

NASA/TM-2009-215784



# Engine Concept Study for an Advanced Single-Aisle Transport

*Mark D. Guynn  
Langley Research Center, Hampton, Virginia*

*Jeffrey J. Berton, Kenneth L. Fisher, William J. Haller, and Michael T. Tong  
Glenn Research Center, Cleveland, Ohio*

*Douglas R. Thurman  
Army Research Laboratory, Cleveland, Ohio*

---

August 2009

## NASA STI Program . . . in Profile

Since its founding, NASA has been dedicated to the advancement of aeronautics and space science. The NASA scientific and technical information (STI) program plays a key part in helping NASA maintain this important role.

The NASA STI program operates under the auspices of the Agency Chief Information Officer. It collects, organizes, provides for archiving, and disseminates NASA's STI. The NASA STI program provides access to the NASA Aeronautics and Space Database and its public interface, the NASA Technical Report Server, thus providing one of the largest collections of aeronautical and space science STI in the world. Results are published in both non-NASA channels and by NASA in the NASA STI Report Series, which includes the following report types:

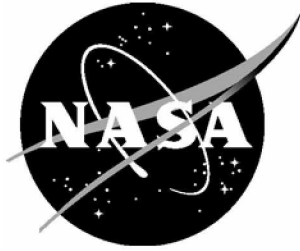
- **TECHNICAL PUBLICATION.** Reports of completed research or a major significant phase of research that present the results of NASA programs and include extensive data or theoretical analysis. Includes compilations of significant scientific and technical data and information deemed to be of continuing reference value. NASA counterpart of peer-reviewed formal professional papers, but having less stringent limitations on manuscript length and extent of graphic presentations.
- **TECHNICAL MEMORANDUM.** Scientific and technical findings that are preliminary or of specialized interest, e.g., quick release reports, working papers, and bibliographies that contain minimal annotation. Does not contain extensive analysis.
- **CONTRACTOR REPORT.** Scientific and technical findings by NASA-sponsored contractors and grantees.
- **CONFERENCE PUBLICATION.** Collected papers from scientific and technical conferences, symposia, seminars, or other meetings sponsored or co-sponsored by NASA.
- **SPECIAL PUBLICATION.** Scientific, technical, or historical information from NASA programs, projects, and missions, often concerned with subjects having substantial public interest.
- **TECHNICAL TRANSLATION.** English-language translations of foreign scientific and technical material pertinent to NASA's mission.

Specialized services also include creating custom thesauri, building customized databases, and organizing and publishing research results.

For more information about the NASA STI program, see the following:

- Access the NASA STI program home page at <http://www.sti.nasa.gov>
- E-mail your question via the Internet to [help@sti.nasa.gov](mailto:help@sti.nasa.gov)
- Fax your question to the NASA STI Help Desk at 443-757-5803
- Phone the NASA STI Help Desk at 443-757-5802
- Write to:  
NASA STI Help Desk  
NASA Center for AeroSpace Information  
7115 Standard Drive  
Hanover, MD 21076-1320

NASA/TM-2009-215784



# Engine Concept Study for an Advanced Single-Aisle Transport

*Mark D. Guynn  
Langley Research Center, Hampton, Virginia*

*Jeffrey J. Berton, Kenneth L. Fisher, William J. Haller, and Michael T. Tong  
Glenn Research Center, Cleveland, Ohio*

*Douglas R. Thurman  
Army Research Laboratory, Cleveland, Ohio*

National Aeronautics and  
Space Administration

Langley Research Center  
Hampton, Virginia 23681-2199

August 2009

## **Acknowledgments**

The authors would like to thank Fay Collier, Principal Investigator for the Subsonic Fixed Wing Project of NASA's Fundamental Aeronautics Program, for his support of this study. Craig Nickol and Dennis Bartlett of NASA Langley Research Center are also acknowledged for their review and critique of the study approach and results.

The use of trademarks or names of manufacturers in this report is for accurate reporting and does not constitute an official endorsement, either expressed or implied, of such products or manufacturers by the National Aeronautics and Space Administration.

Available from:

NASA Center for AeroSpace Information  
7115 Standard Drive  
Hanover, MD 21076-1320  
443-757-5802

# Contents

List of Tables .....	v
List of Figures.....	vi
List of Acronyms, Symbols, and Abbreviations .....	ix
Abstract.....	1
1.0 Introduction.....	1
2.0 Study Objectives and Approach.....	3
3.0 Modeling and Analysis Methodology .....	3
3.1 Propulsion System Modeling.....	3
3.2 Aircraft Sizing Analysis .....	7
3.2.1 Baseline Airframe Model.....	7
3.2.2 ASAT Airframe Model.....	10
3.2.3 Propulsion-Airframe Integration.....	11
3.2.3.1 Landing Gear Length Estimation .....	11
3.2.3.2 Drag Increment for One-Engine-Out Conditions.....	13
3.2.3.3 Vertical Tail Sizing.....	15
3.2.3.4 Nacelle Drag .....	16
3.3 Noise Analysis.....	16
3.3.1 Noise Analysis Validation .....	17
3.3.2 Advanced Noise Reduction Technology Assumptions.....	22
4.0 Spiral 1 .....	24
4.1 Spiral 1 Engine Design .....	24
4.1.1 Low Work Engines .....	24
4.1.2 High Work Engines .....	25
4.1.3 Engine Comparison.....	27
4.2 Spiral 1 Aircraft Sizing.....	30
4.2.1 Low Work Cases.....	30
4.2.2 High Work Cases .....	33
4.2.3 Comparison of Results.....	35
4.2.4 Potential ASAT, Spiral 1 Technology Benefits .....	38
4.3 Spiral 1 Certification Noise Analysis .....	41
5.0 Spiral 2.....	45
5.1 Spiral 2 Engine Design .....	45
5.2 Spiral 2 Aircraft Sizing.....	49
5.2.1 Comparison of Results.....	49
5.2.2 Potential ASAT, Spiral 2 Technology Benefits .....	54

5.3 Spiral 2 Certification Noise Analysis .....	57
6.0 Spiral 3 .....	60
6.1 Spiral 3 Engine Design .....	60
6.2 Spiral 3 Aircraft Sizing.....	63
6.2.1 Airframe Modifications .....	63
6.2.2 Comparison of Results.....	66
6.2.3 Potential ASAT, Spiral 3 Technology Benefits .....	71
6.3 Spiral 3 Certification Noise Analysis .....	72
7.0 Summary .....	75
8.0 Conclusions.....	81
9.0 References .....	82

## List of Tables

Table 1. Advanced Engine Material Assumptions for Projected 2015 Technology .....	6
Table 2. General Characteristics of Spiral 1, Low Work Engine Models.....	26
Table 3. General Characteristics of Spiral 1, High Work Engine Models .....	26
Table 4. Aircraft Sizing Results for Spiral 1, Low Work Engines (162 Passenger, 3250nm Design Mission).....	32
Table 5. Aircraft Sizing Results for Spiral 1, High Work Engines (162 Passenger, 3250nm Design Mission) .....	34
Table 6. General Characteristics of Spiral 2, Low Work Engine Models.....	47
Table 7. General Characteristics of Spiral 2, High Work Engine Models .....	47
Table 8. Aircraft Sizing Results for Spiral 2, Low Work Engines (162 Passenger, 3250nm Design Mission).....	50
Table 9. Aircraft Sizing Results for Spiral 2, High Work Engines (162 Passenger, 3250nm Design Mission) .....	51
Table 10. General Characteristics of Spiral 3, Low Work Engine Models.....	61
Table 11. General Characteristics of Spiral 3, High Work Engine Models .....	61
Table 12. Aircraft Sizing Results for Spiral 3, Low Work Engines (162 Passenger, 3250nm Design Mission).....	67
Table 13. Aircraft Sizing Results for Spiral 3, High Work Engines (162 Passenger, 3250nm Design Mission) .....	68
Table 14. Spiral 1 Trade-Off Analysis.....	79
Table 15. Spiral 2 Trade-Off Analysis.....	79
Table 16. Spiral 3 Trade-Off Analysis.....	80

## List of Figures

Figure 1. Assumed fan tip speed as a function of design fan pressure ratio. ....	5
Figure 2. Variation in fan efficiency with pressure ratio at ADP (TOC) conditions. ....	5
Figure 3. Comparison of predicted and actual $C_D$ versus Mach number for cruise representative $C_L$ condition. ....	8
Figure 4. Comparison of predicted and actual drag polars at representative cruise Mach number. ....	9
Figure 5. Nacelle ground clearance geometry. ....	12
Figure 6. Nose gear collapse geometry. ....	13
Figure 7. Noise certification points. ....	17
Figure 8. Comparison of FLOPS generated and INM generated departure altitudes. ....	19
Figure 9. Comparison of FLOPS generated and INM generated departure airspeeds. ....	19
Figure 10. Comparison of FLOPS generated and INM generated departure thrust. ....	20
Figure 11. Comparison of FLOPS generated and INM generated approach altitudes. ....	21
Figure 12. Comparison of FLOPS generated and INM generated approach airspeeds. ....	21
Figure 13. Comparison of FLOPS generated and INM generated approach thrusts. ....	22
Figure 14. Regression fit of acoustic liner performance (emission yaw angle of $95^\circ$ from inlet). ....	23
Figure 15. Overall acoustic liner suppression map. ....	23
Figure 16. Variation of bypass ratio with fan pressure ratio, top-of-climb conditions, Spiral 1. ....	27
Figure 17. Relationship between fan pressure ratio and TSFC, top-of-climb conditions, Spiral 1. ....	28
Figure 18. Variation of nacelle maximum diameter with fan pressure ratio, Spiral 1. ....	28
Figure 19. Variation of engine+nacelle weight with fan pressure ratio, Spiral 1. ....	29
Figure 20. Variation of block fuel with fan pressure ratio and engine type, Spiral 1. ....	36
Figure 21. Variation of ramp weight with fan pressure ratio and engine type, Spiral 1. ....	36
Figure 22. Variation in total mission $NO_x$ emissions with fan pressure ratio and engine type, Spiral 1. ....	37
Figure 23. Variation in LTO $NO_x$ emissions with fan pressure ratio and engine type ( $D_p/F_{oo}$ ), Spiral 1. ....	38
Figure 24. Variation in $NO_x$ emissions per LTO cycle with fan pressure ratio and engine type, Spiral 1. ....	38
Figure 25. Potential ramp weight reduction from application of ASAT, Spiral 1 technologies. ....	39
Figure 26. Potential block fuel reduction from application of ASAT, Spiral 1 technologies. ....	40
Figure 27. Potential block $NO_x$ reduction from application of ASAT, Spiral 1 technologies. ....	40

Figure 28. Potential LTO NO <sub>x</sub> reduction from application of ASAT, Spiral 1 technologies.....	41
Figure 29. Variation in lateral (sideline) noise with fan pressure ratio and engine type, Spiral 1.....	42
Figure 30. Variation in flyover noise with fan pressure ratio and engine type, Spiral 1.....	42
Figure 31. Variation in approach noise with fan pressure ratio and engine type, Spiral 1.....	43
Figure 32. Variation in cumulative noise reduction with fan pressure ratio and engine type, Spiral 1.....	44
Figure 33. Stage 4 cumulative margin, Spiral 1.....	44
Figure 34. Relationship between fan pressure ratio and TSFC, top-of-climb conditions, Spiral 2.....	48
Figure 35. Variation of engine+nacelle weight with fan pressure ratio, Spiral 2.....	48
Figure 36. Variation in TOC NO <sub>x</sub> Emission Index with fan pressure ratio and engine type, Spiral 2.....	49
Figure 37. Variation of block fuel with fan pressure ratio and engine type, Spiral 2.....	52
Figure 38. Variation of ramp weight with fan pressure ratio and engine type, Spiral 2.....	52
Figure 39. Variation in total mission NO <sub>x</sub> emissions with fan pressure ratio and engine type, Spiral 2.....	53
Figure 40. Variation in LTO NO <sub>x</sub> emissions with fan pressure ratio and engine type (D <sub>p</sub> /F <sub>oo</sub> ), Spiral 2.....	54
Figure 41. Variation in NO <sub>x</sub> emissions per LTO cycle with fan pressure ratio and engine type, Spiral 2.....	54
Figure 42. Potential block fuel reduction from application of ASAT, Spiral 2 technologies.....	55
Figure 43. Potential ramp weight reduction from application of ASAT, Spiral 2 technologies.....	55
Figure 44. Potential block NO <sub>x</sub> reduction from application of ASAT, Spiral 2 technologies.....	56
Figure 45. Potential LTO NO <sub>x</sub> reduction from application of ASAT, Spiral 2 technologies.....	56
Figure 46. Variation in lateral (sideline) noise with fan pressure ratio and engine type, Spiral 2.....	57
Figure 47. Variation in flyover noise with fan pressure ratio and engine type, Spiral 2.....	58
Figure 48. Variation in approach noise with fan pressure ratio and engine type, Spiral 2.....	58
Figure 49. Variation in cumulative noise reduction with fan pressure ratio and engine type, Spiral 2.....	59
Figure 50. Stage 4 cumulative margin, Spiral 2.....	59
Figure 51. Variation of engine+nacelle weight with fan pressure ratio, Spiral 3.....	62
Figure 52. Relationship between fan pressure ratio and TSFC, top-of-climb conditions, Spiral 3.....	62
Figure 53. Variation in NO <sub>x</sub> Emission Index with fan pressure ratio and engine type, Spiral 3.....	63
Figure 54. Comparison of Spiral 1/2 and Spiral 3 airframe geometry.....	64
Figure 55. Comparison of 737-800 and Spiral 3 design drag rise.....	64

Figure 56. Comparison of aerodynamic efficiency for Spiral 1/2 and Spiral 3. ....	65
Figure 57. Variation of block fuel with fan pressure ratio and engine type, Spiral 3. ....	69
Figure 58. Variation of ramp weight with fan pressure ratio and engine type, Spiral 3. ....	70
Figure 59. Variation in total mission NO <sub>x</sub> emissions with fan pressure ratio and engine type, Spiral 3. ....	70
Figure 60. Variation in LTO NO <sub>x</sub> emissions with fan pressure ratio and engine type (D <sub>p</sub> /F <sub>oo</sub> ), Spiral 3. ....	71
Figure 61. Variation in NO <sub>x</sub> emissions per LTO cycle with fan pressure ratio and engine type, Spiral 3. ....	71
Figure 62. Variation in lateral (sideline) noise with fan pressure ratio and engine type, Spiral 3. ....	72
Figure 63. Variation in flyover noise with fan pressure ratio and engine type, Spiral 3. ....	73
Figure 64. Variation in approach noise with fan pressure ratio and engine type, Spiral 3. ....	73
Figure 65. Variation in cumulative noise reduction with fan pressure ratio and engine type, Spiral 3. ....	74
Figure 66. Stage 4 cumulative margin, Spiral 3. ....	74
Figure 67. Minimum ramp weight. ....	76
Figure 68. Minimum block fuel. ....	76
Figure 69. Minimum block NO <sub>x</sub> . ....	77
Figure 70. Minimum LTO NO <sub>x</sub> . ....	77
Figure 71. Minimum noise. ....	78

## List of Acronyms, Symbols, and Abbreviations

$a$  – speed of sound

$a_x$  – empirical coefficients for NO<sub>x</sub> estimation relationship

$b$  – wing span

$C_D$  – Coefficient of Drag

$C_L$  – Coefficient of Lift

$C_{Lmax}$  – Maximum Coefficient of Lift

$C_{L\alpha}$  – lift curve slope versus angle of attack

$C_N$  – Coefficient of Yawing Moment

$C_{l\beta}$  – aircraft stability derivative, change in rolling moment with sideslip

$C_{n\beta}$  – aircraft stability derivative, change in yawing moment with sideslip

$C_{y\beta}$  – aircraft stability derivative, change in sideforce with sideslip

$d_i$  – engine inlet diameter

$d_{nac}$  – nacelle maximum diameter

$D_{wm}$  – engine windmilling drag

$f_a$  – combustor fuel-to-air ratio

$L$  – required landing gear distance from ground to attach point (compressed)

$L/D$  – lift-to-drag ratio

$l_v$  – vertical tail moment arm

$M$  – Mach number

$P_{i3}$  – compressor exit/combustor entrance total pressure

$R$  – aircraft cruise range

$S_{vt}$  – vertical tail reference area

$S_{wing}$  – wing reference area

$T$  – engine thrust

$T_{i3}$  – compressor exit/combustor entrance total temperature

$V$  – aircraft velocity

$V_{mc}$  – minimum control speed during takeoff

$VL_{max}$  – maximum allowable vertical tail loading

$W_f$  – aircraft weight at end of cruise

$W_i$  – aircraft weight at beginning of cruise

$Y$  – side force provided by vertical tail

$y_{gear}$  – main landing gear spanwise location

$y_{nac}$  – nacelle spanwise location

$z_{min}$  – minimum nacelle ground clearance

$\Gamma$  – wing dihedral angle

$\Delta x_{fus}$  – horizontal distance between fuselage ground contact point during nose gear collapse and main landing gear ground contact point

$\Delta x_{nac}$  – horizontal distance between nacelle maximum diameter and main landing gear ground contact point

$\Delta z_{fus}$  – vertical distance between main landing gear attach and fuselage ground contact point during nose gear collapse

$\Delta z_{nac}$  – nacelle-wing offset

$\Delta\phi$  – combustor cooling air percentage

$\rho$  – air density

ADP – Aerodynamic Design Point

ANOPP – Aircraft Noise Prediction Program

ASAT – Advanced Single-Aisle Transport

ASDL – Aerospace Systems Design Laboratory

BPR – Bypass Ratio

EDS – Environmental Design Space

EI – Emission Index, grams of emission per kg of fuel consumed

EIS – Entry-Into-Service

EPNL – Effective Perceived Noise Level

FAR – Federal Aviation Regulations

FLOPS – Flight Optimization System

HPC – High Pressure Compressor

HPT – High Pressure Turbine

ISA – International Standard Atmosphere

LPC – Low Pressure Compressor

LPT – Low Pressure Turbine

LTO – Landing-Takeoff Cycle

NPSS – Numerical Propulsion System Simulation

OEW – Operating Empty Weight

PDCYL – Point Design of Cylindrical-bodied aircraft

TOC – Top-Of-Climb

TSFC – Thrust Specific Fuel Consumption

UHB – Ultra-High Bypass ratio

WATE – Weight Analysis of Turbine Engines

## Abstract

*The desire for higher engine efficiency has resulted in the evolution of aircraft gas turbine engines from turbojets, to low bypass ratio, first generation turbofans, to today's high bypass ratio turbofans. It is possible that future designs will continue this trend, leading to very-high or ultra-high bypass ratio (UHB) engines. Although increased bypass ratio has clear benefits in terms of propulsion system metrics such as specific fuel consumption, these benefits may not translate into aircraft system level benefits due to integration penalties. In this study, the design trade space for advanced turbofan engines applied to a single aisle transport (737/A320 class aircraft) is explored. The benefits of increased bypass ratio and associated enabling technologies such as geared fan drive are found to depend on the primary metrics of interest. For example, bypass ratios at which mission fuel consumption is minimized may not require geared fan technology. However, geared fan drive does enable higher bypass ratio designs which result in lower noise. Regardless of the engine architecture chosen, the results of this study indicate the potential for the advanced aircraft to realize substantial improvements in fuel efficiency, emissions, and noise compared to the current vehicles in this size class.*

## 1.0 Introduction

As aircraft manufacturers Boeing and Airbus continue to develop and mature new twin-aisle, wide body aircraft designs in the 210-350 seat class, for scheduled first deliveries in 2010 and 2013 respectively, it is anticipated that the next major development undertaking for both companies will be a new narrow body aircraft in the Boeing 737/Airbus A320 class. At present, there is not much urgency for these new designs because of robust sales of their current offerings in this size class. However, current projections are that new designs will be introduced in the latter half of the next decade. Boeing and Airbus have been engaged in studies to investigate replacement designs for the 737 and A320, respectively, and published reports indicate that both manufacturers are depending on a next generation engine to power these new designs (ref. 1). The large fuel consumption and operating cost reductions necessary to make a new design economically viable will require substantial improvements in propulsion system efficiency. It is well known in aircraft propulsion system design that it is more efficient to generate thrust by accelerating a large mass of air a small amount than by accelerating a small mass of air a large amount; propulsive efficiency increases as the ratio of exhaust velocity to free stream velocity decreases. For a turbofan engine, this can be accomplished by reducing the fan pressure ratio, which decreases the amount of fan air stream acceleration, and increasing the fan mass flow to maintain thrust. An increase in fan mass flow for a given core engine size leads to higher bypass ratio. The desire for higher engine efficiency has resulted in the evolution of aircraft gas turbine engines from turbojets (BPR=0), to low bypass ratio, first generation turbofans (BPR=1-2), to today's high bypass ratio turbofans (BPR=5-10). It is possible that future designs will continue this trend, leading to very-high or ultra-high bypass ratio (UHB) engines. Increased bypass ratio has complementary benefits in addition to improving fuel efficiency. Increasing bypass ratio also reduces engine noise due to the strong relationship between noise and the velocity of the air exiting the engine. Low pressure ratio fans also typically require lower tip speeds which can result in lower fan noise. The lower jet velocities and lower fan tip speeds associated with low fan pressure ratio can lead to substantial engine noise reduction.

Design studies for the Boeing 737 and Airbus A320 replacement concepts are closely guarded by the companies and it is not currently known what engine concepts are under consideration. Improving fuel efficiency by using advanced engines with lower fan pressure ratio and higher bypass ratio is one approach that certainly will be explored. There is a practical limit, however, to how much bypass ratio can be increased before significant penalties arise which begin to erode the benefits. Ultra-high bypass ratio engines have large, low speed fans. In a conventional turbofan engine, the relatively low rotational speed of this fan creates low-spool weight and performance issues because of a mismatch between the optimum fan speed and optimum low pressure turbine (LPT) speed. This mismatch can be avoided by connecting the fan and low-spool through a gearbox, which enables the fan and low-spool to operate at different rotational speeds. Use of a gear system does, however, introduce a separate set of concerns such as gearbox reliability, weight, and cost. In addition to issues which arise in the engine design itself, increasing bypass ratio at constant thrust increases engine and nacelle diameter. This increases engine installation penalties, such as nacelle weight and drag, and makes it more difficult to integrate the engine with the airframe. Integration is particularly difficult in the case of a conventional under-wing installation on a low wing aircraft. It is not readily apparent, therefore, whether the propulsion efficiency benefits of lower fan pressure ratio and higher bypass ratio lead to benefits at the aircraft system level.

Because of the potential for lower noise and improved propulsive efficiency, the use of UHB engines has been studied many times over the past several decades and there are numerous publications addressing the topic. One early example is reference 2, published in 1972, which includes a discussion of the potential noise benefits, a comparison of geared fan and direct drive fan systems, a presentation of gear system design details, and an assessment of gear system reliability. Reference 3 provides another example, 15 years later. This paper includes a theoretical treatment of the efficiency implications of higher bypass ratio and presents results for BPR=12-14 engines applied to Boeing 747 and 767 aircraft. As noted in reference 3, "Studies of very high BPR engines have occurred many times over the history of large wide-body airplanes. These studies were abandoned each time because of the unfavorable trades between the TSFC (*thrust specific fuel consumption*) advantages and the weight and drag penalties, and between fuel costs and engine development costs." A more recent example is the engine diameter study conducted by Boeing in support of NASA's Ultra-Efficient Engine Technology project (ref. 4). This study compared advanced engines, varying in bypass ratio from ~7.5 to ~21.5, applied to a 777-200ER based airframe. Optimum bypass ratio was found to be in the range of 11 to 14.

Results published over the years include both positive and negative assessments of UHB engines, depending on the assumptions made and the metrics of interest. Over time the baseline technologies, market environment (e.g., fuel cost), metrics of interest, and target applications change, dictating that concepts such as the UHB engine be periodically revisited. In recent years, fuel efficiency, emissions, and noise have become key metrics for aircraft/engine performance. Rising fuel costs have greatly elevated the importance of fuel efficiency to the overall profitability of airlines and the success of an aircraft design. Noise and emissions are also projected to be of increasing importance in aircraft design as the demand for air travel grows. Substantial reductions in aircraft noise and emissions are required to enable unconstrained aviation growth without a sharply increasing negative impact on the environment. The 737/A320 class aircraft considered in this study represent a significant portion of the global airline fleet. Sixty-five percent of the new aircraft produced over the next 20 years are projected to be in this class (ref. 5). Advances made to reduce the noise and emissions of these aircraft could provide a considerable positive contribution to the goal of minimizing the future environmental impact of aviation. What has not been determined, at least not external to the Boeing and Airbus in-house studies, is the most attractive advanced engine design for this class of aircraft in light of the current metrics of interest in the aviation industry.

## 2.0 Study Objectives and Approach

The primary objective of the advanced single-aisle transport\* (ASAT) engine concept study was to determine if the TSFC and noise benefits of lower fan pressure ratio/higher bypass ratio engines translate into overall aircraft system level benefits for a 737 class vehicle. (The scope of this study was limited to ducted turbofan engines, open rotor designs may also be viable candidates for a future ASAT aircraft and are the focus of a separate study.) The approach taken was to develop a series of analytical engine models, apply them to a common airframe model, and assess the overall performance and noise characteristics. The main parameter of interest for the study was design fan pressure ratio (bypass ratio). However, it was quickly determined during the initial stages of the study that other key engine design choices have significant impact on the effects of fan pressure ratio. One key design parameter is the fan drive philosophy. Engine manufacturer Pratt & Whitney is pursuing a geared turbofan design for the 737/A320 replacement vehicles (ref. 6). However, to obtain a more complete understanding of the design space, engines with both geared and direct drive fans were developed for this study. Another potential discriminator in the engine design is the compression work split between the low-spool and high-spool compressors. Engine manufacturers have adopted different high-pressure spool designs based on their company's strategic philosophy. This difference can have an influence on the effects of fan pressure ratio and fan gearing, so work split was added to the study trades. The impact of engine overall pressure ratio and design cruise Mach number on the results was also investigated.

## 3.0 Modeling and Analysis Methodology

### 3.1 Propulsion System Modeling

Since the propulsion system was the primary area of focus for this study, a substantial amount of effort was applied to building analytical models of the study engines. Unfortunately, there is little information available on which to base models of possible future engine systems. Developing models which were adequately representative of engines that could be available for a 737/A320 replacement aircraft was an important objective. However, equally important was the requirement of consistency among the engine models. After reviewing available material on projected advanced propulsion technologies, the propulsion systems analysis team developed a common design approach and set of technology assumptions that were utilized throughout to enable this consistency. The unique characteristics of individual engine architectures may make some assumptions less appropriate for certain engine types. This makes applying consistent ground rules and technology assumptions across such a wide range of engine designs problematic. The degree to which the resulting study engines are truly equivalent in technology and design optimality is uncertain. Cycle analysis for the engines was performed with the NPSS (Numerical Propulsion System Simulation) code (refs. 7, 8, 9). Analysis of the aeromechanical characteristics and estimates of the engine weight (including fan gearbox if applicable) were performed with the WATE (Weight Analysis of Turbine Engines) code (ref. 10-12).

The basic engine architecture for all the engines in this study is the two spool, separate flow turbofan. The variations evaluated include the fan drive approach (geared vs. direct drive), the fan pressure ratio, the low spool-high spool compression work split, the type of fan nozzle (fixed or variable geometry), the overall pressure ratio, and the design Mach number. For a given analysis spiral, all engines were

---

\* "Single-Aisle Transport" is a common way to refer to a 737/A320 class airplane; although there are other types of single-aisle aircraft (e.g., regional jets). Even though it is possible that the future 737/A320 replacements designed by Boeing and Airbus will not have single-aisle passenger layouts, the term "single-aisle transport" will be used in this report to refer to a 737/A320 class airplane.

developed with the same Aerodynamic Design Point (ADP) (Mach number, altitude, and thrust) and same overall pressure ratio at the ADP. The ADP was selected to represent a nominal top-of-climb (TOC) condition for the ASAT airframe. Although for a given spiral the overall pressure ratio is the same for all the engines, two different compressor work splits were considered for each fan pressure ratio/fan drive case. For a given fan pressure ratio and overall pressure ratio, the “low work” engines have a lower pressure rise across the low pressure compressor (and a higher pressure rise across the high pressure compressor) compared to the “high work” engines. Inlet mass flow for each engine was selected to achieve the net thrust requirement at ADP. The bypass ratio was set to achieve an extraction ratio (ratio of total pressures for bypass nozzle and core nozzle) of 1.25 at the design point. In addition to meeting a thrust target at TOC conditions, a sea-level-static (SLS) thrust target of 23,000 lb (hot day, ISA+27°F) was also met by adjusting design point burner fuel-to-air ratio. Low fan pressure ratio engines inherently have a greater loss of thrust with airspeed (thrust lapse) than high fan pressure ratio engines. To achieve equal ADP thrust capability, the low fan pressure ratio engines must be operated at higher temperatures. The ADP operating temperatures for the low fan pressure ratio engines were below the maximums allowed for the materials assumed, but the higher temperatures could still lead to shorter engine hot section life and greater maintenance requirements than the high fan pressure ratio engines. Engine life and maintenance issues were not assessed as part of this study.

Assumptions for fan and compressor design tip speeds and efficiencies were based on technology trend curves recently developed by the Aerospace Systems Design Laboratory (ASDL) at Georgia Tech for use in the FAA’s Environmental Design Space (EDS) system (ref. 13). These curves have been reviewed by the EDS Independent Review Group, which includes industry representatives. Since the ASDL trend curves represent current technology, adjustments were made to reflect advanced technology capabilities. A target entry-into-service (EIS) date of 2015 was assumed in projecting adjustments for advanced technology. Variation in fan tip speed with pressure ratio is shown in Figure 1. Figure 2 shows the fan efficiency at the ADP design condition as a function of fan pressure ratio. Although varying slightly among the engines, the low pressure compressor (LPC) polytropic efficiency at ADP was ~0.89. High pressure compressor polytropic efficiency was ~0.91 at ADP conditions. All of the engines were designed to have the same turbine loadings. Since turbine efficiency trends with loading, equal turbine efficiencies were used across all of the engines; adiabatic efficiency of 0.90 for the high pressure turbine (HPT) and 0.94 for the LPT. The LPT has significantly higher efficiency than the HPT because it is uncooled. For the geared engines the mechanical efficiency of the gearbox was assumed to be 0.99.

A maximum turbine inlet temperature (T4) of 3460°R and maximum HPT rotor inlet temperature (T41) of 3310°R were assumed. The turbine cooling required was estimated assuming use of advanced high temperature materials. A maximum LPT rotor inlet temperature of 2460°R was used, which was considered a reasonable limit that would allow the LPT to be uncooled with use of advanced materials. A complete summary of the advanced engine materials assumed is contained in Table 1. Additional requirements associated with gearbox cooling for the geared fan designs were not assessed.

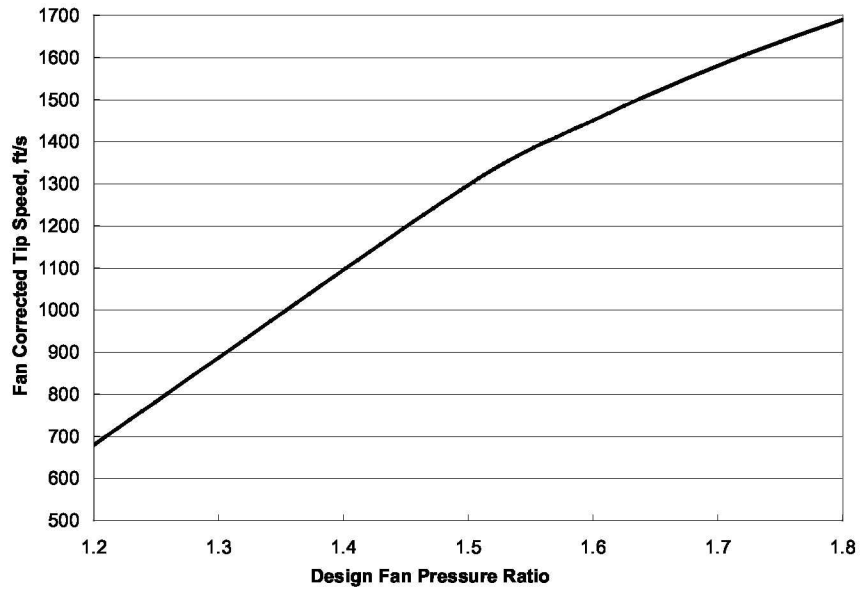


Figure 1. Assumed fan tip speed as a function of design fan pressure ratio.

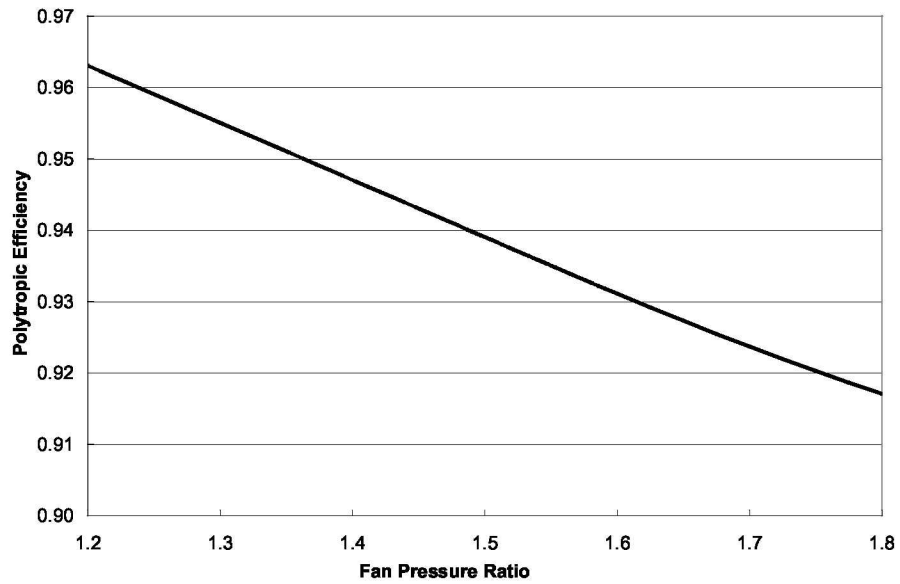


Figure 2. Variation in fan efficiency with pressure ratio at ADP (TOC) conditions.

Table 1. Advanced Engine Material Assumptions for Projected 2015 Technology

Component	Blade	Vane	Disk	Case
Fan	Polymer matrix composite	Polymer matrix composite		Polymer matrix composite wrapped by Zylon
LPC	Titanium aluminide	Titanium aluminide		Polymer matrix composite
HPC (hot section)	Titanium aluminide	Titanium aluminide		Titanium metal matrix composite
HPT	5th generation nickel-based alloy	5th generation nickel-based alloy	Nickel-based powder metallurgy alloy	
LPT	5th generation nickel-based alloy	5th generation nickel-based alloy	Nickel-based powder metallurgy alloy	
Inlet/Nacelle				Polymer matrix composite

Estimates for engine NO<sub>x</sub> emission indices (grams of NO<sub>x</sub> emitted from the engine per kilogram of fuel consumed by the engine) were obtained from a correlation developed by NASA combustor technologists during the latter stages of NASA's Ultra-Efficient Engine Technology program. The correlation (shown below) reflects advanced combustor technology consistent with NASA's goals for the 2015 EIS timeframe.

$$EINO_x = a_0 \times (P_{t3})^{a_1} \times \left[ e^{\left( \frac{T_{t3} - 459.67}{a_2} \right)} \right] \times \left( \frac{f_a}{\Delta\phi} \right)^{a_3};$$

where,

- $a_0$  =  $f$ (% combustor cooling air, combustor technology level)
- $a_1$  = 0.35
- $a_2$  = 300
- $a_3$  = 2.4
- $P_{t3}$  = compressor exit/combustor entrance total pressure (psia)
- $T_{t3}$  = compressor exit/combustor entrance total temperature (°R)
- $f_a$  = combustor fuel-to-air ratio
- $\Delta\phi$  = combustor cooling air percentage

The combustor testing used to develop this correlation was limited to high power settings (i.e., takeoff and climbout). EIs for approach and idle power settings were estimated based on EI values projected for other advanced technology, low NO<sub>x</sub> combustors under concurrent development during the NASA program.

Low fan pressure ratio engine cycles generally require some type of variable geometry for proper operation across the flight envelope. Two approaches commonly considered are variable pitch fan blades and a variable area fan exhaust nozzle. Because variable pitch fan blades present additional technological challenges, the use of a variable area nozzle was examined in this study. The variable area nozzle was assessed a 10% weight penalty compared to an equivalent fixed-area design. Engines across the fan pressure ratio spectrum were initially developed both with and without use of a variable area nozzle. Then for a given fan pressure ratio, the need for, or benefit of, the variable area nozzle was assessed. For the low fan pressure ratio cases, a variable area nozzle was needed to achieve a desired 20% fan surge margin throughout the operating envelope. For the high fan pressure ratio cases, an acceptable surge margin was achievable with fixed geometry and the extra weight of a variable area nozzle was not justified. At a fan

pressure ratio of 1.5, engines with both fixed and variable nozzle area were carried forward to the aircraft sizing analysis with the final choice made based on overall aircraft system performance. Throat area of the variable area nozzle was varied at off-design to maintain the fan operating conditions equal to, or very close to, the fan peak efficiency operating line. The amount of area variation required for the lowest fan pressure ratio (1.3) was 7.5%.

The engine design approach and technology assumptions used for this study are not exclusive. There are a number of possible variations in the design approach; such as different choices for ADP and/or thrust sizing conditions, a different LPT cooling philosophy, or a different choice for extraction ratio. Furthermore, assumptions based on projected technology advances are not definitive. Changes in the technology assumptions and design approach can affect the absolute engine performance and weight, as well as the relative differences among the engine types. The results of this study should be viewed, therefore, in light of the assumptions and approach used.

### **3.2 Aircraft Sizing Analysis**

To evaluate and compare aircraft system level performance, the study engines were combined with an advanced technology, single-aisle commercial transport airframe model. The aircraft sizing and synthesis computer code FLOPS (Flight Optimization System) (ref. 14) was used as the primary aircraft level sizing and analysis tool. Since the objective of the study was a comparison of engine concepts, the primary modeling focus was the propulsion system. However, inaccuracies in the airframe model can skew the system level impacts of the engine designs and influence the overall conclusions. Special sizing considerations introduced by large diameter engines were addressed through simplifying assumptions and enhancements to the FLOPS analysis. Spreadsheet analyses were used to determine landing gear length, engine-out drag, and vertical tail size so that impacts of large diameter engines could be properly captured. Enhancements to basic FLOPS capabilities were also made in the structural weight and aerodynamics areas. The wing and fuselage structure weight estimates of FLOPS were replaced with estimates from PDCYL (ref. 15). PDCYL offers a less empirical, more analytical weight estimation methodology that is more sensitive to parameters such as engine weight and location. FLOPS aerodynamic predictions were enhanced through a model calibration process incorporating details of the 737-800 high speed and low speed aerodynamic performance.

#### ***3.2.1 Baseline Airframe Model***

The Boeing 737-800 (with winglets) was used as a starting point for development of an advanced single-aisle transport (ASAT) airframe model. A baseline FLOPS model of a 737-800 like aircraft (162 passenger, mixed-class configuration) was developed using a combination of publicly available data on the 737-800 geometry, weight, and performance characteristics (ref. 16); a CFM56-7B based engine model developed at NASA Glenn; and proprietary aerodynamic data.

Model weight predictions were calibrated by setting maximum ramp weight and landing weight to the Boeing reported values (174,700 lb and 146,300 lb respectively) and comparing the predicted operating empty weight (OEW) to the Boeing data. Lower level weight data were not available for the 737-800 and errors in individual component weights could not be ascertained. Since FLOPS and PDCYL do not include weight estimates for winglets, this calibration was first performed for the 737-800 without winglets. The predicted OEW without calibration was 90,927 lb compared to 91,300 lb from reference 16. This predicted OEW estimate includes PDCYL-based fuselage and wing weight estimates; FLOPS estimates for empennage structure, landing gear, systems and equipment, and operating items; and CFM56-7B engine/nacelle weight estimates provided by NASA Glenn and supplied as input to FLOPS

and PDCYL. (Note that the PDCYL-based wing and fuselage total weight estimates include an empirical factor applied to the PDCYL analytically derived structural weight estimates. This empirical factor accounts for additional, non-optimal structural weight as well as non-structural components that contribute to the total weight. The factor is based on a linear regression of PDCYL-predicted primary structure weight compared to actual total weight for eight subsonic commercial transport type aircraft.) Although the model OEW matches the Boeing data to within 0.5%, calibration adjustments were made to the model to match OEW exactly. The increase in empty weight associated with blended winglets is not explicitly available from reference 16. Estimates for the weight impact of the winglets are given in numerous places. In reference 17 the additional weight is given as 170-235 kg (375-520 lb). Reference 18, which is an article on blended winglets published by Boeing, presents a number of winglet characteristics but a specific weight penalty is not given. However, in this article the OEW for the 737-800 with winglets is given as 91,660 lb. A factor was therefore applied to the PDCYL wing weight estimate to result in the model matching this slightly higher OEW weight.

One significant feature of the baseline model is calibration of the FLOPS aerodynamic predictions to 737-800 high speed aerodynamic data. Although it was not possible to exactly match the 737-800 data at all conditions, it was possible to obtain an excellent match around the cruise flight conditions as shown in Figures 3 and 4. This agreement is most important for matching overall mission performance since the large majority of mission time and fuel consumption is at cruise conditions.

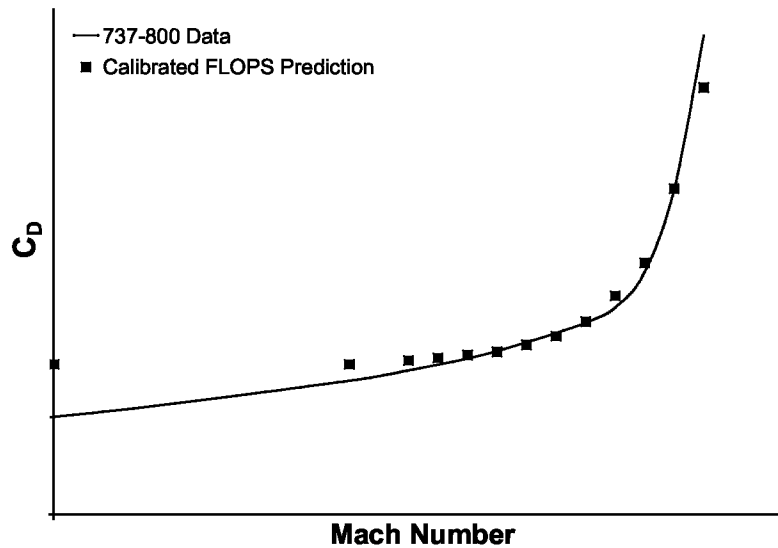


Figure 3. Comparison of predicted and actual  $C_D$  versus Mach number for cruise representative  $C_L$  condition.

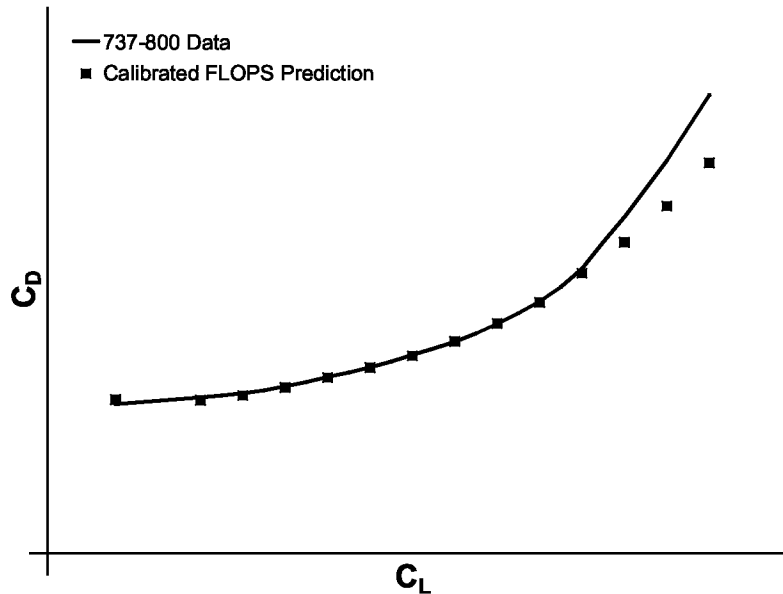


Figure 4. Comparison of predicted and actual drag polars at representative cruise Mach number.

FLOPS predicted mission performance was calibrated to a specific point on the 737-800 payload-range diagram provided in reference 16. Assuming a payload of 32,400 lb (162 passengers at 200 lb per passenger), OEW plus payload is 124,060 lb. At maximum fuel capacity of 46,063 lb, ramp weight for the calibration mission is 170,123 lb. According to the payload-range diagram, at this operating point the range is ~3060 nm. This mission performance was used as the calibration point for the FLOPS model. Assuming the weight characteristics are accurate, range performance is impacted most directly by the mission profile, engine TSFC, and aircraft aerodynamic efficiency (lift-to-drag ratio, L/D). Although a detailed mission profile is not provided in reference 16, some parameters are specified in the payload-range diagram: 31-35-39,000 ft step cruise, cruise speed at Long Range Cruise Mach, typical mission reserves, and a 200 nm alternate airport. Additional insight into the likely Boeing mission rules was obtained from reference 19, which includes a “typical” mission profile diagram from Boeing. Prior to calibration, the FLOPS predicted range for this mission was 3178 nm (~4% high). Assuming that the mission profile is adequately modeled and the aerodynamic model is accurate, the higher FLOPS range is indicative of an under prediction of engine TSFC at cruise. The NASA-developed engine deck was therefore adjusted to match the 3060 nm published range capability. Note that it is not possible to separate the impacts of inaccuracies in mission profile, engine TSFC, and aircraft L/D when matching range performance. Even though adjustment was only made to the engine model, the discrepancy is most likely due to a combination of differences in engine characteristics, aerodynamic characteristics, and mission definition. For example, the step cruise specified in reference 16 was approximated in FLOPS by cruising at optimum altitude (“cruise-climb”). This more efficient cruise profile may be partly responsible for the initial FLOPS model resulting in a range higher than the published range capability.

Evaluation and calibration of the FLOPS model was also performed for low speed performance; that is, takeoff and landing performance. Low speed aerodynamic characteristics at any given point are dependent on many different factors. Although FLOPS offers a detailed, time-stepping takeoff and landing analysis, it is not possible to capture all the detailed dynamics associated with an actual takeoff and landing. For example, because of the mutual interaction of air flow around the landing gear and the rest of the vehicle, landing gear drag may be a function of aircraft lift coefficient. FLOPS, on the other hand, has a single input value for landing gear drag. Using the available 737-800 low speed data, representative values for the required FLOPS inputs were developed. Takeoff and landing performance

data from reference 16 for standard day, dry runway were then used for validation of the FLOPS model. After some adjustment to the inputs, takeoff and landing distances were matched to within ~1.0% of the reported values for a single set of conditions. Good agreement of the model with reported data at one point does not necessarily imply, however, that the model is accurate enough to replicate variation of takeoff and landing distances with weight, airport altitude, temperature, etc.

The final step in development of a baseline model representative of a 737-800 type aircraft was ensuring that the FLOPS vehicle sizing was consistent with the actual aircraft. For basic FLOPS sizing the parameters varied are engine thrust and wing area, with an objective to minimize the gross weight required to meet the mission. One of the difficulties in sizing for this particular case is that the design mission described above is at a gross weight below the maximum gross weight. Performance constraints such as initial cruise altitude capability and takeoff field length need to be met when the mission starts at the maximum weight. A more significant issue is that the wing area and thrust of the actual aircraft can be sized by considerations outside the scope of FLOPS. For example, the wing or engine may be oversized for a future “growth version” of the aircraft. In the case of the 737, a range of different thrust engines are available and the same engines are available on the 737-800 and 737-900, which have different maximum weights. If performance constraints such as rate-of-climb can be met for the larger, heavier 737-900 with a given engine, they will likely be exceeded for the smaller, lighter 737-800. The sizing routine in FLOPS would therefore tend to reduce the engine thrust of a 737-800 type vehicle. The only way to mitigate this tendency in the FLOPS model is to specify additional constraints which force the sizing to replicate the 737-800 performance. For example, constraining takeoff field length to be “as good as” the 737-800 for the same takeoff weight will relax the tendency for FLOPS to size down the engines to eliminate excess thrust capability at top-of-climb. With a takeoff field length constraint of 7000 ft (approximate sea level, standard day performance of 737-800 with CFM56-7B26 engines at takeoff weight of 170,123 lb) the FLOPS sizing results in a vehicle with a gross weight of 169,685 lb (170,123 lb actual), a OEW of 91,620 lb (91,660 actual), a wing area of 1365 ft<sup>2</sup> (1341 ft<sup>2</sup> actual), and a sea level static thrust of 25,828 lb per engine (26,300 lb actual).

### ***3.2.2 ASAT Airframe Model***

The ASAT airframe model is a derivative of the 737-800 like baseline model intended to be representative of a potential advanced technology 737 replacement aircraft. A conventional airframe-engine layout like the 737-800 was assumed based on the hypothesis that unconventional approaches are not sufficiently mature to support the expected EIS date for this vehicle. The primary airframe technology advancement assumed was extensive use of composite materials for the airframe structure. For the Boeing 787 currently in development, as much as 50 percent of the primary structure is made of composite materials (ref. 20). This composite construction was assumed to result in a 15% reduction in weight of the wing, fuselage, and empennage compared to the metal construction of the 737-800. Other minor technology improvements based on the 787 included an increase in hydraulic pressure to 5000 psi, and a 1% reduction in drag. Changes were also made to the design mission to reflect performance enhancements projected for an advanced aircraft in this vehicle class. Cruise Mach was increased to 0.8 (typical cruise Mach for the 737-800 is 0.785 (ref. 21)) and design range (with 32,400 lb payload) was increased from 3060 nm to 3250 nm. The basic 737-800 geometry was not changed for the ASAT model, except for a slight increase in wing sweep to enable efficient cruise at Mach=0.8. (Increasing wing sweep increases the “drag-rise Mach number,” the Mach number at which compressibility drag begins to greatly reduce aerodynamic efficiency.) Changes to wing weight associated with the increased wing sweep were captured in the PDCYL analysis.

### 3.2.3 Propulsion-Airframe Integration

Proper propulsion-airframe integration requires consideration of many issues. Typically, for a high-level comparative study of this type most of these issues are not directly addressed. Rather, they are addressed indirectly by developing aircraft analysis models based on, or similar to, existing aircraft, for which proper propulsion-airframe integration has already been performed. Propulsion-airframe integration is one of the key considerations for large diameter, UHB engines, however. Reference 4 provides an excellent summary of the integration issues associated with large diameter engines and was used as a basis for the current study. Concerns highlighted in reference 4 include nacelle drag, ground clearance, windmilling drag, thrust reverser operation, and engine placement. These concerns were addressed to varying degrees in the current study. A simple geometric method was developed to estimate the required landing gear length. Windmilling and engine-out drag estimates were made using handbook methods (ref. 22) and the vertical tail was sized based on consideration of both tail volume coefficient and one-engine-out control. Detailed descriptions of these approximate methods are given below. Other propulsion-airframe integration issues were addressed through existing FLOPS capability or not included as part of the study. Examples of issues outside the scope of this study include impacts of nacelle diameter on pylon and flap design and potential changes in thrust reverser operation associated with large diameter engines. (An estimate of thrust reverser weight was included for all engines.)

#### 3.2.3.1 Landing Gear Length Estimation

Nacelle ground clearance has been an issue for the Boeing 737 aircraft since introduction of the high bypass ratio CFM56-3 engines on the second generation 737-300,-400, and -500 models. The original 737-100 and -200 aircraft were equipped with low bypass ratio JT8D engines, having a diameter of ~42 inches (ref. 23). The minimum nacelle ground clearance on the 737-100 and -200 was only 20 inches (ref. 16). Integration of the higher bypass ratio CFM56-3 (BPR=6), which has a fan diameter of 60 inches (ref. 24), required side mounted engine accessories and a “squashed” nacelle shape to arrive at a minimum nacelle ground clearance of 18 inches (ref. 16). This arrangement was retained for integration of the newer CFM56-7B engine on the 737-600, -700, -800, -900 aircraft. Given the extreme measures required to integrate a 60 inch diameter engine on the 737, it is not likely that a larger engine could be retrofitted to a current 737-800 without other configuration changes. Although the basic 737-800 geometry was used for the airframe in this study, adjustment in landing gear length was necessary to accommodate larger engines. A simple geometric method was developed to estimate the required landing gear length based on two constraints. First, a minimum nacelle ground clearance constraint is applied. This minimum clearance was set at 18 inches, the same clearance as the current 737-800. A second constraint is then applied to avoid the potential of engine damage in the case of a nose gear collapse, which was identified as a potential gear length sizing constraint in reference 4. These calculations were automated in a spreadsheet and linked to the FLOPS analysis to capture changes in required landing gear length during aircraft sizing.

The main landing gear length required to meet the minimum nacelle ground clearance is a function of the nacelle maximum diameter, the spanwise location of the nacelle, the wing dihedral, the spanwise location of the main gear, and the “nacelle-wing offset” (defined here as the vertical distance between the top of the nacelle and the local wing chord line):

$$L_1 = z_{\min} + d_{nac} - ((y_{nac} - y_{gear}) \tan(\Gamma) - \Delta z_{nac});$$

where, as shown in Figure 5,

- $L_1$  = required distance from ground to attach point (compressed)
- $z_{min}$  = minimum ground clearance (1.5 ft in this case)
- $d_{nac}$  = nacelle maximum diameter, ft
- $y_{nac}$  = nacelle spanwise location (distance from centerline, ft)
- $y_{gear}$  = main gear spanwise location (distance from centerline, ft)
- $\Gamma$  = wing dihedral
- $\Delta z_{nac}$  = nacelle-wing offset, ft

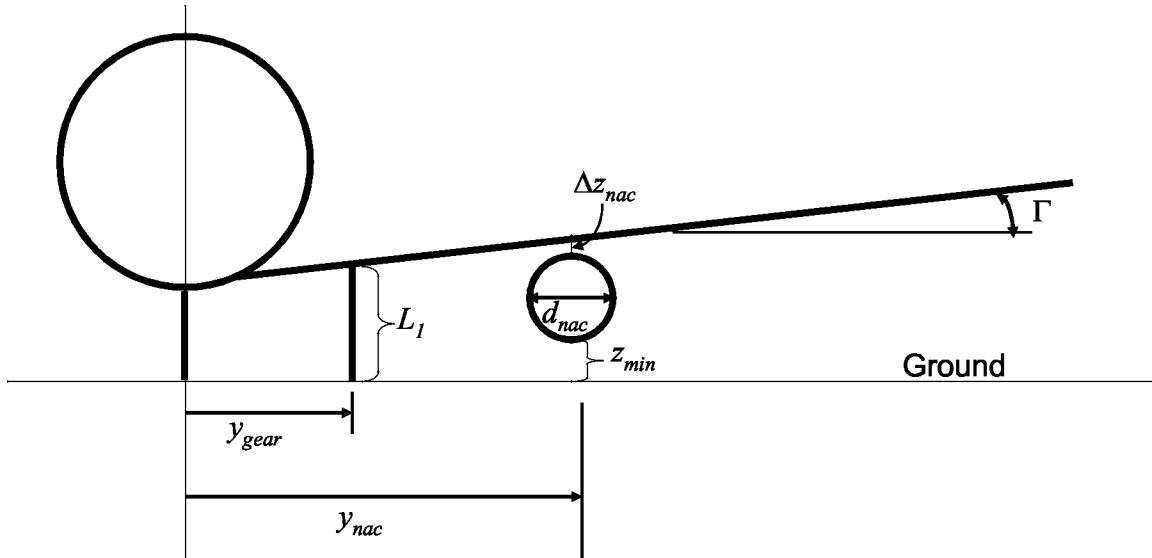


Figure 5. Nacelle ground clearance geometry.

Nacelle diameter was based on the engine model characteristics, scaled in proportion to the square root of engine thrust during thrust sizing. Note that although the current 737 designs have a “squashed” nacelle shape, circular nacelles were assumed for this study. The unique shape of the 737 nacelles resulted from constraints imposed by a derivative design situation and it is unlikely that such a measure would be taken in the case of a completely new aircraft design. The gear location and wing dihedral inputs were based on the 737-800 geometry. Nacelle-wing offset was assumed to be 5% of nacelle diameter based on drawings of nacelle-wing interfaces contained in reference 4. The vertical offset for the CFM56-7B installation on a 737-800 is much smaller than this typical value because of the limited space available to accommodate the nacelle. Although the capability to vary engine spanwise location was included in the method, changes in engine placement were not investigated as part of this study and the relative spanwise locations of the study engines (i.e., fraction of semi-span) were assumed to be the same as the CFM56-7B on the 737-800.

The main landing gear length necessary to avoid engine damage in the case of nose gear collapse is more dependent on the overall geometric layout of the airplane than the length necessary to maintain basic nacelle clearance. Additional relevant geometric parameters include: horizontal distance between nacelle maximum diameter point (ground contact point) and main landing gear ground contact point, horizontal distance between the lowest forward fuselage point (i.e., point that would contact the ground in case of nose gear collapse) and main landing gear contact point, vertical distance between main landing gear attachment point and lowest forward fuselage point. These parameters are illustrated in Figure 6. The required main landing gear length is given by:

$$L_2 = \frac{1}{\left(1 - \frac{\Delta x_{nac}}{\Delta x_{fus}}\right)} \times \left\{ d_{nac} - \left( \frac{\Delta x_{nac}}{\Delta x_{fus}} \right) \Delta z_{fus} - ((y_{nac} - y_{gear}) \tan(\Gamma) - \Delta z_{nac}) \right\};$$

where, as shown in Figure 6,

- $L_2$  = required distance from ground to attach point (compressed)
- $\Delta x_{nac}$  = horizontal distance between nacelle maximum diameter and main landing gear contact, ft
- $\Delta x_{fus}$  = horizontal distance between fuselage contact and main landing gear contact, ft
- $\Delta z_{fus}$  = vertical distance between main landing gear attach and fuselage contact, ft

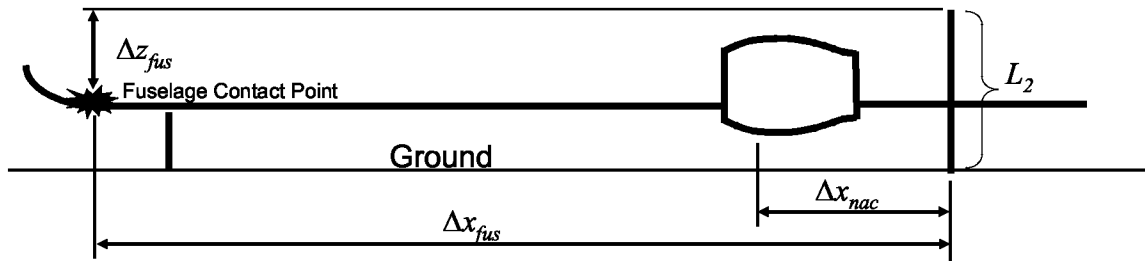


Figure 6. Nose gear collapse geometry.

Values for  $\Delta x_{fus}$  and  $\Delta z_{fus}$  were estimated based on the 737-800 geometry and held fixed for all the ASAT cases. For  $\Delta x_{nac}$  an approximate value was obtained using the nacelle length determined by the propulsion modeling, placing the engine nacelle at a “typical” chordwise location on the wing (with variation based on spanwise engine location) and maintaining the chordwise location of the main gear the same as on the 737-800.

The final main landing gear length estimate was based on the larger of  $L_1$  and  $L_2$ . Since these lengths are from the main landing gear ground contact point to the attachment point while in a compressed state, to arrive at the extended strut length for input to FLOPS the tire radius was subtracted and the length was increased 20% (based on 737-800 landing gear compression). Available under-wing volume and articulation requirements for gear retraction were not addressed. Nose gear length was assumed to be 70% of main gear length, consistent with the FLOPS internal nose gear length estimation assumptions.

### 3.2.3.2 Drag Increment for One-Engine-Out Conditions

When one engine of the aircraft fails, there is an increase in drag due to a combination of the windmilling drag of the inoperative engine and an increase in airframe drag associated with balancing the yawing moment induced by an asymmetric thrust condition. The larger physical size of UHB engines leads to larger engine-out drag which can impact the performance and stability and control of the vehicle.

Windmilling drag estimates for each of the study engines were made using a method from reference

22. Reference 22 provides approximations for both additional external drag and internal drag of a windmilling engine. External drag is approximated by:

$$(C_D S)_{ext} = 0.1 * \left(\frac{\pi}{4}\right) d_i^2;$$

where,

$$d_i = \text{engine inlet diameter}$$

An estimate for internal drag is obtained from:

$$(C_D S)_{in} = \frac{2}{1 + 0.16M^2} A_N \frac{V_N}{V} \left(1 - \frac{V_N}{V}\right);$$

where,

$$M = \text{free stream Mach number}$$

$$A_N = \text{nozzle area}$$

$$V_N/V = \text{nozzle velocity ratio (suggested values based on engine type are provided in ref. 22.)}$$

The internal drag expression is evaluated separately for the core and bypass airflows and the results added together along with  $(C_D S)_{ext}$  to arrive at the total windmilling drag estimate.

When one engine is inoperative, there is a yawing moment induced by the thrust of the operative engine and windmilling drag of the inoperative engine. This yawing moment must be counteracted by the airframe to maintain steady, controlled flight. The yawing moment coefficient induced,  $C_{Noeo}$ , is given by:

$$C_{Noeo} = \frac{(T + D_{wm}) y_{nac}}{\frac{1}{2} \rho V^2 S_{wing} b}$$

where,

$$S_{wing} = \text{wing reference area, ft}^2$$

$$b = \text{wingspan, ft}$$

$$T = \text{thrust of operating engine, lb}$$

$$D_{wm} = \text{windmilling drag of inoperative engine, lb}$$

$$\rho = \text{air density, slugs/ft}^3$$

$$V = \text{flight velocity, ft/s}$$

The drag associated with counteracting this moment depends on the stability and control characteristics of the vehicle. A detailed stability and control analysis was not performed for the ASAT configurations. However, available low speed aerodynamic data for the 737-800 included  $\Delta C_D$  versus  $C_N$ . This was used to approximate control drag increments for the ASAT analysis.

The estimation of total engine-out drag was automated in a spreadsheet linked to the FLOPS analysis so that engine-out drag was updated during aircraft sizing. The engine-out analysis was conducted at sea level and, as in reference 4, at a Mach number of 0.2 since FLOPS uses engine-out drag in takeoff analysis, impacting takeoff performance and engine thrust needed to meet minimum climb gradients for the one-engine-out conditions. Estimated engine-out drag was also used in vertical tail sizing as will be

described below. Another potential impact of increased engine-out drag is reduction in ETOPS (Extended Twin-Engine Operations) capability (i.e., how far a twin-engine aircraft's route can be from an alternate, emergency airport based on performance in the one-engine-out flight condition). ETOPS performance was not addressed in this study.

### 3.2.3.3 Vertical Tail Sizing

As defined in the Federal Aviation Regulations (FAR 25.149), a minimum control speed,  $V_{MC}$ , must be established at which, "when the critical engine is suddenly made inoperative, it is possible to maintain control of the airplane with that engine still inoperative and maintain straight flight with an angle of bank of not more than 5 degrees." (ref. 25) ( $V_{MC}$  is a takeoff parameter, minimum control speeds are also defined in FAR 25.149 for ground roll and landing approach.) FAR 25.149 specifies that this minimum control speed cannot exceed the reference stall speed ( $V_{SR}$ ) by more than 13%.  $V_{MC}$  is a function of the stability and control characteristics of the aircraft, maximum thrust of the operating engine, and windmilling drag of the inoperative engine. For a conventional airframe, the yawing moment needed to counteract the asymmetric thrust of a one-engine-out condition is provided primarily by the vertical tail. Because large diameter engines have larger windmilling drag, it is possible that the vertical tail size of the 737-800 is insufficient to achieve a suitable  $V_{MC}$  for the study configurations. A simple vertical tail sizing routine was developed that considers two constraints, a minimum tail volume coefficient and a maximum "vertical tail loading" during one-engine-out conditions. This calculation was automated in a spreadsheet and linked to the FLOPS analysis to capture variation in required tail size during aircraft sizing.

Since no stability and control analyses were performed for the ASAT configurations, the vertical and horizontal tail volume coefficients of the 737-800 were assumed to be the minimum values for which acceptable stability and control characteristics could be achieved. This assumption provided a minimum vertical tail size:

$$S_{VT\min} = V_{V\min} S_{wing} \left( \frac{b}{l_V} \right);$$

where,

- $V_{V\min}$  = minimum acceptable vertical tail volume coefficient
- $S_{wing}$  = wing reference area, ft<sup>2</sup>
- $b$  = wingspan, ft
- $l_V$  = vertical tail moment arm (distance between wing and tail aerodynamic centers), ft

Wing reference area and span vary as aircraft sizing is performed by FLOPS. The tail moment arm was assumed to be essentially constant and was based on the 737-800 geometry.

Determining whether or not one-engine-out trimmed flight can be achieved within the FAR mandated 5° bank angle limit requires knowledge of stability parameters such as  $C_{n\beta}$ ,  $C_{y\beta}$ , and  $C_{l\beta}$ . A simplified approach was implemented for this study considering only the forces and moments generated by the engines and the vertical tail. Using engine thrust, windmilling drag, spanwise engine location, and vertical tail moment arm, the side force on the tail,  $Y_{oeo}$ , required to balance the engine-out yawing moment can be estimated:

$$Y_{oeo} = \frac{(T + D_{wm})y_{nac}}{l_v}$$

Given a maximum “vertical tail loading” (lb/ft<sup>2</sup>), the tail area required to provide the necessary side force,  $Y_{oeo}$ , can be calculated.

$$S_{VT_{oeo}} = \frac{Y_{oeo}}{VL_{max}};$$

where,

$$S_{VT_{oeo}} = \text{required tail size based on one-engine-out condition, ft}^2$$

$$VL_{max} = \text{maximum allowable vertical tail loading, lb/ft}^2$$

To arrive at a reasonable estimate for  $VL_{max}$ , the loading of a 737-600 vertical tail during one-engine-out conditions was examined. The 737-600 has a much shorter fuselage than the 737-800 and, even though the engine thrust is lower, the side force required to balance an engine-out condition is greater than for the 737-800. Based on the geometry of the 737-600 and an engine windmilling drag estimate using the methods described above, the vertical tail loading for the 737-600 was estimated to be 26.1 lb/ft<sup>2</sup>. This value was then used as a limit in the ASAT analysis. The greater of  $S_{VT_{min}}$  and  $S_{VT_{oeo}}$  was used for the vertical tail area input to FLOPS.

#### 3.2.3.4 Nacelle Drag

FLOPS internally estimates nacelle profile drag based on the nacelle diameter and length (provided by WATE output). The larger nacelle size of an UHB engine directly impacts the profile drag estimate. In addition to profile drag, the nacelle can also contribute wave drag, interference drag, and excrescence drag. The FLOPS aerodynamic analysis does not directly address these additional drag components, but includes a “miscellaneous drag” which is a percentage of the profile drag. For this study it was assumed that the miscellaneous drag percentage did not vary with nacelle diameter. That is, the increase in interference drag, excrescence drag, and wave drag due to a larger nacelle was assumed to be proportional to the increase in profile drag. One might expect that as the size of the nacelle relative to the wing increases, nacelle-wing interference issues and their contribution to total nacelle drag would also increase. There are indications, however, that pylon shape and orientation can mitigate these issues. For example, results in reference 26 indicate a lower installation drag penalty for a “superfan” nacelle (BPR~18) than for a conventional BPR~6 engine nacelle. It is even possible that positive wing-nacelle interference effects could be realized through optimum wing and nacelle shaping. This potential for favorable interference was not included as part of the current study.

### 3.3 Noise Analysis

The primary tools used for the noise analysis included: NPSS for the engine cycle analysis; WATE for the engine aeromechanical and flowpath analysis; FLOPS for the aircraft trajectory simulation; and ANOPP (Aircraft Noise Prediction Program) Level 26 (refs. 27, 28) for the source noise prediction and propagation. The NPSS and WATE codes were used to generate input data necessary for the ANOPP source noise modeling. Adjustments for noise reduction technologies were made to the source noise spectra prior to propagation. ANOPP noise propagation modeling included spherical spreading, atmospheric attenuation, ground effects, reflections, and lateral attenuation. The Effective Perceived Noise Level (EPNL) was calculated at the noise certification points defined in FAR Part 36 (ref. 29, see Figure 7). EPNL is an integration of the ground observer perceived noise time history which depends on

aircraft trajectory, noise spectra propagation, frequency integration, and tonal content and amplitude penalties.

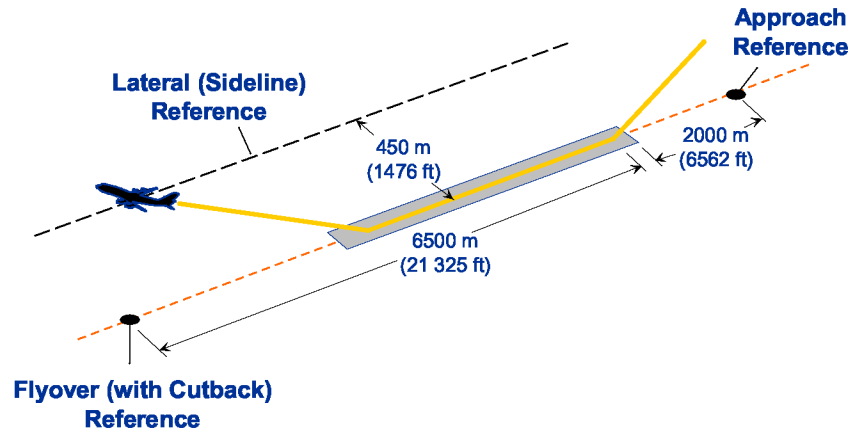


Figure 7. Noise certification points.

### 3.3.1 Noise Analysis Validation

The noise analysis tools were first used to model a 737-800/CFM56-7B and the analytical results were compared to noise certification data for that airplane. The CFM56-7B engine was analytically modeled in NPSS using data available from several public-domain sources; no company proprietary data were used. The thermodynamic, aeromechanical, and geometric predictions for the CFM56-7B were used as inputs to ANOPP's propulsion source noise prediction methods. Freefield, lossless, 1/3<sup>rd</sup> octave band sound pressure level predictions were made for the CFM56-7B fan, jet, and core sources using the methods reported in references 30, 31, and 32, respectively. The predicted hardwall fan noise spectra were analytically adjusted by ANOPP to account for the presence of conventional acoustic treatment according to the method in reference 33. Freefield, lossless, 1/3<sup>rd</sup> octave band spectra for flap, slat, gear, and trailing edge airframe noise sources were predicted using the method in reference 34.

Using an assumption of acoustic superposition, the freefield noise sources were analytically summed in the vicinity of the aircraft and propagated to certification observers on the ground in accordance with specifications for certification measurements. Noise propagation effects accounted for included spherical spreading, Doppler shift and convective amplification, atmospheric attenuation, ground reflections based on data for grass-covered ground, and extra ground attenuation. The propagated acoustic spectra were predicted at half-second intervals at each measurement location. From these spectra, ANOPP computed the PNL, PNL<sub>T</sub>, and EPNL certification noise metrics for the aircraft.

Good agreement between the certification data and analytical prediction was obtained for the lateral (sideline) and approach conditions. Noise at the flyover condition was over predicted by approximately 4 EPNdB. Through more detailed analysis and comparison of predicted source noise levels to proprietary data it was determined that the ANOPP fan noise predictions could be about 5 dB too high at the flyover, cutback power setting. There are many sources of uncertainty in the noise analysis process, however, including the engine cycle and aeromechanical modeling (NPSS and WATE), the trajectory and throttle setting assumptions, and many other potential discrepancies. Because the exact cause of the error cannot be readily determined and the level of error in the results was deemed acceptable for this comparative study, no attempt was made to calibrate the noise analysis tools and eliminate the discrepancy between

predicted and actual 737-800 noise levels.

The noise analysis approach, methods, and assumptions were examined by acoustics experts at NASA Glenn and NASA Langley in an acoustic tool benchmarking assessment (refs. 35, 36). Scrutiny of the ANOPP source noise methodologies did not reveal any fundamental issues with regard to the study analysis. Comparisons of ANOPP component source noise predictions to experimental component data indicated that the ANOPP methods are generally applicable to aircraft with ultra-high bypass ratio engines (refs. 37, 38, 39). One area of particular concern was the applicability of the fan noise module to modern fan designs. Benchmarking of this module against experimental acoustic test data indicated that the fan noise module is generally applicable to modern, wide-chord, highly-contoured fan blade designs (ref. 37).

Higher bypass ratio, lower fan pressure ratio engines have inherently higher thrust lapse (i.e., available thrust decreases more rapidly with increase in aircraft speed). The impact of higher thrust lapse is manifested in changes in climb rates, airspeeds, and throttle settings for takeoff and landing trajectories. Certification noise is impacted by these trajectory changes since propulsion noise is a strong function of throttle setting, airframe noise is a strong function of airspeed, and altitude and distance from the observer strongly affect noise from all sources. These engine dependent trajectory characteristics can be captured in the analysis by the modeling of detailed departure and approach trajectories in FLOPS, which in turn enables the influence of trajectory on the noise results to be properly captured. (Note, however, that except for engine-out drag, the low speed aerodynamic characteristics were held constant across all the study configurations.) To verify the accuracy of the FLOPS low speed model, trajectory results from the FLOPS model were compared to trajectories from SAE AIR-1845 INM (Integrated Noise Model) empirical procedures (ref. 40). In Figures 8 through 10, altitude, airspeed, and thrust histories from FLOPS using the INM specified departure procedures are compared to the INM trajectory results. The FLOPS output shows excellent agreement with the INM trajectories, especially through the distances of interest for noise calculations at the certification points. Note that the FLOPS model is based on the 737-800 with winglets, whereas the INM results are for a basic 737-800. One of the benefits of winglets is improved takeoff and climb performance (ref. 18) and this configuration difference may be responsible for some of the discrepancies in the trajectory results.

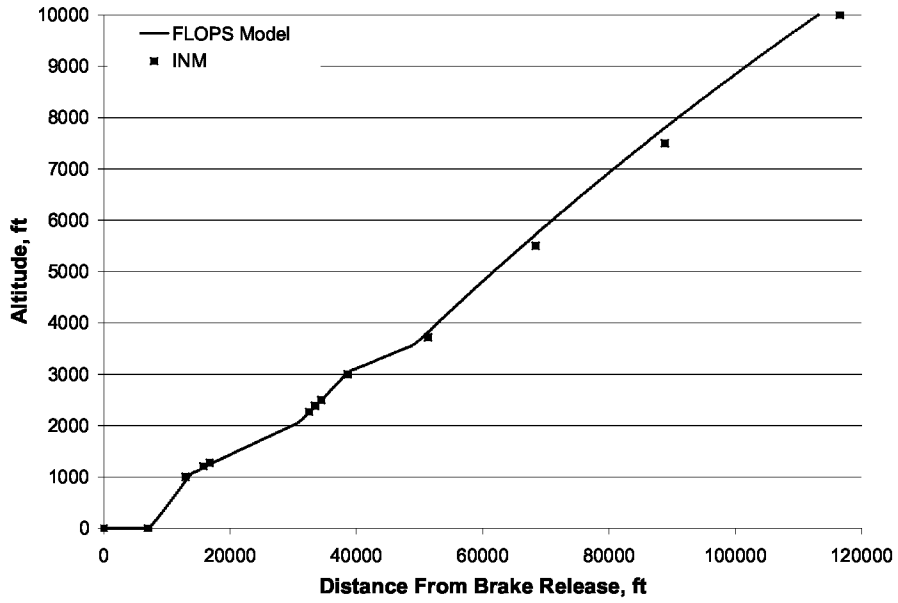


Figure 8. Comparison of FLOPS generated and INM generated departure altitudes.

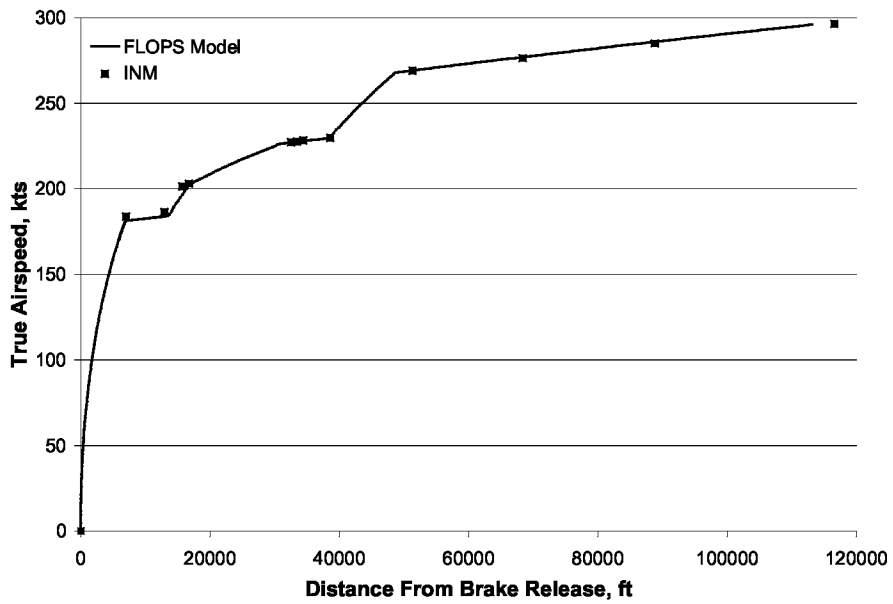


Figure 9. Comparison of FLOPS generated and INM generated departure airspeeds.

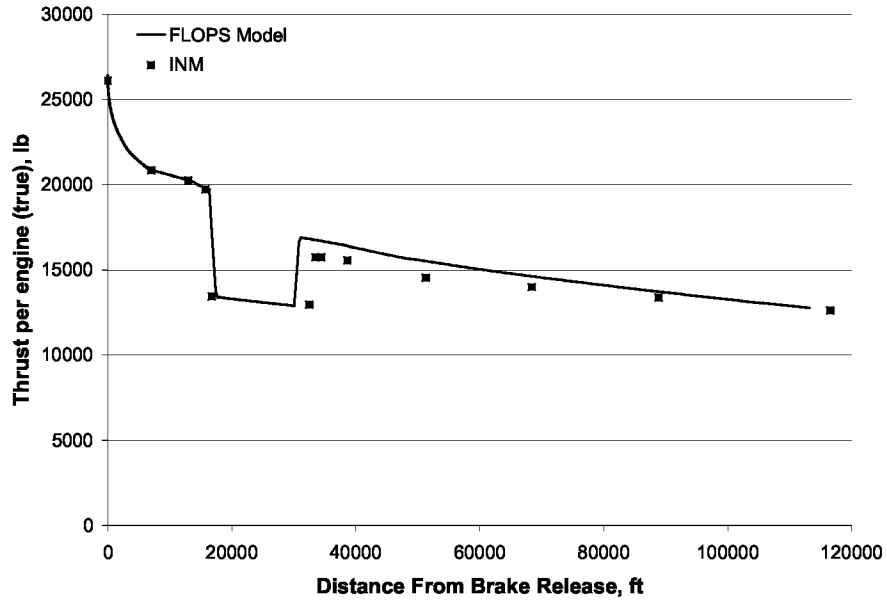


Figure 10. Comparison of FLOPS generated and INM generated departure thrust.

In Figures 11 through 13, altitude, airspeed, and thrust histories from FLOPS are compared to the INM trajectory results for approach. There are slightly larger discrepancies between FLOPS and INM in the case of approach. It does not appear, however, that the same basic approach procedures are reflected in both cases. The approach angle indicated by the INM results is slightly greater than the 3° standard approach angle specified in the FLOPS input. Approach speed is also higher for the INM trajectory. By default, the approach speed selected by FLOPS is the minimum allowable approach speed based on the aircraft stall characteristics. With these differences the FLOPS model also predicts a thrust which is ~8% lower than in the INM approach profile. The results in Figures 8 to 13 indicate that the FLOPS detailed profile calculations are capable of adequately modeling departure and approach procedures and therefore can be used to introduce vehicle specific trajectory variations in the noise analysis.

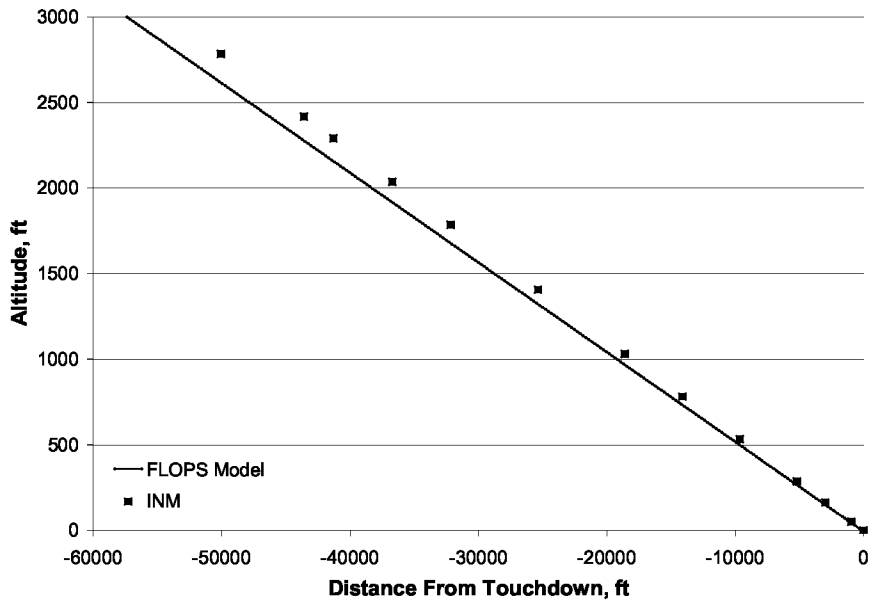


Figure 11. Comparison of FLOPS generated and INM generated approach altitudes.

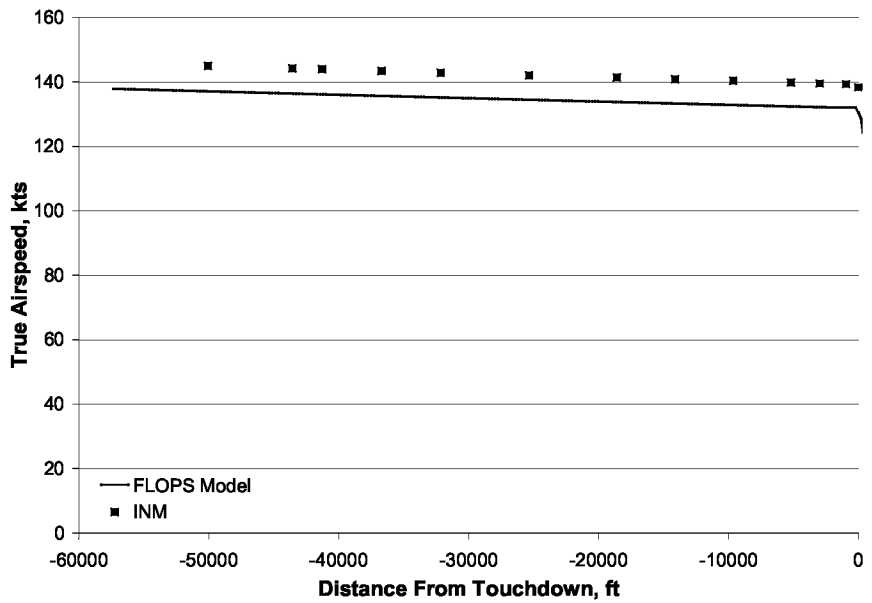


Figure 12. Comparison of FLOPS generated and INM generated approach airspeeds.

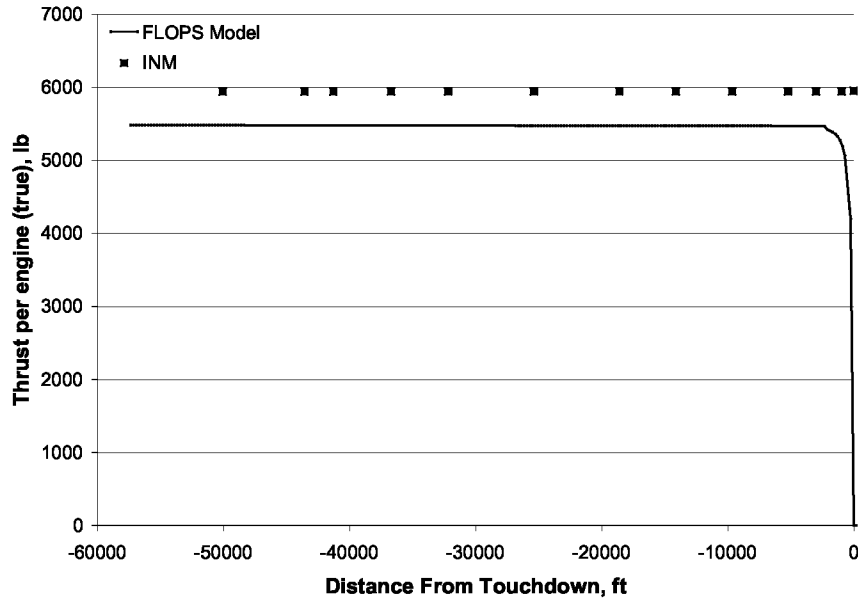


Figure 13. Comparison of FLOPS generated and INM generated approach thrusts.

### 3.3.2 Advanced Noise Reduction Technology Assumptions

A series of advanced noise reduction technologies were applied to the study configurations consistent with the 2015 EIS target for the vehicle.

Chevrans were applied to all core nozzles and to all fixed-area bypass nozzles. Chevrons were not applied to bypass nozzles of the low fan pressure ratio engines with variable area nozzles due to potential conflict with the variable area nozzle design. Jet noise benefits of the nozzle chevrons were determined analytically using the 2004 Stone jet noise prediction method in ANOPP (ref. 31). This method is based on 1997 acoustic measurements of chevron-equipped nozzles from NASA Glenn’s Aeroacoustic Propulsion Laboratory’s Nozzle Acoustic Test Rig freejet facility (ref. 41). The Stone chevron method predicts reductions in large- and intermediate-scale jet mixing noise and an increase in small-scale (high frequency) jet mixing noise near the nozzle exit plane.

Conventional inlet, interstage, and aft fan duct liners were applied to reduce fan inlet and discharge noise. The benefits of these liners were modeled by applying an acoustic suppression “map” of 1/3<sup>rd</sup> octave band sound pressure level decrements to the hardwall fan source spectra predicted by ANOPP. This approach differs from the 737-800/CFM56-7B validation study described above, where ANOPP’s built-in treatment suppression prediction module was used (ref. 33), since a more aggressive treatment configuration would likely be used in an advanced engine. The liner suppression map was based on measured acoustic data of 22-inch diameter fan test articles in NASA Glenn’s 9×15 Low Speed Wind Tunnel (ref. 42). The most effective treatment tested proved to be double degree of freedom liners applied to the inlet, interstage, and aft bypass duct areas. These liners were tuned to attack the discrete interaction tone’s second harmonic at maximum takeoff-rated power. An initial treatment suppression map was generated based on the measured differences between the treated and hardwall measurements. This simple map was scaled from the 22-inch model dimensions to full scale using standard FAR 36 frequencies. The data were then smoothed with a regression technique to fit a modified Weibull probability density function as shown in Figure 14. A Weibull-shaped curve was chosen since liner effectiveness is small at low frequencies and increases to a maximum near its tuned frequency. The logarithm of the ratio of inlet

diameter to wavelength is an appropriate choice for the independent parameter. Low-frequency liner self noise, caused by air flow and surface roughness, is small and is ignored in this regression. The complete treatment suppression map is shown in Figure 15. Maximum effectiveness is approximately 12 dB at an emission yaw angle of 99° from the inlet.

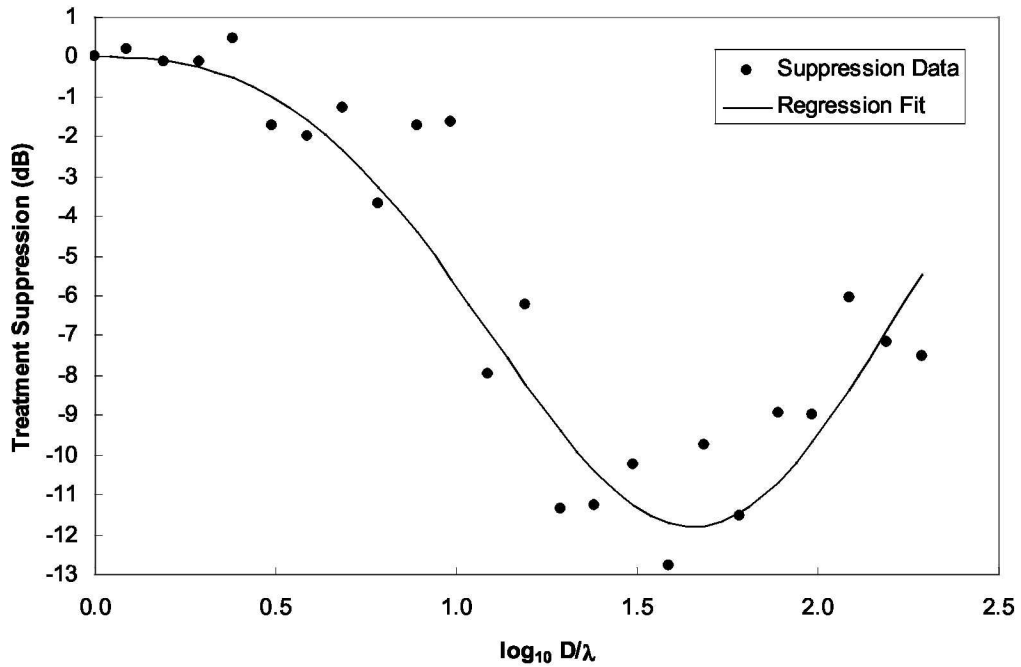


Figure 14. Regression fit of acoustic liner performance (emission yaw angle of 95° from inlet).

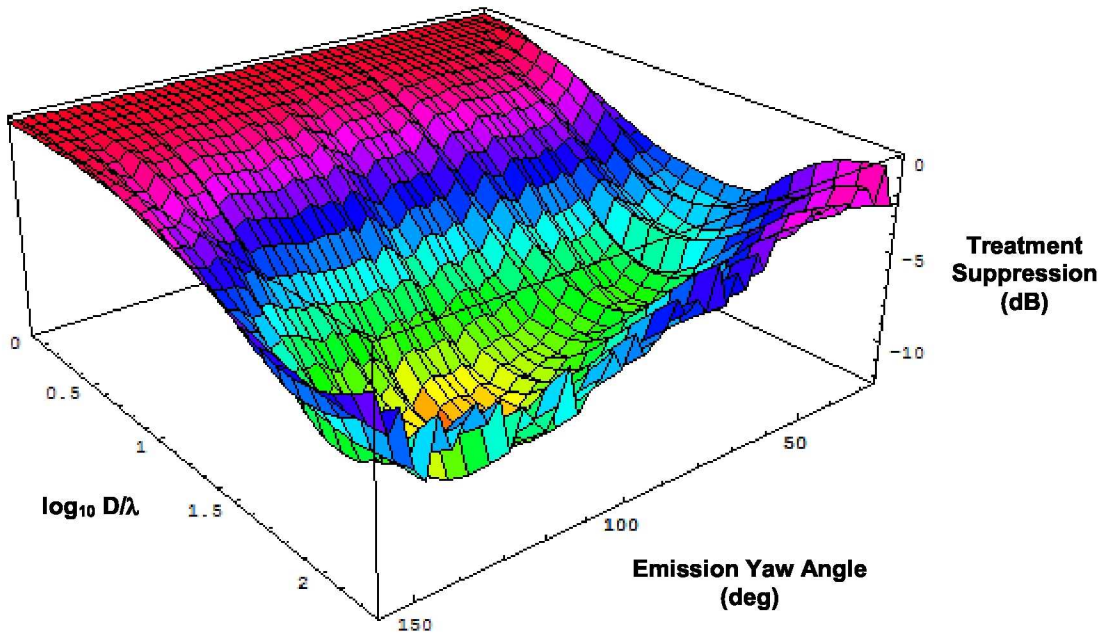


Figure 15. Overall acoustic liner suppression map.

In addition to conventional liners, two advanced technologies were applied for fan noise reduction; soft vane stators and over-the-rotor foam metal treatment (refs. 43, 44). Both of these technologies are applications of acoustic treatment in areas of the engine which currently do not have treatment: the fan vanes and above the fan rotor tips. The treatments in these locations attenuate both fan broadband and tone noise and are anticipated to work together without conflict to produce additive fan noise reduction benefits. Acoustic tests of both of these technologies were conducted at NASA Glenn in 2008. Based on these tests, a system-level decrement of -4 dB was applied to the freefield hardwall fan source noise predictions made by ANOPP. This system-level decrement was applied as a simple constant to the predicted fan sound pressure levels across all 1/3<sup>rd</sup> octave band frequencies, directions, and throttle settings.

Airframe noise reduction technologies included innovative slat cove designs, flap porous tips, and landing gear fairings. These technologies are considered mature enough to be commensurate with the 2015 EIS timeframe (ref. 45). The flap porous tips and slat cove filler technologies were modeled by subtracting 4 dB across all frequencies and directions from the freefield 1/3<sup>rd</sup> octave band sound pressure levels predicted by ANOPP's Fink method (ref. 34) for flap and slat noise. The landing gear fairing technology was modeled by subtracting 3 dB from the Fink gear method prediction for all directions, but only above 250 Hz. These benefit assumptions were based on consultation with acoustic researchers in NASA's Subsonic Fixed Wing project.

## **4.0 Spiral 1**

### **4.1 Spiral 1 Engine Design**

NPSS was utilized to develop a series of advanced, separate-flow turbofan engines under the study assumptions and ground rules discussed in Section 3.1. Because of the multiple performance requirements placed on the engine, engines were modeled using a "multi-point design" philosophy. This approach combines the ability to size turbomachinery components at the aerodynamic design point (ADP) while concurrently determining the necessary turbine cooling levels at sea-level where the maximum cycle temperatures are experienced. A range of cycles were produced to span the fan pressure ratio, high-spool/low-spool compression split, fan drive type, and fan nozzle type design space. All engines in Spiral 1 were nominally sized to produce 5000 lb of thrust at top-of-climb (ADP point) and 23,000 lb of thrust at sea-level static conditions. After completing the thermodynamic modeling, an engine weight and flowpath approximation was performed with WATE utilizing a consistent set of aeromechanical and material assumptions.

#### ***4.1.1 Low Work Engines***

General characteristics of the Spiral 1, low work engines are shown in Table 2. The following naming convention is used in Table 2 and throughout this report to identify the engine designs: *spiral-LPC work (Lo or Hi)-fan drive (g for geared or dd for direct)-fan pressure ratio*. "S1-Lo-g-1.3" therefore indicates a Spiral 1 engine with a low work LPC and geared fan having a fan pressure ratio of 1.3. Overall pressure ratio for the Spiral 1 engines is 32 at the top-of-climb, ADP conditions of 35,000 ft and M=0.80 (overall pressure ratio of 32 is based on a multiplication of component pressure ratios and does not account for duct pressure losses). This overall pressure ratio is achieved with a HPC pressure ratio of 13.5 and a LPC pressure ratio which varies depending on fan pressure ratio. Engine models include geared fan configurations with fan pressure ratios (ADP) of 1.3 to 1.6 (bypass ratios of 24.7 to 10.6) and direct drive configurations with fan pressure ratios (ADP) of 1.4 to 1.7 (bypass ratios of 17.3 to 8.8). TSFC at ADP

decreases from 0.554 lb/(lb-h) with a fan pressure ratio of 1.7 to 0.495 lb/(lb-h) with a fan pressure ratio of 1.3 (-11%), reflecting the improvement in propulsive efficiency associated with increasing bypass ratio from 8.8 to 24.7. However, this improvement comes with a significant increase in engine weight. The weight of the geared, FPR=1.3 engine is 70% more than the direct drive, FPR=1.7 design. For a given fan pressure ratio, the geared and direct drive engines have similar size and fuel consumption characteristics. The only cycle performance difference associated with the fan drive approach is the inclusion of a small efficiency loss in the low-spool to account for gearbox losses, other losses and component efficiencies are assumed to be the same for both fan drive types. This results in a slightly larger LPT work requirement for the geared engines, reducing the bypass ratios slightly. The primary difference between geared and direct drive engines is the engine weight.

The geared, FPR=1.3 and direct drive, FPR=1.4 engines have been labeled “impractical” designs. An extremely low SLS fan pressure ratio of 1.2 and a very large engine diameter are issues for the geared, FPR=1.3 engine. The large diameter leads to an unrealistically long landing gear given the propulsion-airframe integration approach assumed for the study. The direct drive, FPR=1.4, BPR=17 design is an extreme case for the direct drive engine architecture. Under the design ground rules used for this study, the slow low-spool speed necessitates a large number of LPT stages, leading to an extremely heavy and long engine. Both of these engines were carried through the remainder of the analyses, however, in order to investigate performance trends as fan pressure ratio is decreased to the extreme. There are also potential practicality issues for the high fan pressure ratio geared engines. Although the gear ratio for the FPR=1.3 engine is 3.0, this ratio decreases to only 1.2 for the FPR=1.6 geared engine. Gear ratios close to 1.0 are difficult to justify from a mechanical design standpoint since any weight or performance benefits that might result would likely be overwhelmed by the increased design and operational costs associated with the gearbox.

#### ***4.1.2 High Work Engines***

General characteristics of the Spiral 1, high work engines are shown in Table 3. The high work engines have the same ADP conditions as the low work engines. The difference is in how the overall pressure ratio of 32 is achieved. For the high work engines, the HPC pressure ratio was assumed to be 10. Consequently, a larger amount of the compression work is done by the LPC. LPC pressure ratios were selected to produce an overall pressure ratio of 32 as fan pressure ratio varied. High work engine models include geared fan configurations with fan pressure ratios (ADP) of 1.3 to 1.6 (bypass ratios of 23.4 to 9.9) and direct drive configurations with fan pressure ratios (ADP) of 1.4 to 1.7 (bypass ratios of 16.4 to 8.3). As with the low work engines, there is an 11% decrease in TSFC from the highest of 0.558 lb/(lb-h) for a fan pressure ratio of 1.7 to the lowest of 0.498 lb/(lb-h) for a fan pressure ratio of 1.3. The weight variation across the fan pressure ratio range is not as large as for the low work designs and this architecture appears to benefit more from fan gearing. As was the case for the low work engines, the geared and direct drive high work engines have a small performance difference resulting from gearbox losses. The primary difference again between direct drive and geared fan systems for a given fan pressure ratio is in the engine weight. Gear ratios for the high work engines vary from 3.3 at the lowest fan pressure ratio to 1.5 at the highest fan pressure ratio. The slightly higher gear ratios for the high work engines compared to the low work engines are reflective of the larger mismatch between the fan and low spool optimum speeds when the low spool is designed to perform more compression work. The lowest fan pressure ratio geared and direct drive cases again lead to impractical designs under the study assumptions.

Table 2. General Characteristics of Spiral 1, Low Work Engine Models

	S1-Lo-g-1.3*		S1-Lo-g-1.4		S1-Lo-dd-1.4*		S1-Lo-g-1.5		S1-Lo-dd-1.5		S1-Lo-g-1.6		S1-Lo-dd-1.6		S1-Lo-dd-1.7	
Fan Drive/Gear Ratio	Geared/3.0		Geared/2.0		Direct Drive		Geared/1.5		Direct Drive		Geared/1.2		Direct Drive		Direct Drive	
Fan Diameter, in	92		80		80		73		73		68		68		64	
Fan Nozzle Geometry	Variable		Variable		Variable		Fixed		Fixed		Fixed		Fixed		Fixed	
Engine+Nacelle Weight, lb	9695		7921		10127		6967		7453		6622		6211		5682	
Nacelle Max Diameter, ft	9.4		8.2		8.2		7.5		7.5		6.9		6.9		6.5	
Operating Conditions	SLS	TOC	SLS	TOC	SLS	TOC	SLS	TOC	SLS	TOC	SLS	TOC	SLS	TOC	SLS	TOC
Fan Pressure Ratio	1.2	1.3	1.3	1.4	1.3	1.4	1.39	1.5	1.39	1.5	1.49	1.6	1.49	1.6	1.6	1.7
Bypass Ratio	24.1	24.7	16.8	17.1	16.9	17.3	13.3	13.1	13.5	13.3	10.9	10.6	11.0	10.7	9.2	8.8
Overall Pressure Ratio	22.9	32	24.8	32	24.8	32	25.7	32	25.7	32	26.7	32	26.7	32	27.6	32
Net Thrust, lb	23002	5000	22984	5000	23002	5000	22981	5000	23001	5000	22981	5000	23002	5000	23001	5000
TSFC, lb/(lb-h)	0.218	0.495	0.251	0.509	0.249	0.504	0.273	0.526	0.271	0.521	0.296	0.542	0.293	0.537	0.316	0.554
NO <sub>x</sub> Emission Index (g/kg)	15.9	7.2	17.6	6.1	17.6	6.1	18.3	5.7	18.3	5.7	19.1	5.4	19.1	5.4	19.9	5.1

\*Design ground rules lead to impractical design for these cases.

Table 3. General Characteristics of Spiral 1, High Work Engine Models

	S1-Hi-g-1.3*		S1-Hi-g-1.4		S1-Hi-dd-1.4*		S1-Hi-g-1.5		S1-Hi-dd-1.5		S1-Hi-g-1.6		S1-Hi-dd-1.6		S1-Hi-dd-1.7	
Fan Drive/Gear Ratio	Geared/3.3		Geared/2.3		Direct Drive		Geared/1.8		Direct Drive		Geared/1.5		Direct Drive		Direct Drive	
Fan Diameter, in	92		80		80		73		73		68		68		64	
Fan Nozzle Geometry	Variable		Variable		Variable		Fixed		Fixed		Fixed		Fixed		Fixed	
Engine+Nacelle Weight, lb	8813		7336		10545		6472		8019		6047		6784		5949	
Nacelle Max Diameter, ft	9.4		8.2		8.2		7.5		7.5		6.9		6.9		6.5	
Operating Conditions	SLS	TOC	SLS	TOC	SLS	TOC	SLS	TOC	SLS	TOC	SLS	TOC	SLS	TOC	SLS	TOC
Fan Pressure Ratio	1.2	1.3	1.3	1.4	1.3	1.4	1.4	1.5	1.4	1.5	1.5	1.6	1.49	1.6	1.6	1.7
Bypass Ratio	23.1	23.4	16.0	16.2	16.2	16.4	12.7	12.4	12.8	12.5	10.3	9.9	10.4	10.0	8.6	8.3
Overall Pressure Ratio	22.7	32	24.6	32	24.6	32	25.6	32	25.6	32	26.6	32	26.6	32	27.5	32
Net Thrust, lb	23005	5000	23003	5000	23023	5000	22998	5000	23017	5000	22999	5000	23016	5000	23023	5000
TSFC, lb/(lb-h)	0.220	0.498	0.254	0.512	0.251	0.507	0.277	0.529	0.274	0.524	0.300	0.546	0.297	0.541	0.321	0.558
NO <sub>x</sub> Emission Index (g/kg)	15.0	6.6	16.5	5.6	16.5	5.6	17.2	5.2	17.2	5.2	18.0	4.9	18.0	4.9	18.8	4.6

\*Design ground rules lead to impractical design for this case

### 4.1.3 Engine Comparison

Figures 16 through 19 present the engine data in a graphical form to enable easier comparison among the multiple Spiral 1 engines. The dashed-line portions of the curves extending out to the lowest fan pressure ratio points indicate these designs are impractical given the ground rules used for this study.

Figure 16 indicates a smooth and consistent variation of bypass ratio with fan pressure ratio. With the modeling approach used for this study, the choice of fan drive system has minimal impact on the relationship between fan pressure ratio and bypass ratio. For a given fan pressure ratio, the low work engines have a slightly higher bypass ratio. This is a result of the high-spool/low-spool work split assumption. Typically, the LPC is a less efficient component than the HPC. As such, at a given fan pressure ratio the overall power required from the turbines is greater for a high work engine since more of the compression is performed by the less efficient LPC. The core flow required is therefore larger, reducing the bypass ratio. The impact of design fan pressure ratio on TOC specific fuel consumption is approximately linear as shown in Figure 17. For a given fan pressure ratio and fan drive type, the low work engines have somewhat lower TSFC than the corresponding high work engines because of their higher bypass ratio. The difference in TSFC is rather small, however, at less than 1%. The effect of fan drive configuration on TSFC is also less than 1%, with the geared drive engines having slightly higher TSFC than their direct drive counterparts due to gearbox losses. The nacelle diameter variation with design fan pressure ratio (Figure 18) is insensitive to the choice of fan drive approach and compressor work split. This is expected since regardless of how the fan is mechanically driven or how the compression work is split between the low spool and high spool, achieving the same thrust with the same fan pressure ratio should require the same amount of mass flow and thus the same size fan/nacelle. This consistency in engine size is also reflected in the fan diameters (see Table 2 and Table 3). Nacelle diameters for the Spiral 1 engines vary from 6.5 to 9.4 ft. By comparison, the nacelle diameter for the NASA CFM56-7B type engine model is 7.0 ft. (The actual CFM56-7B engine nacelle is not cylindrical and the nacelle height, critical for airframe integration, is less than 7 ft).

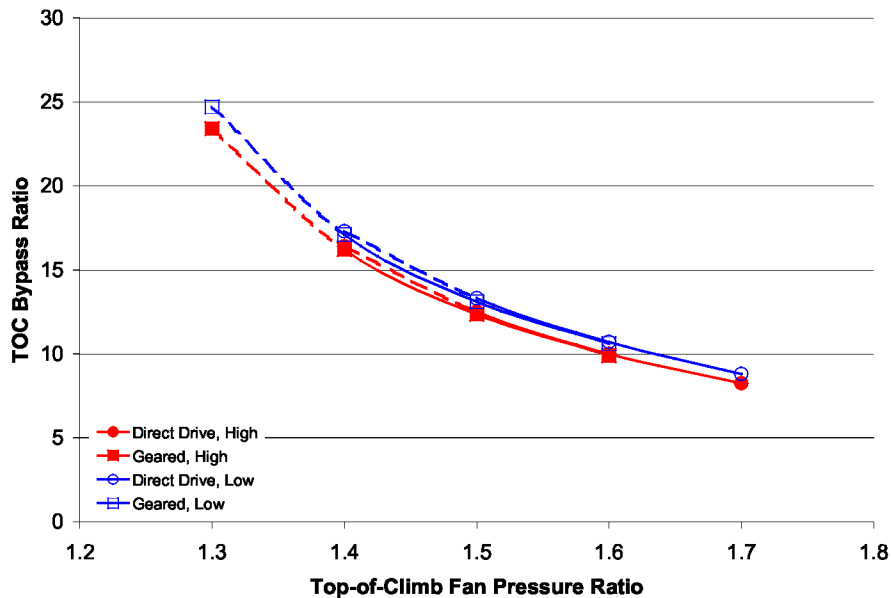


Figure 16. Variation of bypass ratio with fan pressure ratio, top-of-climb conditions, Spiral 1.

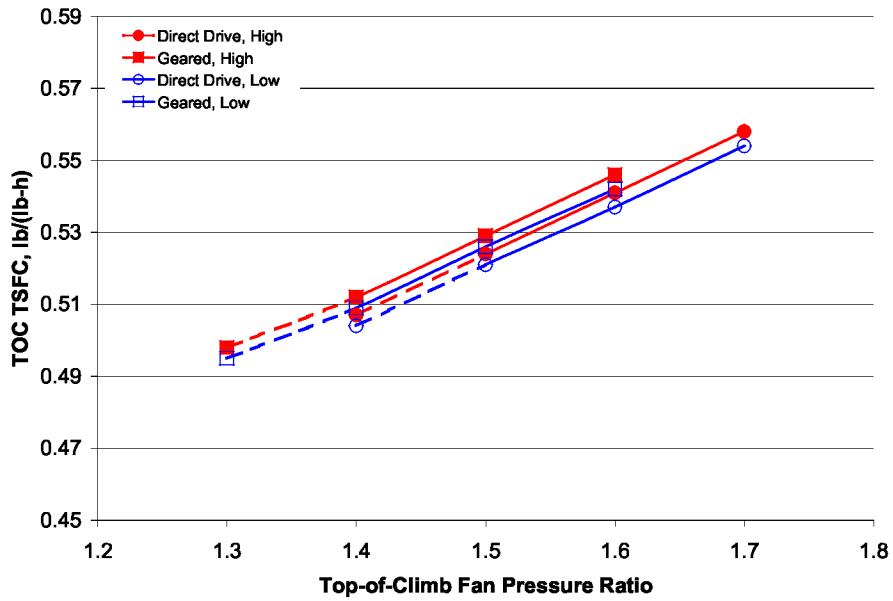


Figure 17. Relationship between fan pressure ratio and TSFC, top-of-climb conditions, Spiral 1.

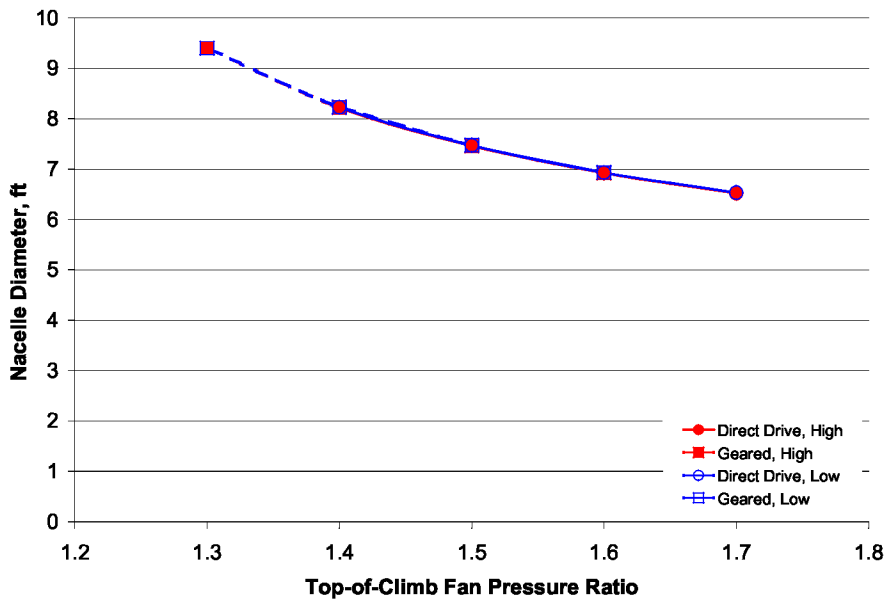


Figure 18. Variation of nacelle maximum diameter with fan pressure ratio, Spiral 1.

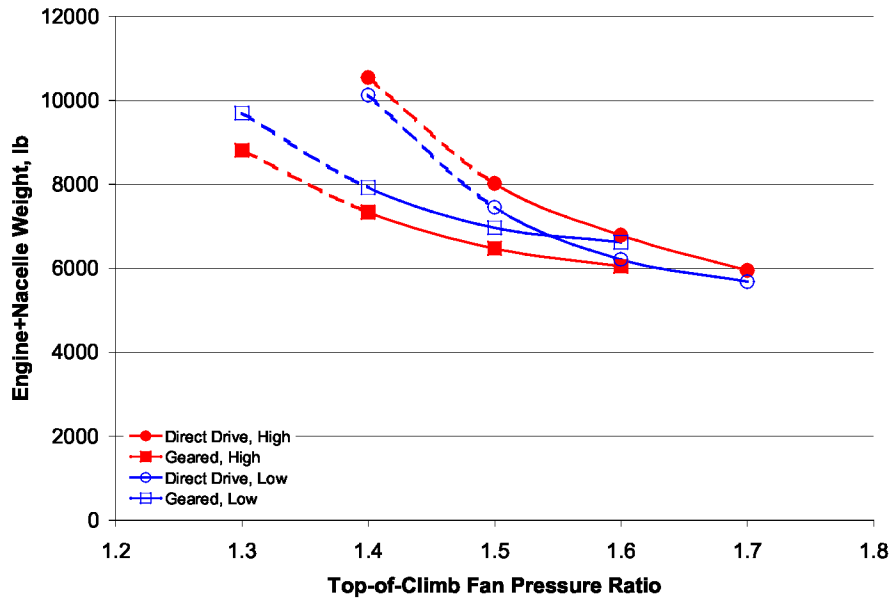


Figure 19. Variation of engine+nacelle weight with fan pressure ratio, Spiral 1.

Engine architecture has the largest impact on engine weight as shown in Figure 19. For a direct drive configuration, the low work designs have lower weight than the corresponding high work designs. The magnitude of this benefit is fairly constant across the fan pressure ratio range. This lower weight is due primarily to the high work systems having a larger and heavier LPC and a larger core size than the equivalent low work engine. Conversely, the high work, geared engines are lighter than their low work counterparts. The low work engines are not able to take full advantage of the fan gearing benefits because of the different low-spool/high-spool work split. For all engine types there is a significant weight increase associated with lower fan pressure ratios. The magnitude of the weight increase depends on the engine type, however. As the fan pressure ratio and tip speed of the direct drive system decrease, the LPT length and weight begin to increase rapidly. The growth in LPT size for the direct drive engines could be mitigated to some extent by changing the LPT design approach; for example, increasing the stage loading and reducing the number of stages. However, maximum stage loading was considered a technology limit and increasing loading would require deviating from the design ground rules and assumptions established for the study engines. Using a geared fan drive system enables the low pressure spool to operate at a more optimal speed, resulting in a reasonable number of turbine stages. The use of a geared fan drive system significantly decreases the variation in engine weight with fan pressure ratio, but the engine weight still grows as fan pressure ratio is decreased because of the larger fan and nacelle required. In the case of the high work engines, there is a weight benefit from using a geared fan approach up to at least a fan pressure ratio of 1.6 (based on the shape of the curves, it appears that direct drive may be a lighter weight approach at 1.7). For the low work engines, there is less weight benefit associated with a geared fan than for the high work designs. This is because there is less demand on the low pressure compressor and turbine and less benefit to be gained, therefore, from increasing the speed of the low pressure spool. As a result, the cross-over point at which gearing is no longer beneficial is at a lower fan pressure ratio (~1.55). At higher fan pressure ratios, the benefits of a geared system, such as reduced LPT stage count, are not sufficient to offset the penalties (e.g., weight of the gear system). For fan pressure ratios up to 1.6, the geared, high work engines provide the overall lowest weight designs; above this fan pressure ratio the low work, direct drive engine is lightest.

## 4.2 Spiral 1 Aircraft Sizing

FLOPS, with additional external analyses for landing gear size, vertical tail size, and engine-out drag, was used to size/optimize the gross weight, wing area, and thrust needed to perform the design mission for each of the engine design cases. Other design parameters such as wing aspect ratio and wing taper ratio were held fixed at the 737-800 values. Thrust sizing was performed using the baseline engine models described in Section 4.1 and FLOPS scaling laws. Constraints used in wing and engine sizing included: wing fuel capacity, approach speed, missed approach climb, second segment climb, takeoff field length, and initial cruise altitude capability (expressed as minimum potential rate-of-climb of 300 ft/min at  $M=0.8$ , 35,000ft). Other performance aspects of the configurations (e.g., landing field length) were also checked for reasonableness following completion of the sizing/optimization.

### 4.2.1 Low Work Cases

Results of the aircraft sizing and analysis are summarized in Table 4 for the Spiral 1, low work engines. Also shown in Table 4 for reference are results for a 1998 EIS technology level vehicle (equivalent technology to 737-800/CFM56-7B), sized to match the study design mission of 3250 nm with a cruise speed of  $M=0.8$ . The numbers in bold in Table 4 indicate the “best” value for that particular parameter (e.g., lowest ramp weight, highest cruise range factor, etc.). The low work engine results indicate block fuel consumption is minimized with a direct drive fan and a fan pressure ratio of 1.6 (TOC). The bypass ratio for this engine is 11 at SLS conditions. Note that the cruise range factor, which is an approximate measure of combined aerodynamic and propulsive efficiency, increases as the fan pressure ratio is reduced. However, this higher efficiency is insufficient to offset the increase in weight that occurs for the lower fan pressure ratio engines. This clearly illustrates the well-known system level trade-offs that occur for higher bypass ratio engines, the benefit of lower engine TSFC versus the penalty of higher drag and higher engine weight. The geared fan system is able to mitigate to some extent the penalties associated with decreasing fan pressure ratio and increasing bypass ratio. This benefit can be seen by comparing the FPR=1.4 results for the two fan drive approaches. The aircraft with the geared fan engine has a lower empty weight, lower ramp weight, lower block fuel consumption, lower total  $\text{NO}_x$  (“block  $\text{NO}_x$ ” in the table) and lower landing-takeoff cycle (LTO)  $\text{NO}_x$  emissions. But, even in the case of the lighter weight geared designs, minimum block fuel occurs at a fan pressure ratio of 1.5. Although the direct drive, FPR=1.6 engine has the overall lowest block fuel consumption, the fuel consumption for the FPR=1.5, geared fan design is <1% higher. Lowest total  $\text{NO}_x$  emissions are obtained for a higher fan pressure ratio case, the direct drive, FPR=1.7 engine. LTO  $\text{NO}_x$  emissions are lowest for the geared, FPR=1.3 engine; but, the variation in LTO  $\text{NO}_x$  is relatively small among all the cases. Although the minimum fuel consumption case is the direct drive, FPR=1.6 case, the minimum gross weight occurs with FPR=1.7. In other words, the decrease in engine weight for that configuration is sufficient to offset the increase in fuel weight to arrive at a lower total gross weight. Clearly, identifying a “best” engine design depends on the metric of interest. Ultimately the primary metric is life cycle cost, and historically gross weight has been used as a surrogate for life cycle cost in aircraft design and optimization. However, recent increases in fuel cost have made fuel consumption a more important factor in life cycle cost. It may no longer be valid to assume the lowest gross weight configuration has the lowest life cycle cost.

In all the sizing cases, the sized configuration has lower wing loading than is typical for a 737-800 like design. For the chosen design mission and constraints, takeoff field length is the primary sizing constraint. The required takeoff distance can be met by a range of different engine and wing sizes. The penalty of increasing wing size is diminished somewhat for the ASAT configurations relative to current designs due to the use of composite materials. For the ASAT designs, the preferred (lower gross weight) approach tends to be a larger wing (low wing loading) rather than a larger engine (high thrust-to-weight).

Even so, for the low fan pressure ratio cases the SLS thrust of the sized configurations is much larger than the engine design value of 23,000 lb. The low fan pressure ratio engines have higher thrust lapse during takeoff and require additional SLS thrust to achieve the same takeoff performance as the high fan pressure ratio cases. This reduction in engine takeoff performance, coupled with higher aircraft weight leading to higher thrust required, results in relatively large engine scale factors for these cases. Although engine scaling laws were used to provide approximate characteristics for these higher thrust engines, the low fan pressure ratio cases could potentially benefit from redesigned engines that meet takeoff thrust requirements without scaling.

Table 4. Aircraft Sizing Results for Spiral 1, Low Work Engines (162 Passenger, 3250nm Design Mission)

	<i>1998 Tech. Baseline</i>	<b>S1-Lo-g-1.3*</b> (BPR ~ 25)	<b>S1-Lo-g-1.4</b> (BPR ~ 17)	<b>S1-Lo-dd-1.4*</b> (BPR ~ 17)	<b>S1-Lo-g-1.5</b> (BPR ~ 13)	<b>S1-Lo-dd-1.5</b> (BPR ~ 13)	<b>S1-Lo-g-1.6</b> (BPR ~ 11)	<b>S1-Lo-dd-1.6</b> (BPR ~ 11)	<b>S1-Lo-dd-1.7</b> (BPR ~ 9)
OEW, lb	94700	106100	91700	103200	85250	86750	83600	82200	<b>80200</b>
Mission Fuel, lb	50350	43200	40500	43100	38400	38500	38900	<b>38100</b>	38600
Payload Weight, lb	32400	32400	32400	32400	32400	32400	32400	32400	32400
Ramp Weight, lb	177550	181700	164600	178700	156100	157700	155000	152700	<b>151200</b>
Wing Area, ft <sup>2</sup>	1470	1760	1400	1660	1380	1400	1365	1340	1315
W/S, lb/ft <sup>2</sup>	121	103	116	107	113	113	114	114	115
Thrust(SLS), lb	26100	29800	26700	28000	23600	23800	23200	23000	22600
T/W (takeoff)	0.294	0.328	0.325	0.314	0.303	0.302	0.300	0.301	0.299
Takeoff field length, ft	7000	7000	7000	7000	7000	7000	7000	7000	7000
Landing field length, ft	6020	5440	5850	5570	5720	5720	5750	5750	5790
~Cruise Range Factor V*(L/D)/TSFC, nm	12450	<b>15200</b>	14600	14900	14550	14700	14250	14350	14000
Block Fuel, lb	42600	36400	34100	36350	32500	32600	32900	<b>32250</b>	32600
Block NO <sub>x</sub> , lb	555	219	186	200	175	176	172	169	<b>164</b>
LTO NO <sub>x</sub> , lb per cycle	22.2	<b>9.7</b>	10.4	10.7	9.8	9.7	10.3	10.1	10.8

\*Design ground rules lead to impractical design for these cases.

#### **4.2.2 High Work Cases**

Sizing results for the Spiral 1, high work engine cases are given in Table 5. For the high work engines, which experience a larger weight benefit from the geared fan approach than the low work engines, the lowest block fuel consumption occurs for one of the geared engine cases. The FPR=1.5, geared fan engine has 2% lower fuel burn than the best direct drive case. The SLS bypass ratio of this engine is 12.7. As with the low work engines, there is a trade-off between the improved propulsive efficiency associated with lower fan pressure ratio and the increase in engine weight and drag. The FPR=1.3 and FPR=1.4 geared fan cases have higher cruise efficiency, but higher block fuel consumption. The direct drive, FPR=1.7 case provides the lowest total NO<sub>x</sub> emissions and lowest ramp weight, consistent with the low work engine results. The lowest LTO NO<sub>x</sub> emissions occur at the completely opposite end of the fan pressure ratio spectrum, at FPR=1.3.

Table 5. Aircraft Sizing Results for Spiral 1, High Work Engines (162 Passenger, 3250nm Design Mission)

	<i>1998 Tech. Baseline</i>	<b>S1-Hi-g-1.3*</b> (BPR ~ 23)	<b>S1-Hi-g-1.4</b> (BPR ~ 16)	<b>S1-Hi-dd-1.4*</b> (BPR ~ 16)	<b>S1-Hi-g-1.5</b> (BPR ~ 12)	<b>S1-Hi-dd-1.5</b> (BPR ~ 12)	<b>S1-Hi-g-1.6</b> (BPR ~ 10)	<b>S1-Hi-dd-1.6</b> (BPR ~ 10)	<b>S1-Hi-dd-1.7</b> (BPR ~ 8)
OEW, lb	94700	101900	89500	106150	83700	88950	81800	83950	<b>81000</b>
Mission Fuel, lb	50350	42400	40200	44650	<b>38300</b>	39700	38900	39100	39450
Payload Weight, lb	32400	32400	32400	32400	32400	32400	32400	32400	32400
Ramp Weight, lb	177550	176700	162100	183200	154400	161000	153100	155500	<b>152800</b>
Wing Area, ft <sup>2</sup>	1470	1700	1400	1720	1370	1420	1340	1350	1300
W/S, lb/ft <sup>2</sup>	121	104	116	106	113	113	114	115	117
Thrust(SLS), lb	26100	29150	26350	28500	23350	24200	23000	23400	23050
T/W (takeoff)	0.294	0.330	0.325	0.311	0.303	0.301	0.300	0.301	0.302
Takeoff field length, ft	7000	7000	7000	7000	7000	7000	7000	7000	7000
Landing field length, ft	6020	5440	5830	5540	5720	5750	5780	5800	5870
~Cruise Range Factor V*(L/D)/TSFC, nm	12450	<b>15000</b>	14500	14700	14400	14500	14100	14200	13900
Block Fuel, lb	42600	35700	33900	37700	<b>32450</b>	33600	32900	33200	33300
Block NO <sub>x</sub> , lb	555	203	176	199	161	167	157	158	<b>150</b>
LTO NO <sub>x</sub> , lb per cycle	22.2	<b>9.2</b>	9.7	10.3	9.3	9.6	9.9	10.0	10.7

\*Design ground rules lead to impractical design for these cases.

### 4.2.3 Comparison of Results

The sizing results in Tables 4 and 5 lead to some interesting conclusions. These can be better highlighted by presenting some of the key results graphically as done in Figures 20 through 24. The variation of fuel consumption with fan pressure ratio and engine type is shown in Figure 20. Note the geared FPR=1.3 and direct drive FPR=1.4 cases are connected with dashed lines because these particular cases do not represent practical designs. However, it is helpful to examine the trends out to those extreme points. Compressor work split has little to no impact on fuel burn in the case of a geared fan engine. Evidently, when the low spool is able to operate at its optimal speed, both high and low LPC pressure ratios can be accommodated with equal effectiveness and efficiency. When the low spool is directly connected to the fan, the work split has a noticeable impact. The fuel burn curve for the low work direct drive engines has a shape similar to the high work cases, but is shifted downward. For the high work engines, the “cross-over” point above which the direct drive configurations have lower fuel consumption than the geared engines is around FPR=1.6 (perhaps slightly higher). However, because of the better performance of the low work direct drive engines, this “cross-over” point is shifted to FPR=1.5 for the low work engines. For a low work approach, a direct drive, FPR=1.6 fan design provides the lowest fuel consumption. For a high work approach, a geared, FPR=1.5 fan design provides the lowest fuel consumption. Whether a direct drive or geared fan design provides the lowest fuel burn clearly depends on other engine design parameters, such as fan pressure ratio and compressor work split. The difference in fuel consumption for these two distinctly different engine designs is less than 1%. Given the level of accuracy expected for this type of conceptual design study, the two approaches can be considered essentially equivalent from a fuel consumption perspective. The lower fan pressure ratio design leads to lower noise, however, as will be discussed in Section 4.3.

Figure 21 compares the ramp weight results for the Spiral 1 cases. As with fuel consumption, there is a cross-over point for the direct drive and geared fan approaches. For the low work designs, the direct drive fan results in lower ramp weight when fan pressure ratio is above ~1.52. As with fuel consumption, the cross-over point is higher for the high work engines. Although not within the range of fan pressure ratios considered, the cross-over point for high work engines appears to be greater than FPR=1.6. There is a larger difference between low work and high work geared fan designs in the case of ramp weight than there was in Figure 20 for fuel consumption. Recall from Figures 17 and 19, that the low work geared engines have lower TSFC, but higher weight than their high work counterparts. The lower TSFC and higher weight balance out in the case of fuel consumption but lead to higher ramp weight. As discussed in Section 4.1.3, at a given fan pressure ratio the fundamental difference among the different engine types is engine weight. The cross-over points in ramp weight are therefore similar to the cross-over points in engine weight (see Figure 19).

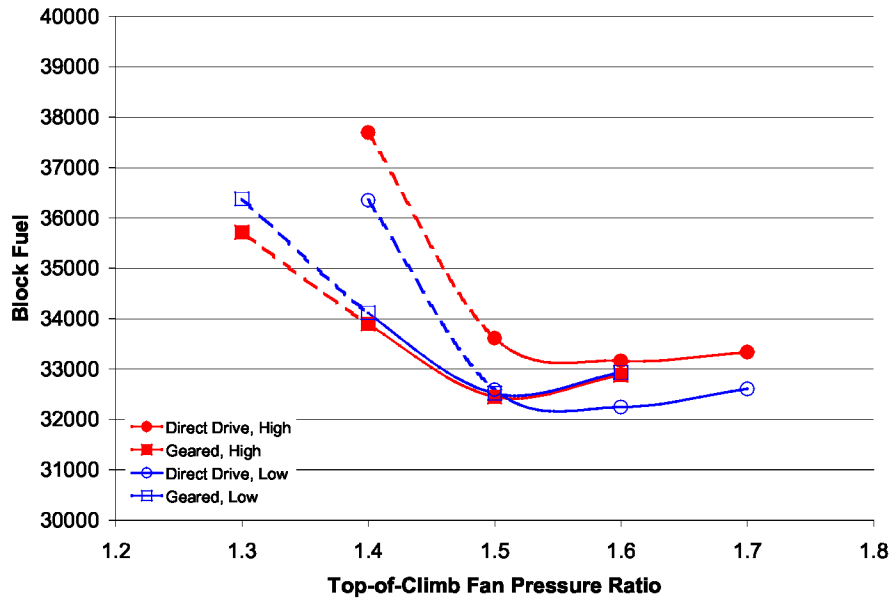


Figure 20. Variation of block fuel with fan pressure ratio and engine type, Spiral 1.

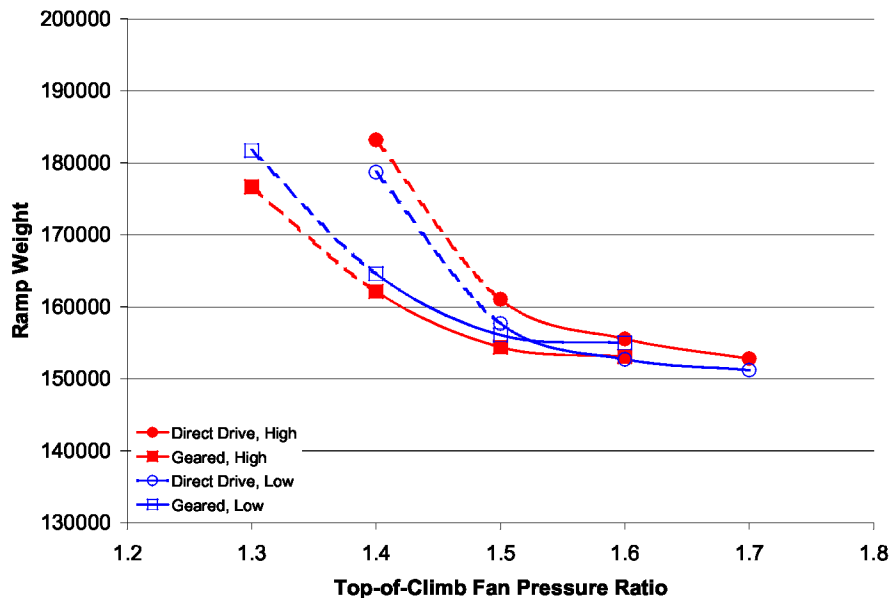


Figure 21. Variation of ramp weight with fan pressure ratio and engine type, Spiral 1.

NO<sub>x</sub> emission characteristics are compared in Figures 22 through 24. These results are based on advanced combustor technology as represented by the NASA low NO<sub>x</sub> correlation described in Section 3.1. Total NO<sub>x</sub> emissions over the entire mission, or block NO<sub>x</sub> emissions, are presented in Figure 22. For both the low work and high work engines, minimum block NO<sub>x</sub> occurs for the FPR=1.7, direct drive engine design. Although the block fuel consumption is higher for the FPR=1.7 cases than for the FPR=1.6 cases, the total NO<sub>x</sub> emitted is lower which indicates the higher fuel consumption is offset by a lower cruise NO<sub>x</sub> emission index. A decrease in emission index as fan pressure ratio is increased is also evident in Tables 2 and 3 for the TOC condition. The NO<sub>x</sub> emission index is most strongly influenced by combustor design and pressure and temperature conditions across the combustor. For the study, all the

engines were assumed to have the same combustor design (i.e., the same emission correlation equation was used). At TOC, the overall pressure ratio is also the same for all the engines. However, the combustor temperature conditions at TOC do vary, with combustor exit temperature increasing as fan pressure ratio decreases. The higher combustor exit temperatures for the low fan pressure ratio engines help to mitigate thrust lapse and improves fuel consumption, but leads to a higher  $\text{NO}_x$  emission index. At a given fan pressure ratio, the low work engines have higher  $\text{NO}_x$  emission indices than the high work engines. A primary reason is the differences in the engine architecture. As mentioned previously, the low work engines have slightly higher bypass ratio. Slightly higher combustor temperatures are needed to achieve the design thrust targets, resulting in higher  $\text{NO}_x$  emissions. In Figure 23 the engine landing-takeoff cycle (LTO)  $\text{NO}_x$  parameter “ $D_p/F_{oo}$ ” is presented. This parameter, defined by the International Civil Aviation Organization (ICAO) and used in FAR Part 34 engine certification, is the grams of  $\text{NO}_x$  emitted over a standard LTO cycle (by a single, uninstalled engine) divided by rated output at SLS conditions. There is a consistent downward trend in  $D_p/F_{oo}$  with decreasing fan pressure ratio; fan drive approach has little impact on this parameter because at a given fan pressure ratio there is little difference in the cycle performance for the two fan drive approaches. As with total  $\text{NO}_x$ , there is an increase in LTO  $\text{NO}_x$  for the low work designs, but the difference is much smaller than it was for total  $\text{NO}_x$ . Although all the engines have the same overall pressure ratio at the top-of-climb design condition, overall pressure ratio at takeoff conditions decreases with decreasing fan pressure ratio. This lower overall pressure ratio for the low fan pressure ratio cases leads to lower LTO  $\text{NO}_x$ . LTO  $\text{NO}_x$  is often presented simply in terms of the ICAO  $D_p/F_{oo}$  emissions parameter. This parameter alone does not account for differences in engine weight and performance which can lead to differences in the required thrust level ( $F_{oo}$ ) when the engine is integrated into an overall aircraft design. Lower  $D_p/F_{oo}$  does not necessarily result in lower total LTO  $\text{NO}_x$  emissions. The estimated  $\text{NO}_x$  per LTO is compared in Figure 24.  $\text{NO}_x$  per LTO has been estimated by multiplying the ICAO  $D_p/F_{oo}$  parameter by the total engine thrust. The  $\text{NO}_x$  per LTO curves do not follow the same trends as  $D_p/F_{oo}$ . For the direct drive engines, the larger thrust needed for the FPR=1.4 cases leads to higher  $\text{NO}_x$  per LTO than the FPR=1.5 case, even though  $D_p/F_{oo}$  is lower. For the geared fan cases,  $\text{NO}_x$  per LTO falls again as fan pressure ratio is decreased to 1.3, indicating the decrease in  $D_p/F_{oo}$  is greater than the increase in thrust required.

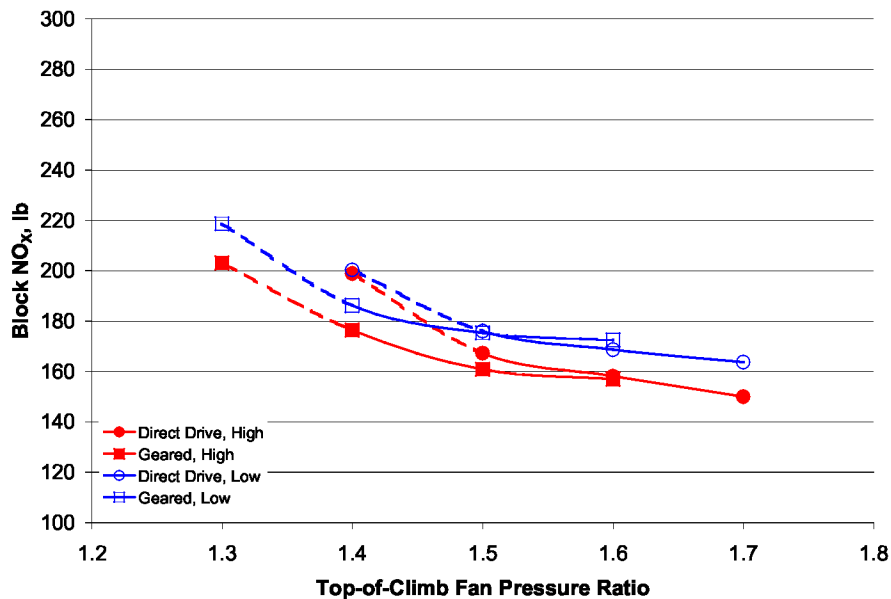


Figure 22. Variation in total mission  $\text{NO}_x$  emissions with fan pressure ratio and engine type, Spiral 1.

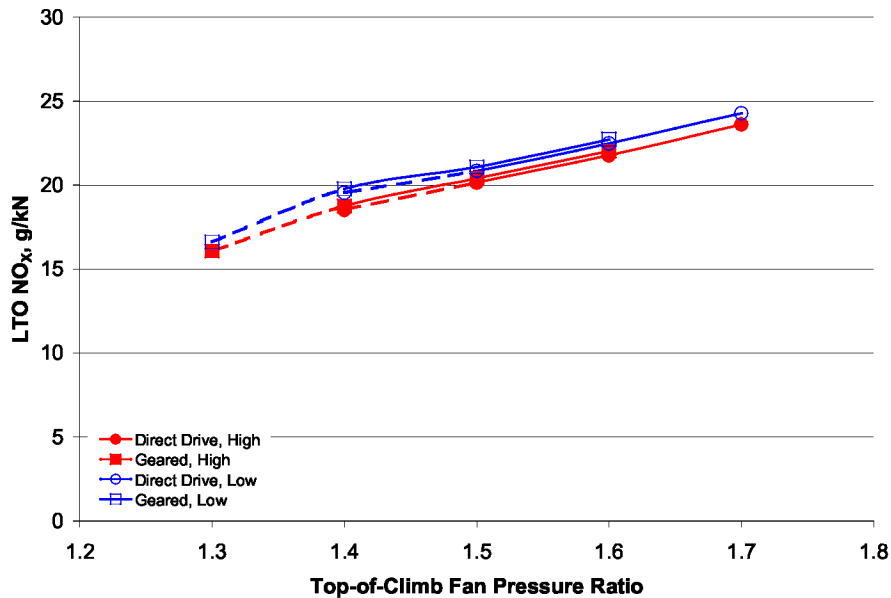


Figure 23. Variation in LTO NO<sub>x</sub> emissions with fan pressure ratio and engine type ( $D_p/F_{\infty}$ ), Spiral 1.

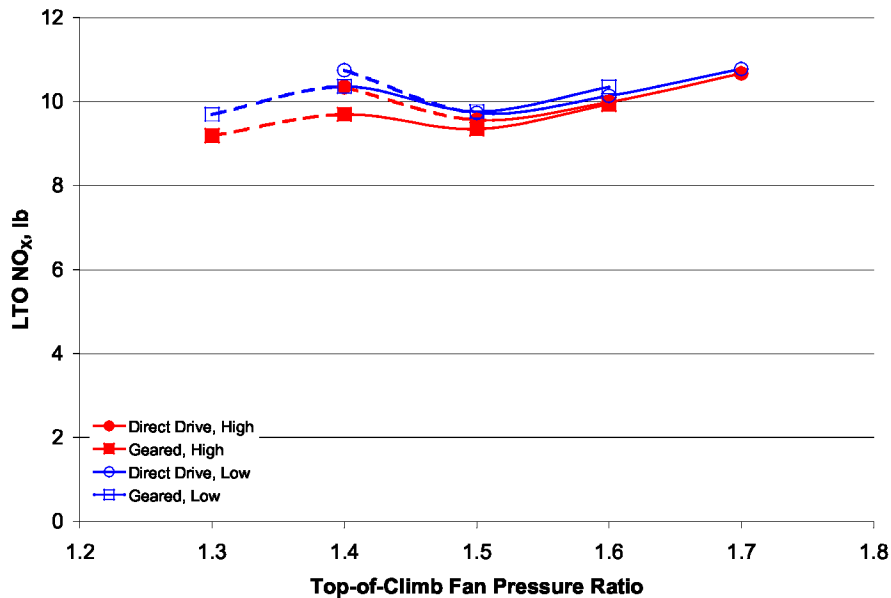


Figure 24. Variation in NO<sub>x</sub> emissions per LTO cycle with fan pressure ratio and engine type, Spiral 1.

#### 4.2.4 Potential ASAT, Spiral 1 Technology Benefits

In Figures 25 through 28, the potential overall benefits of the advanced technologies assumed for the Spiral 1 vehicles are assessed for the key sizing outputs of weight, fuel consumption, and NO<sub>x</sub> emissions. For these figures, the baseline for comparison is a 1998 EIS technology level vehicle (equivalent technology to 737-800/CFM56-7B), sized to match the study design mission of 3250 nm with a cruise speed of  $M=0.8$ . The advanced Spiral 1 vehicles offer up to a 15% reduction in ramp weight, up to a 24% reduction in block fuel consumption, up to a 73% reduction in block NO<sub>x</sub> (block fuel and NO<sub>x</sub> compared for a 3250 nm mission), and up to a 58% reduction in NO<sub>x</sub> emission per landing-takeoff cycle. These

maximum potential reductions occur for different engines designs, and a single vehicle would not achieve all of these reductions. The projected weight, fuel, and emission benefits associated with the ASAT, Spiral 1 technology set are significant. However, Boeing recently revealed that they have curtailed their 737 replacement studies because, according to industry sources, combining the best technology advances in materials, propulsion, aerodynamics, structures, and systems failed to come close to their original goals for a 737 replacement vehicle (ref. 46). According to reference 47, Boeing targeted a 15-20% increase in fuel efficiency, which is exceeded by the vehicles in this study. It is not clear whether it is the fuel efficiency target that has not been met in Boeing's studies, or whether other targets, such as a significant reduction in maintenance cost (not investigated in this study), are the issue. In any case, it is not unusual for NASA's projected advances to be higher than those of industry because of more aggressive assumptions for component level technologies and fewer constraints in the system level design.

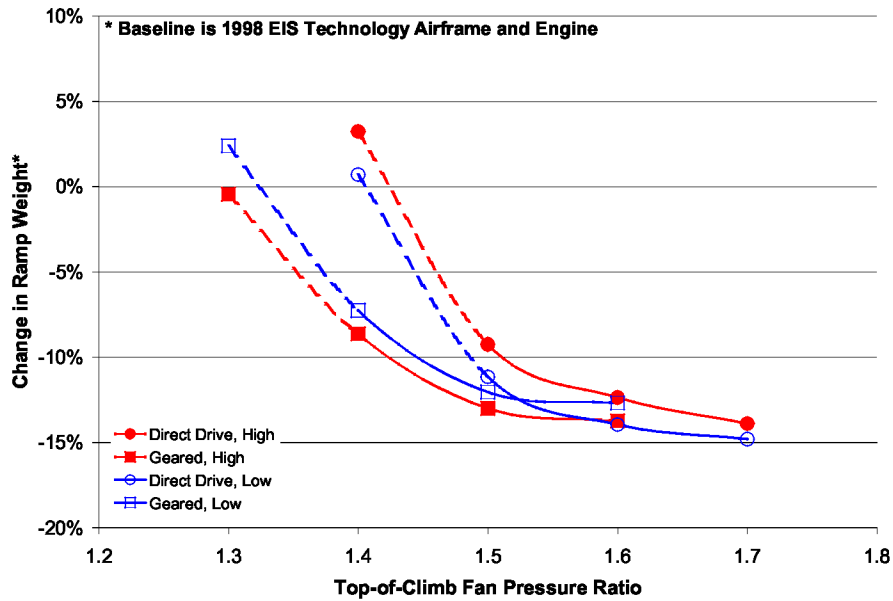


Figure 25. Potential ramp weight reduction from application of ASAT, Spiral 1 technologies.

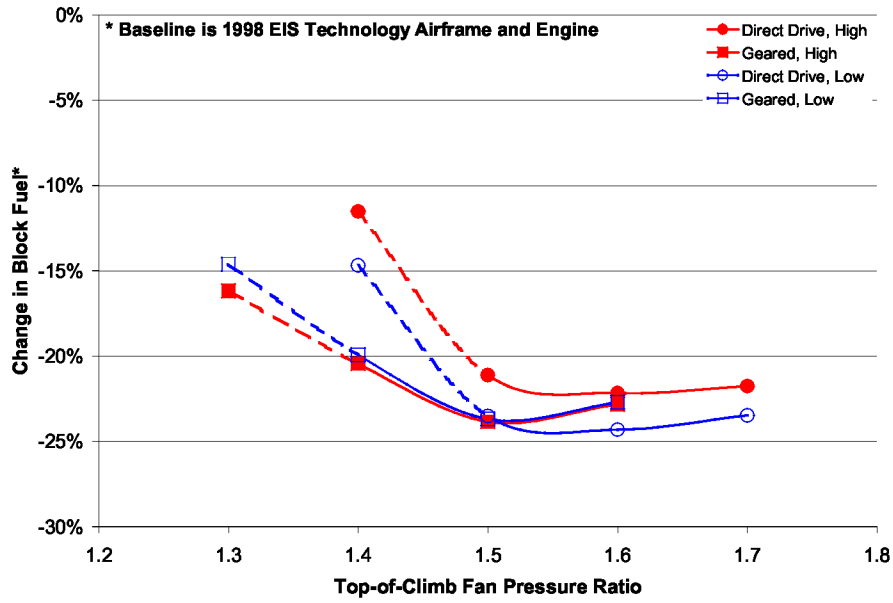


Figure 26. Potential block fuel reduction from application of ASAT, Spiral 1 technologies.

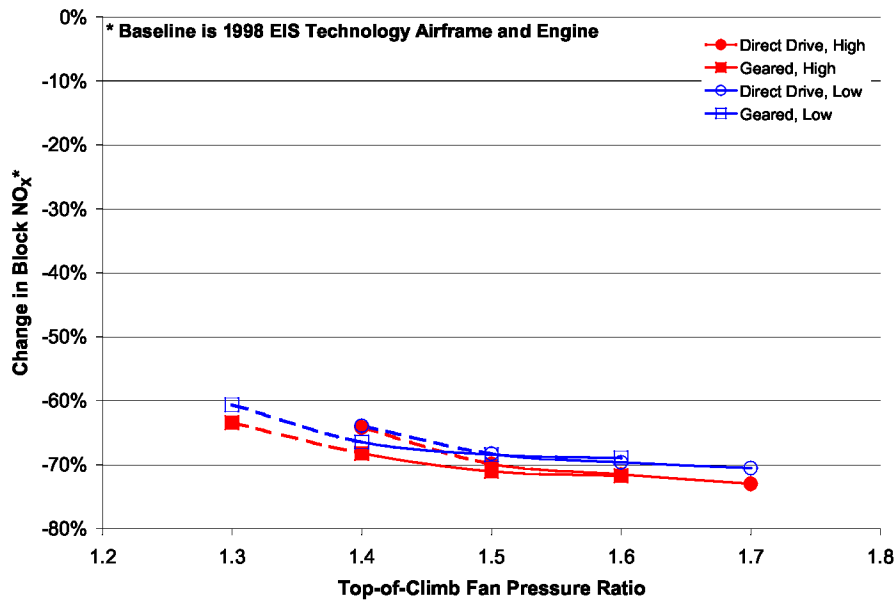


Figure 27. Potential block NO<sub>x</sub> reduction from application of ASAT, Spiral 1 technologies.

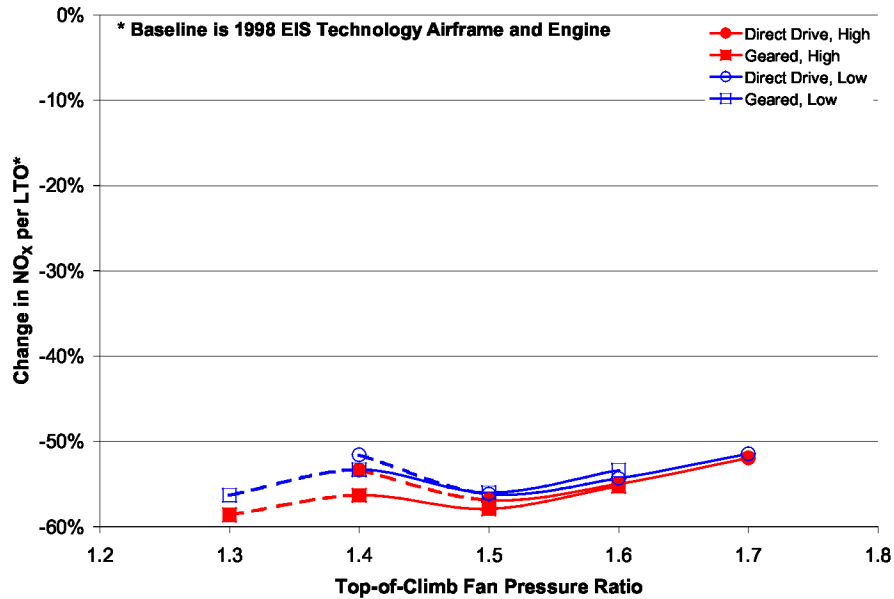


Figure 28. Potential LTO NO<sub>x</sub> reduction from application of ASAT, Spiral 1 technologies.

### 4.3 Spiral 1 Certification Noise Analysis

Certification noise results for the Spiral 1 configurations are presented in Figures 29 to 31, relative to the levels predicted for a 737-800/CFM56-7B26 using similar noise analysis methodologies. Results are presented on a relative basis to minimize the affect of the potential inaccuracies in the analysis methodologies noted in Section 3.3.1. The noise variations in Figures 29 to 31 reflect not only the impact of changes in the engine cycle (fan pressure ratio), but also the differences in engine thrust, aircraft weight, takeoff and approach trajectories, throttling, etc. resulting from the sizing of each aircraft to a common design mission. As with earlier graphs, the lowest fan pressure ratio cases are connected with dashed lines to indicate that these cases do not correspond to practical designs. The expected noise benefits of low fan pressure ratio are confirmed in these results. For all three certification points, the noise level is reduced by pushing fan pressure ratio as low as possible, where low fan tip speeds and low exhaust velocity, high bypass ratio nozzles are found. There is almost no difference in any of the certification noise levels at a given fan pressure ratio for different configurations based on different engine designs. Variation in lateral (sideline) noise is 0.2 EPNdB or less. There is slightly more variation in flyover noise, but the engine configuration still only changes noise by 0.3 EPNdB or less for a given fan pressure ratio. Changes in approach noise are only 0.1 EPNdB or less. The slight differences are primarily associated with the wing/engine sizing and the resulting trajectory performance. All of the Spiral 1 configurations show potential for significant noise reduction relative to the 737-800. The noise reduction is on the order of 8-9 EPNdB at each certification point for an ADP fan pressure ratio of 1.40 (only practical with a geared fan design). The large approach noise reductions are due to effective airframe noise reduction technologies and slower approach speeds for the ASAT designs. The slower approach speeds are the result of the ASAT vehicles sizing to lower wing loadings than the baseline 737-800.

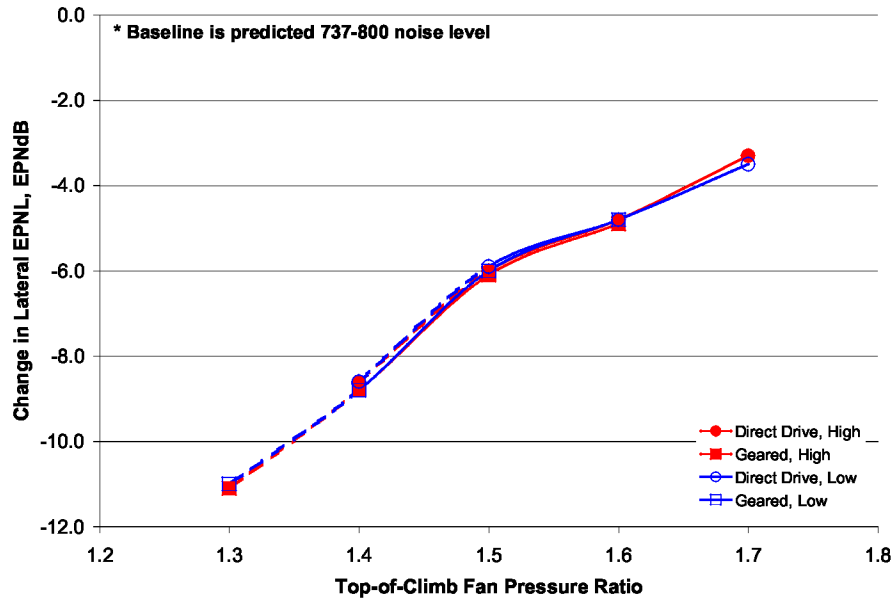


Figure 29. Variation in lateral (sideline) noise with fan pressure ratio and engine type, Spiral 1.

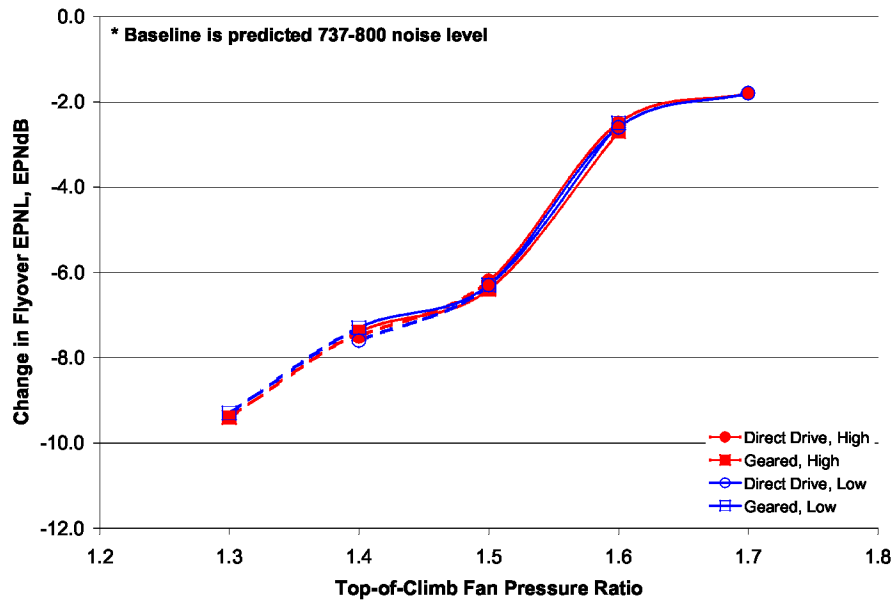


Figure 30. Variation in flyover noise with fan pressure ratio and engine type, Spiral 1.

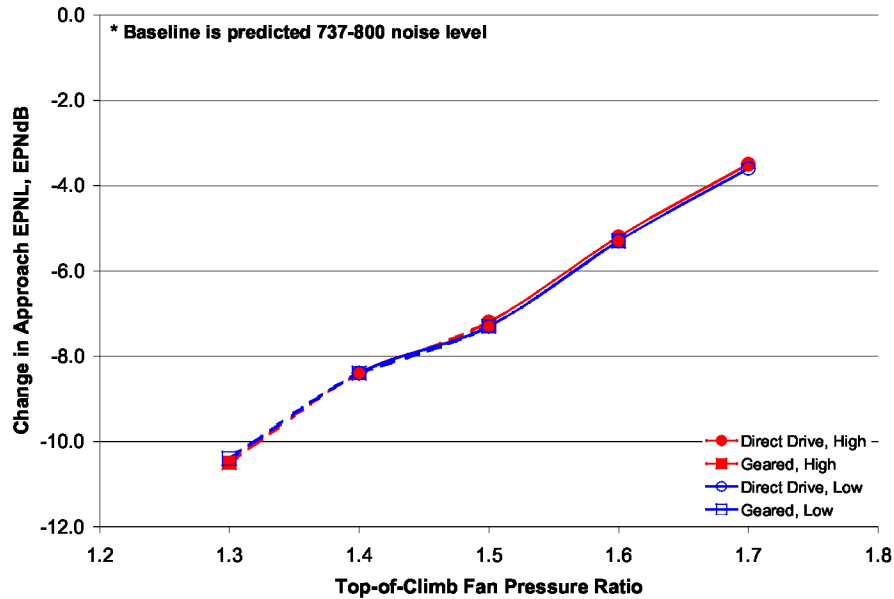


Figure 31. Variation in approach noise with fan pressure ratio and engine type, Spiral 1.

Often certification noise is compared in terms of the algebraic sum of the lateral, flyover, and approach noise levels (“cumulative noise”). The cumulative noise reductions predicted for the Spiral 1 configurations relative to a 737-800 are presented in Figure 32. Again the positive impact of low fan pressure ratio on noise is evident. The cumulative noise reduction achieved by reducing fan pressure ratio from 1.7 to 1.3 is over 22 EPNdB; despite the higher aircraft weight and engine thrust associated with the low fan pressure ratio configuration. The maximum reduction relative to the 737-800 baseline realized for a practical design is 24.5 EPNdB cumulative (geared, FPR=1.4 cases). This reduction is the result of both engine cycle changes and noise reduction technologies. Figure 33 presents the Spiral 1 noise results in terms of cumulative margin relative to the current, “Stage 4” noise regulations (i.e., sum of amount below lateral, flyover, and approach limits based on aircraft weight, ref. 29). For the FPR=1.4, geared engine cases, the predicted cumulative margin relative to Stage 4 regulations is ~25 EPNdB. (Recall from Section 3.3.1 that comparison of the 737-800 predicted noise levels to certification data indicated a possible 4 EPNdB over prediction of flyover noise. If this discrepancy in flyover noise is also present in the Spiral 1 analysis cases, the true cumulative margin for this case would be ~29 EPNdB.) At FPR=1.3, the cumulative margin approaches 32 EPNdB. The FPR=1.3 case in this study does not result in a practical aircraft design with the ground rules used. However, there may be other approaches to the FPR=1.3 geared engine which would enable this additional noise benefit to be realized in a practical aircraft design.

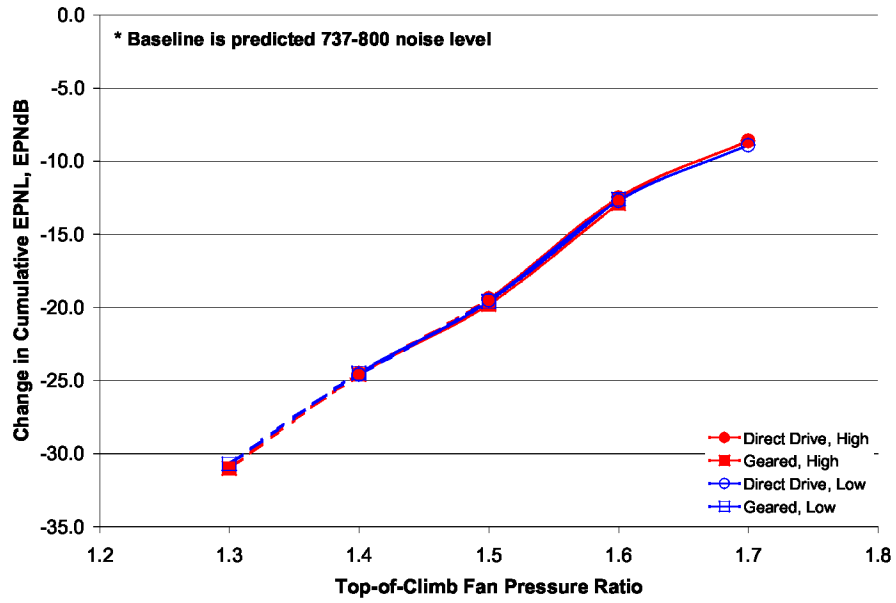


Figure 32. Variation in cumulative noise reduction with fan pressure ratio and engine type, Spiral 1.

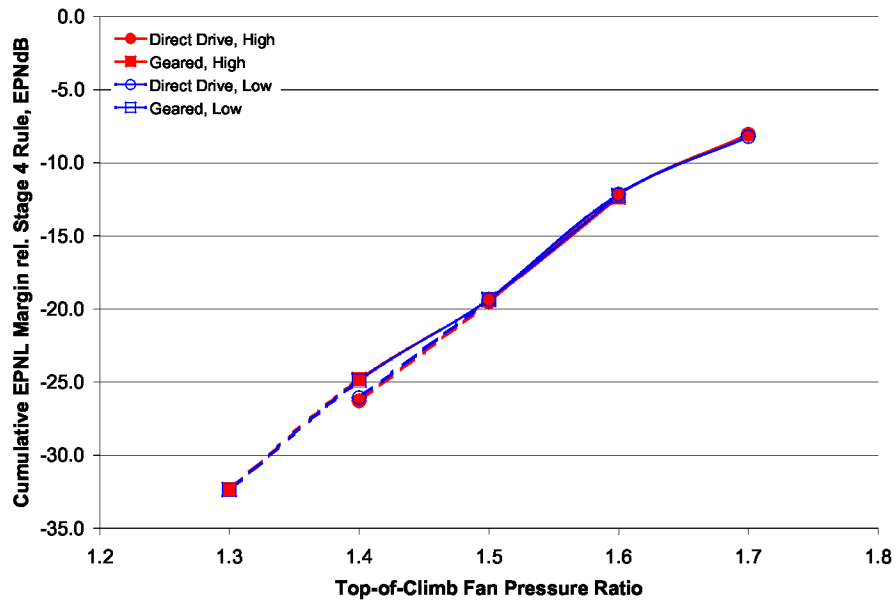


Figure 33. Stage 4 cumulative margin, Spiral 1.

## 5.0 Spiral 2

All of the engines in Spiral 1 are designed with an overall pressure ratio (at the top-of-climb ADP) of 32. This overall pressure ratio is similar to that of the CFM56 engines that are used on the current Boeing 737 and Airbus A320. Current technology large engines can have overall pressure ratios above 40, however. Technology advances can lead to higher overall pressure ratios, but there are physical limits that must be considered. Specifically, as the air is compressed in the compressor and the density increases, each stage (row) in the compressor has to have smaller blades than the stage preceding it. There are physical limits on how small a compressor blade can be manufactured and the smaller the blade becomes, the less aerodynamically efficient it is due to exaggerated blade tip clearance losses and Reynolds number effects. For these reasons it is not possible to simply scale down a high overall pressure ratio, 80,000 lb thrust engine to a 25,000 lb thrust engine. In Spiral 1, a conventional, fairly conservative design approach was taken which enabled design overall pressure ratio of 32 while maintaining blade heights above 0.5 inches. Based on projections of a potential higher overall pressure ratio for a 2015 engine of this class, a second set of analyses, Spiral 2, was conducted with a more aggressive approach to enable increased overall pressure ratio. In particular, the minimum blade height constraint was relaxed. The primary objective of Spiral 2 was to determine if a higher overall pressure ratio had any significant impact on the relative performance of the different engine types.

### 5.1 Spiral 2 Engine Design

General characteristics of the Spiral 2 engines are shown in Table 6 and Table 7 for the low work and high work design approaches, respectively. These engines were designed with the same ADP flight conditions and thrust targets as the Spiral 1 engines, but with an overall pressure ratio of 42 instead of 32. For the low work engines, the higher overall pressure ratio was achieved by increasing the HPC pressure ratio from 13.5 to 17.7, with no change to the LPC. The high work engines have a smaller increase in HPC pressure ratio (from 10 to 12), as well as an increase in LPC pressure ratio as necessary to achieve the overall pressure ratio of 42. The range of fan pressure ratios considered for Spiral 2 are the same as in Spiral 1; 1.3 to 1.6 for geared fan designs and 1.4 to 1.7 for direct drive designs. The FPR=1.3 geared engine and FPR=1.4 direct drive engine continue to be impractical designs for the reasons noted in Section 4.1. With the same fan pressure ratios and thrust levels, fan and nacelle diameters for Spiral 2 are the same as for Spiral 1. Even though engine size and fan pressure ratios are the same as Spiral 1, the bypass ratios are slightly higher. The higher overall pressure ratio in Spiral 2 enables a given fan to be driven with a smaller core, leading to less core airflow and a higher bypass ratio for a given fan pressure ratio. For the low work engines, gear ratios are the same as in Spiral 1, because the LPC pressure ratio is unchanged. For the high work engines, the higher LPC pressure ratio leads to slightly higher gear ratios than in Spiral 1. The high work engine gear ratios vary from 3.5 at the low fan pressure ratios to 1.6 at the high fan pressure ratios. Because of the higher overall pressure ratio, the last stage HPC blade heights are shorter than in Spiral 1. The minimum blade height for the low fan pressure ratio engines is ~0.4 inches, a more aggressive design than in Spiral 1. Increasing minimum blade height to the Spiral 1 limit of 0.5 inches would require a reduction in HPC exit Mach number to about 0.2 (currently 0.3).

The increase in overall pressure ratio from 32 to 42 did not impact the relative characteristics of the different engine designs. In Figure 34, TSFC for the Spiral 2 engines is shown overlaid on the Spiral 1 values. The variation in TSFC with fan pressure ratio is similar for the two different engine sets. For both the low work and high work designs, the decrease in TSFC from FPR=1.7 to FPR=1.3 is ~10%, compared to ~11% for Spiral 1. The weight penalties associated with lower fan pressure ratio are also similar to Spiral 1 as can be seen in Figure 35. Qualitatively, the impact of fan drive on engine TSFC and weight is the same as for the Spiral 1 engines as well; geared engines have slightly higher TSFC and the geared

approach has larger weight benefit when used with a high work low spool design. The “cross-over” fan pressure ratios at which the geared fan approach becomes heavier than a direct drive fan approach are essentially the same for Spiral 1 and Spiral 2. Although the relative comparison of the Spiral 2 engines among each other is similar to that of the Spiral 1 engines, the Spiral 2 engines do differ considerably from the Spiral 1 engines. Increasing overall pressure ratio from 32 to 42 resulted in a 3-5% reduction in TSFC. This did not come without penalties in other areas, however. Engine weight is up to 5% higher depending on the specific case. And,  $\text{NO}_x$  emission indices at SLS and TOC are approximately 40% higher for the Spiral 2 engines. A comparison of  $\text{NO}_x$  EI’s for Spiral 1 and Spiral 2 engines at TOC conditions is shown in Figure 36. This increase in  $\text{NO}_x$  is expected given the higher operating pressure in the engines. When selecting engine overall pressure ratio there is a well known tradeoff between fuel burn and  $\text{NO}_x$  emissions.

Table 6. General Characteristics of Spiral 2, Low Work Engine Models

	S2-Lo-g-1.3*		S2-Lo-g-1.4		S2-Lo-dd-1.4*		S2-Lo-g-1.5		S2-Lo-dd-1.5		S2-Lo-g-1.6		S2-Lo-dd-1.6		S2-Lo-dd-1.7	
Fan Drive/Gear Ratio	Geared/3.0		Geared/2.0		Direct Drive		Geared/1.5		Direct Drive		Geared/1.2		Direct Drive		Direct Drive	
Fan Diameter, in	92		81		81		73		73		68		68		64	
Fan Nozzle Geometry	Variable		Variable		Variable		Fixed		Fixed		Fixed		Fixed		Fixed	
Engine+Nacelle Weight, lb	9742		7953		10482		6991		7552		6808		6293		5772	
Nacelle Max Diameter, ft	9.4		8.3		8.3		7.5		7.5		7.0		7.0		6.6	
Operating Conditions	SLS	TOC	SLS	TOC	SLS	TOC	SLS	TOC	SLS	TOC	SLS	TOC	SLS	TOC	SLS	TOC
Fan Pressure Ratio	1.2	1.3	1.3	1.4	1.3	1.4	1.4	1.5	1.4	1.5	1.5	1.6	1.5	1.6	1.6	1.7
Bypass Ratio	26.0	26.4	18.1	18.4	18.3	18.6	14.4	14.1	14.6	14.3	11.8	11.4	12.0	11.6	10.0	9.6
Overall Pressure Ratio	29.6	42	32.1	42	32.1	42	33.4	42	33.4	42	34.6	42	34.6	42	35.8	42
Net Thrust, lb	23001	5000	22986	5000	23002	5000	22982	5000	23001	5000	22981	5000	23000	5000	23002	5000
TSFC, lb/(lb-h)	0.204	0.473	0.235	0.485	0.233	0.480	0.256	0.501	0.253	0.496	0.276	0.516	0.273	0.511	0.294	0.526
NO <sub>x</sub> Emission Index (g/kg)	22.0	10.2	24.4	8.6	24.4	8.6	25.4	8.0	25.4	8.0	26.4	7.6	26.5	7.6	27.6	7.2

\*Design ground rules lead to impractical design for these cases.

Table 7. General Characteristics of Spiral 2, High Work Engine Models

	S2-Hi-g-1.3*		S2-Hi-g-1.4		S2-Hi-dd-1.4*		S2-Hi-g-1.5		S2-Hi-dd-1.5		S2-Hi-g-1.6		S2-Hi-dd-1.6		S2-Hi-dd-1.7	
Fan Drive/Gear Ratio	Geared/3.5		Geared/2.5		Direct Drive		Geared/1.9		Direct Drive		Geared/1.6		Direct Drive		Direct Drive	
Fan Diameter, in	92		81		81		73		73		68		68		64	
Fan Nozzle Geometry	Variable		Variable		Variable		Fixed		Fixed		Fixed		Fixed		Fixed	
Engine+Nacelle Weight, lb	8842		7353		11064		6475		8350		6028		6824		6136	
Nacelle Max Diameter, ft	9.4		8.3		8.3		7.5		7.5		7.0		7.0		6.6	
Operating Conditions	SLS	TOC	SLS	TOC	SLS	TOC	SLS	TOC	SLS	TOC	SLS	TOC	SLS	TOC	SLS	TOC
Fan Pressure Ratio	1.2	1.3	1.3	1.4	1.3	1.4	1.4	1.5	1.4	1.5	1.5	1.6	1.5	1.6	1.6	1.7
Bypass Ratio	24.4	24.5	16.9	17.0	17.2	17.2	13.4	13.0	13.6	13.2	11.0	10.5	11.1	10.6	9.2	8.7
Overall Pressure Ratio	29.4	42	31.9	42	31.9	42	33.2	42	33.2	42	34.4	42	34.4	42	35.7	42
Net Thrust, lb	23002	5000	22998	5000	23020	5000	22996	5000	23015	5000	22995	5000	23017	5000	23022	5000
TSFC, lb/(lb-h)	0.208	0.478	0.240	0.491	0.237	0.486	0.261	0.507	0.258	0.502	0.283	0.523	0.279	0.518	0.302	0.533
NO <sub>x</sub> Emission Index (g/kg)	21.0	9.2	23.2	7.8	23.2	7.8	24.2	7.3	24.2	7.3	25.3	6.9	25.3	6.9	26.5	6.5

\*Design ground rules lead to impractical design for this case

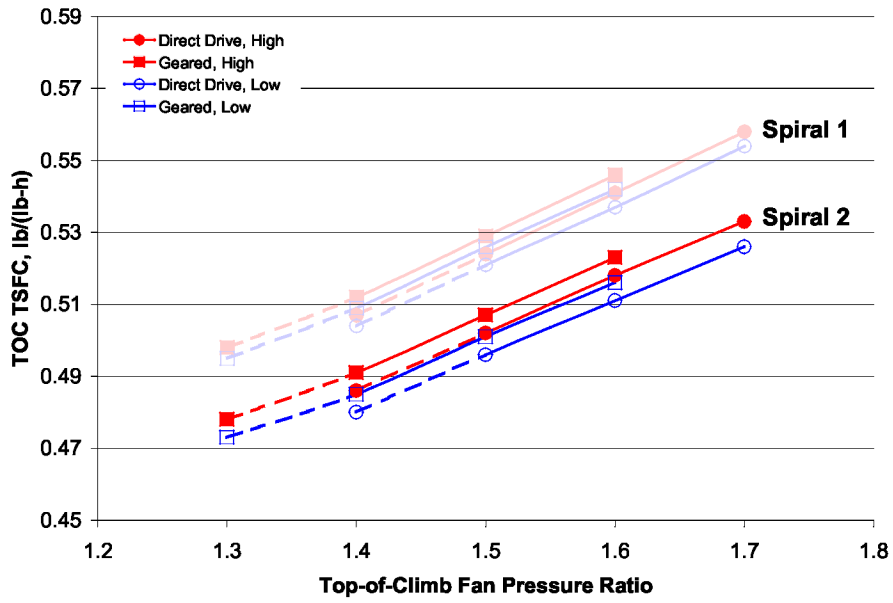


Figure 34. Relationship between fan pressure ratio and TSFC, top-of-climb conditions, Spiral 2.

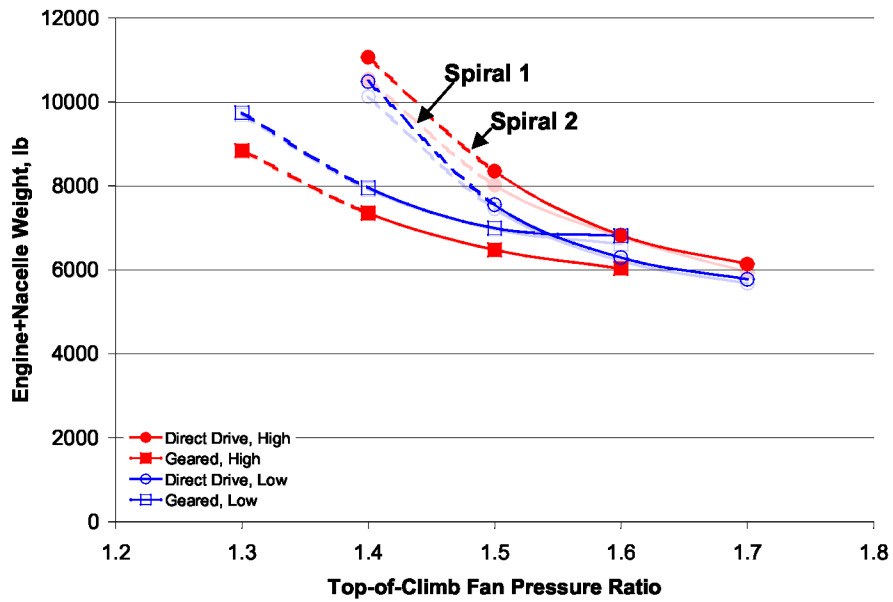


Figure 35. Variation of engine+nacelle weight with fan pressure ratio, Spiral 2.

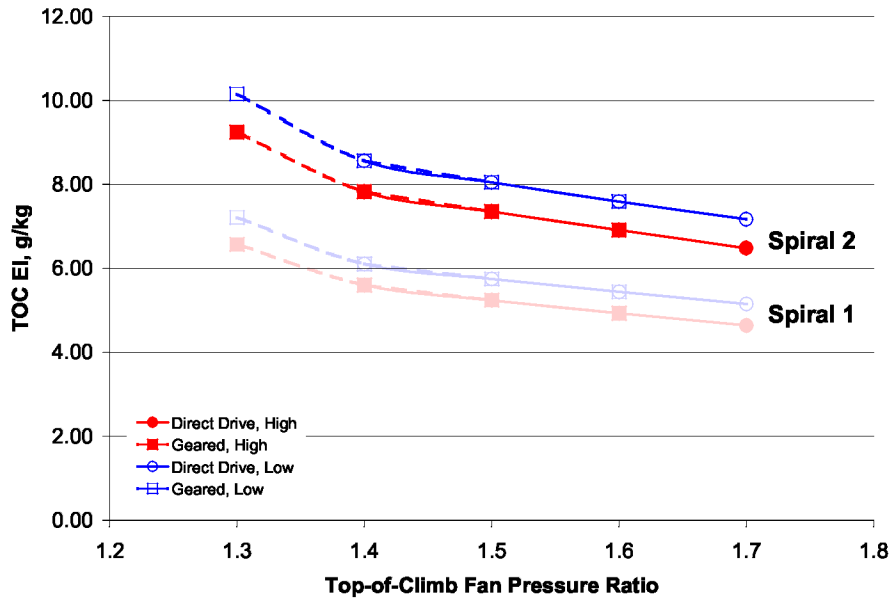


Figure 36. Variation in TOC NO<sub>x</sub> Emission Index with fan pressure ratio and engine type, Spiral 2.

## 5.2 Spiral 2 Aircraft Sizing

The Spiral 2 engines were applied to the same ASAT airframe model as used in Spiral 1 and sizing performed for the same mission requirements. Results of the Spiral 2 aircraft sizing and analysis are summarized in Table 8 for the low work engines and Table 9 for the high work engines. The numbers in bold indicate the “best” value for that particular parameter. Results for a 1998 EIS technology baseline vehicle sized to perform the study design mission are shown in the tables for reference.

### 5.2.1 Comparison of Results

Given the similarity in weight and TSFC trends between the Spiral 1 and Spiral 2 engines, it is not surprising the trends in the sizing results (ramp weight, block fuel consumption, NO<sub>x</sub> emissions, etc.) are also similar between Spiral 1 and Spiral 2. A quick comparison with the Spiral 1 results in Tables 4 and 5 reveals that, for every case except one, the “best” fan pressure ratio and fan drive approach in Spiral 2 is the same as in Spiral 1. For low work designs: operating empty weight, ramp weight, and total NO<sub>x</sub> emissions are minimized with the direct drive, FPR=1.7 engine; total mission fuel and block fuel weight are minimized with the direct drive, FPR=1.6 engine; and cruise efficiency is maximized and LTO NO<sub>x</sub> minimized with the geared, FPR=1.3 engine. These results are the same as for Spiral 1. For high work designs: operating empty weight and total NO<sub>x</sub> emissions are minimized with the direct drive, FPR=1.7 engine; ramp weight is minimized with the geared, FPR=1.6 engine; total mission fuel and block fuel weight are minimized with the geared, FPR=1.5 engine; and the geared, FPR=1.3 engine results in the maximum cruise efficiency and minimum LTO NO<sub>x</sub>. For Spiral 1, the minimum ramp weight for high work engines occurred with the direct drive, FPR=1.7 engine, otherwise these results are the same as in Spiral 1.

Table 8. Aircraft Sizing Results for Spiral 2, Low Work Engines (162 Passenger, 3250nm Design Mission)

	<i>1998 Tech. Baseline</i>	<b>S2-Lo-g-1.3*</b> (BPR ~ 26)	<b>S2-Lo-g-1.4</b> (BPR ~ 18)	<b>S2-Lo-dd-1.4*</b> (BPR ~ 19)	<b>S2-Lo-g-1.5</b> (BPR ~ 14)	<b>S2-Lo-dd-1.5</b> (BPR ~ 14)	<b>S2-Lo-g-1.6</b> (BPR ~ 11)	<b>S2-Lo-dd-1.6</b> (BPR ~ 12)	<b>S2-Lo-dd-1.7</b> (BPR ~ 10)
OEW, lb	94700	105000	90800	103600	84500	86200	83400	81700	<b>79650</b>
Mission Fuel, lb	50350	40500	37900	40800	36000	36100	36600	<b>35700</b>	36250
Payload Weight, lb	32400	32400	32400	32400	32400	32400	32400	32400	32400
Ramp Weight, lb	177550	178000	161100	176800	152900	154700	152400	149800	<b>148300</b>
Wing Area, ft <sup>2</sup>	1470	1730	1400	1650	1360	1383	1350	1330	1270
W/S, lb/ft <sup>2</sup>	121	103	115	107	112	112	113	113	117
Thrust(SLS), lb	26100	29300	26200	27800	23250	23400	22900	22600	22600
T/W (takeoff)	0.294	0.329	0.326	0.315	0.304	0.303	0.301	0.301	0.305
Takeoff field length, ft	7000	7000	7000	7000	7000	7000	7000	7000	7000
Landing field length, ft	6020	5410	5820	5560	5700	5690	5730	5710	5840
~Cruise Range Factor V*(L/D)/TSFC, nm	12450	<b>15800</b>	15300	15600	15200	15400	14900	15050	14700
Block Fuel, lb	42600	34200	32000	34500	30500	30600	31050	<b>30300</b>	30700
Block NO <sub>x</sub> , lb	555	284	241	262	222	223	219	214	<b>200</b>
LTO NO <sub>x</sub> , lb per cycle	22.2	<b>10.0</b>	10.6	11.2	10.3	10.2	10.9	10.7	11.6

\*Design ground rules lead to impractical design for these cases.

Table 9. Aircraft Sizing Results for Spiral 2, High Work Engines (162 Passenger, 3250nm Design Mission)

	<i>1998 Tech. Baseline</i>	S2-Hi-g-1.3* (BPR ~ 24)	S2-Hi-g-1.4 (BPR ~ 17)	S2-Hi-dd-1.4* (BPR ~ 17)	S2-Hi-g-1.5 (BPR ~ 13)	S2-Hi-dd-1.5 (BPR ~ 13)	S2-Hi-g-1.6 (BPR ~ 11)	S2-Hi-dd-1.6 (BPR ~ 11)	S2-Hi-dd-1.7 (BPR ~ 9)
OEW, lb	94700	100900	88800	107800	83100	89500	81100	83450	<b>80900</b>
Mission Fuel, lb	50350	40100	38000	43000	<b>36300</b>	37900	36700	37000	37300
Payload Weight, lb	32400	32400	32400	32400	32400	32400	32400	32400	32400
Ramp Weight, lb	177550	173400	159200	183200	151750	159800	<b>150200</b>	152900	150600
Wing Area, ft <sup>2</sup>	1470	1680	1390	1720	1340	1420	1320	1350	1300
W/S, lb/ft <sup>2</sup>	121	103	115	106	113	113	114	113	116
Thrust(SLS), lb	26100	28700	25900	28600	23200	24200	22700	22900	22600
T/W (takeoff)	0.294	0.331	0.326	0.313	0.306	0.302	0.302	0.300	0.300
Takeoff field length, ft	7000	7000	7000	7000	7000	7000	7000	7000	7000
Landing field length, ft	6020	5420	5800	5540	5720	5730	5750	5740	5810
~Cruise Range Factor V*(L/D)/TSFC, nm	12450	<b>15600</b>	15050	15300	15000	15100	14650	14800	14450
Block Fuel, lb	42600	33800	32100	36350	<b>30800</b>	32200	31100	31400	31600
Block NO <sub>x</sub> , lb	555	265	229	263	209	220	204	207	<b>198</b>
LTO NO <sub>x</sub> , lb per cycle	22.2	<b>9.7</b>	10.4	11.3	10.1	10.4	10.8	10.8	11.5

\*Design ground rules lead to impractical design for these cases.

The Spiral 2 fuel consumption, ramp weight, and NO<sub>x</sub> results are presented graphically in Figures 37 through 41, overlaid on the Spiral 1 results. As shown in Figure 37, the overall variation of fuel burn with fan pressure ratio and engine type is essentially the same for both Spiral 1 and Spiral 2. However, the fuel consumption benefit of higher overall pressure ratio is evident. For the minimum fuel cases (low work, direct drive fan, FPR=1.6), the Spiral 2 engine results in a 6% reduction in block fuel consumption. Again in the case of ramp weight, Figure 38, the Spiral 2 trends are consistent with Spiral 1. The shift in ramp weight for Spiral 2 is less than in the case of block fuel, with the lowest ramp weight case (low work, direct drive fan, FPR=1.7) only 2% below its corresponding Spiral 1 case.

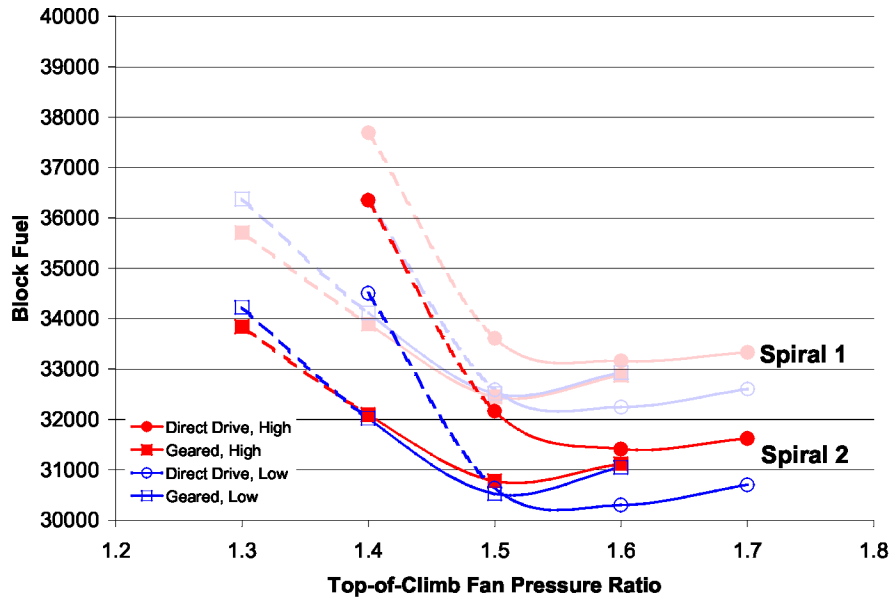


Figure 37. Variation of block fuel with fan pressure ratio and engine type, Spiral 2.

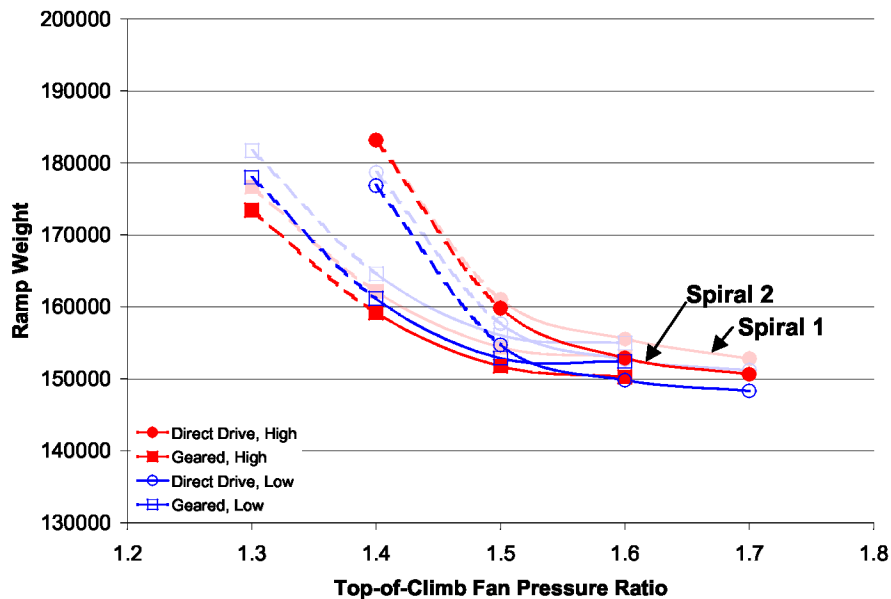


Figure 38. Variation of ramp weight with fan pressure ratio and engine type, Spiral 2.

A comparison of Spiral 1 and Spiral 2 total NO<sub>x</sub> emissions is presented in Figure 39. As with the other parameters, the impact of fan drive type, work split, and fan pressure ratio on total NO<sub>x</sub> is similar for Spiral 1 and 2. Unfortunately, the higher overall pressure ratio of the Spiral 2 engines leads to a significant increase in total NO<sub>x</sub>. NO<sub>x</sub> emissions for the best case (high work, direct drive, FPR=1.7) increase 32% from Spiral 1 to Spiral 2. This reflects a significantly higher NO<sub>x</sub> emission index, as noted in Section 5.1, only partially offset by lower block fuel consumption. The increases in LTO NO<sub>x</sub>, presented in Figures 40 and 41 are not as significant. Minimum D<sub>p</sub>/F<sub>00</sub> is 7% higher and minimum NO<sub>x</sub> per LTO is 5% higher. Although the Spiral 2 engines have significantly higher takeoff and climb NO<sub>x</sub> EIs compared to Spiral 1, EIs for approach and idle are unchanged. (Experimental data at low power settings were not available when the NO<sub>x</sub> emission correlation equation described in Section 3.1 was developed. The idle and approach NO<sub>x</sub> emission indices are fixed values based on observation of other similar advanced combustor technologies and are insensitive to changes in the engine cycle parameters.) Since in this analysis the approach and idle NO<sub>x</sub> emissions (as much as half of the total LTO emissions for advanced, low NO<sub>x</sub> combustors) are not significantly impacted by the differences between the Spiral 1 and Spiral 2 designs, the increase in LTO NO<sub>x</sub> for Spiral 2 is not as large as the increase in total block NO<sub>x</sub>.

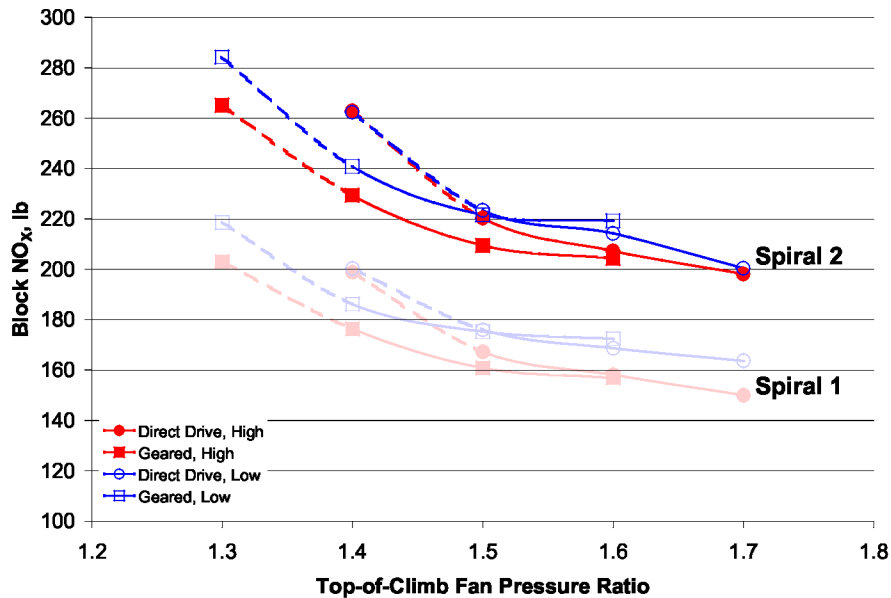


Figure 39. Variation in total mission NO<sub>x</sub> emissions with fan pressure ratio and engine type, Spiral 2.

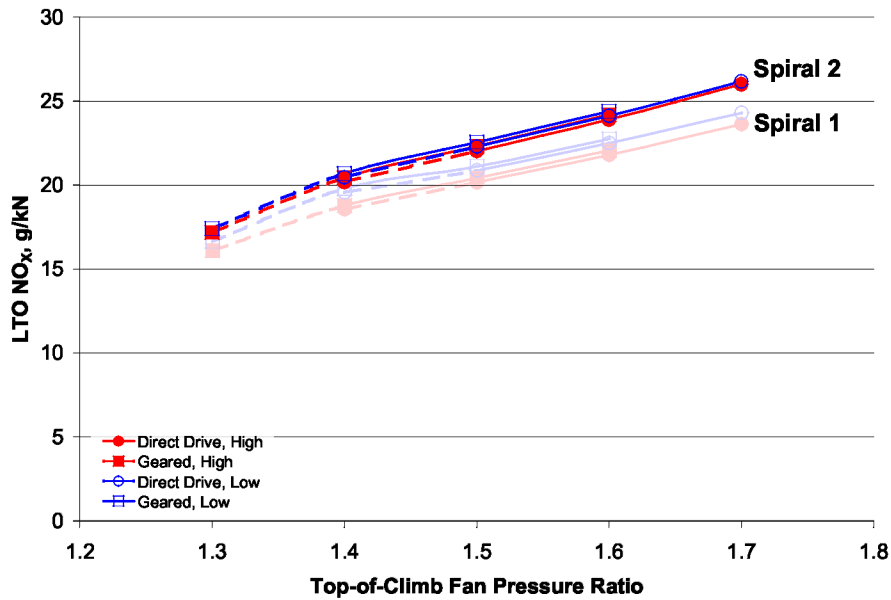


Figure 40. Variation in LTO NO<sub>x</sub> emissions with fan pressure ratio and engine type ( $D_p/F_{oo}$ ), Spiral 2.

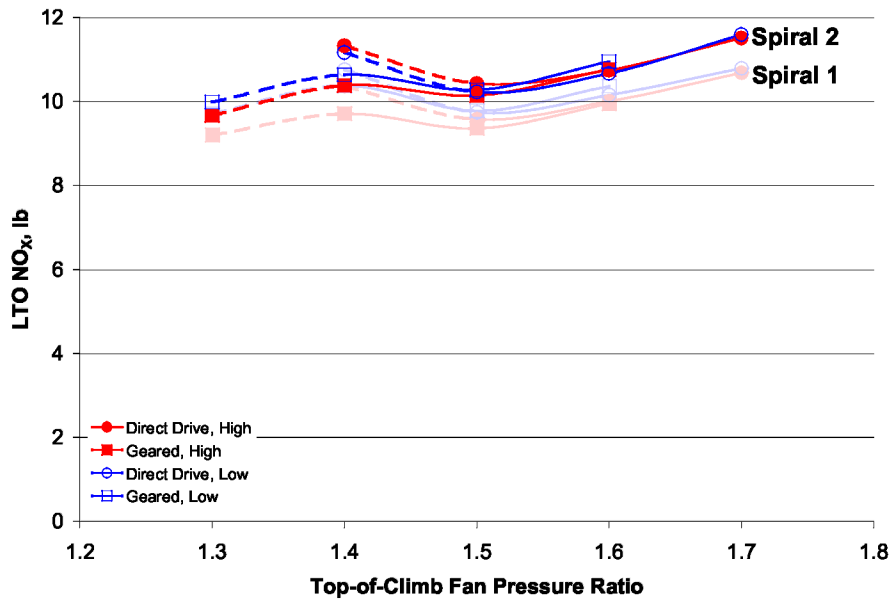


Figure 41. Variation in NO<sub>x</sub> emissions per LTO cycle with fan pressure ratio and engine type, Spiral 2.

### 5.2.2 Potential ASAT, Spiral 2 Technology Benefits

The advanced technology of the Spiral 2 vehicles offers even greater potential than the Spiral 1 vehicles for reducing fuel consumption compared to current single-aisle vehicles. In Figure 42, block fuel for the Spiral 2 vehicles is compared to that of a 1998 EIS technology level vehicle (737-800/CMF56-7B equivalent technology) designed for the same mission. The potential fuel consumption benefit is up to

29%. Ramp weight could be up to 16% less as indicated in Figure 43. The Spiral 2 vehicles have less NO<sub>x</sub> reduction potential than Spiral 1 due to the higher emission indices associated with the higher overall pressure ratio engines. The advanced combustor technology assumed for these engines still results in large NO<sub>x</sub> emission reductions, however. Figure 44 shows up to 64% reduction in block NO<sub>x</sub> emissions, and Figure 45 shows up to a 54% reduction in NO<sub>x</sub> per LTO cycle compared to the 1998 EIS technology baseline vehicle.

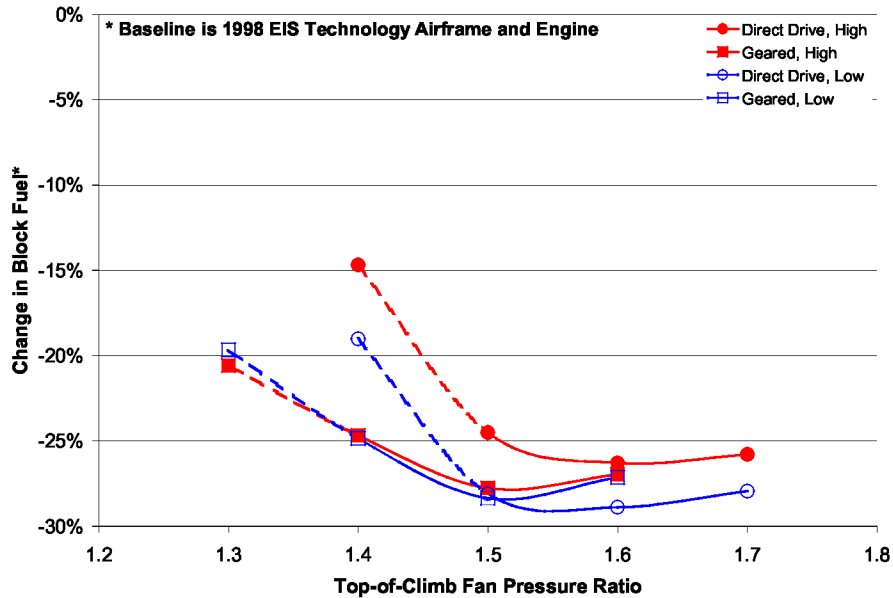


Figure 42. Potential block fuel reduction from application of ASAT, Spiral 2 technologies.

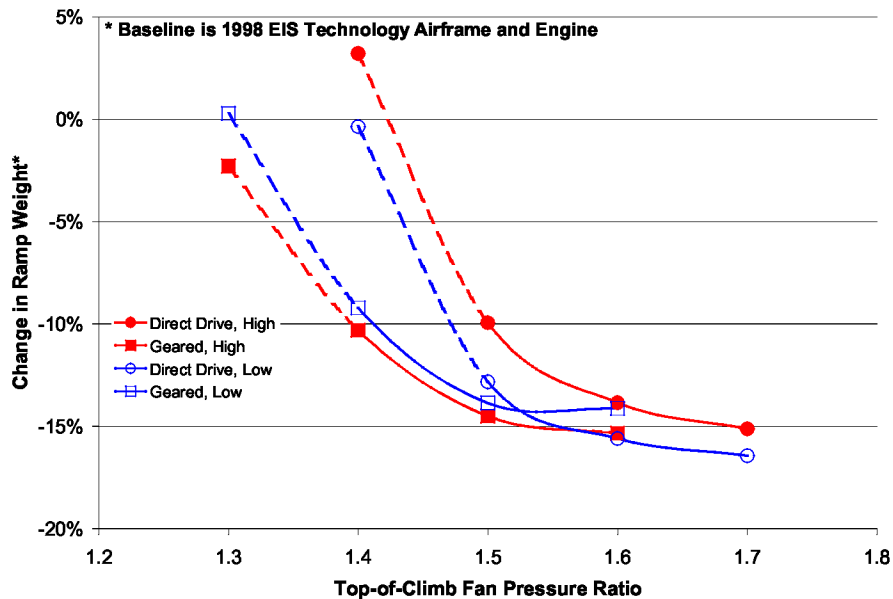


Figure 43. Potential ramp weight reduction from application of ASAT, Spiral 2 technologies.

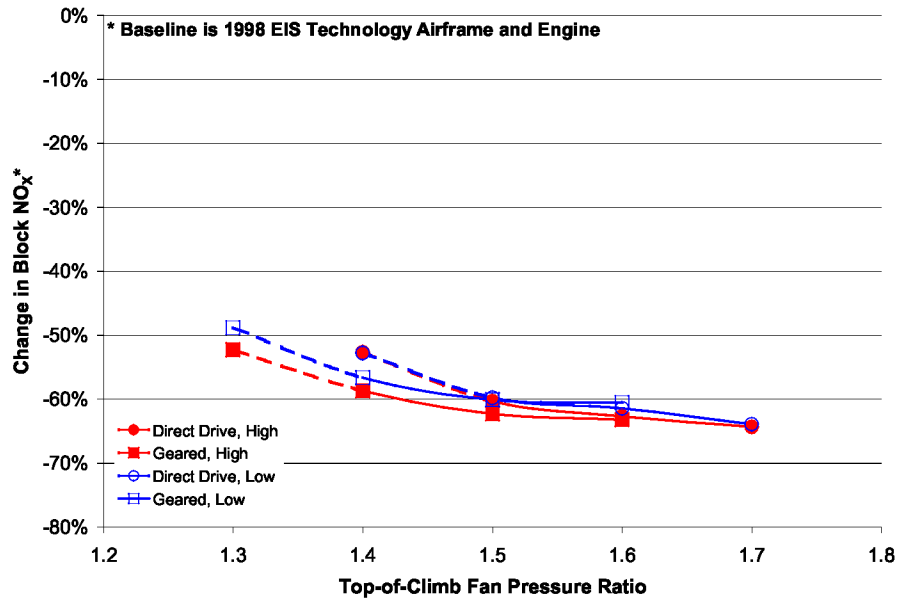


Figure 44. Potential block NO<sub>x</sub> reduction from application of ASAT, Spiral 2 technologies.

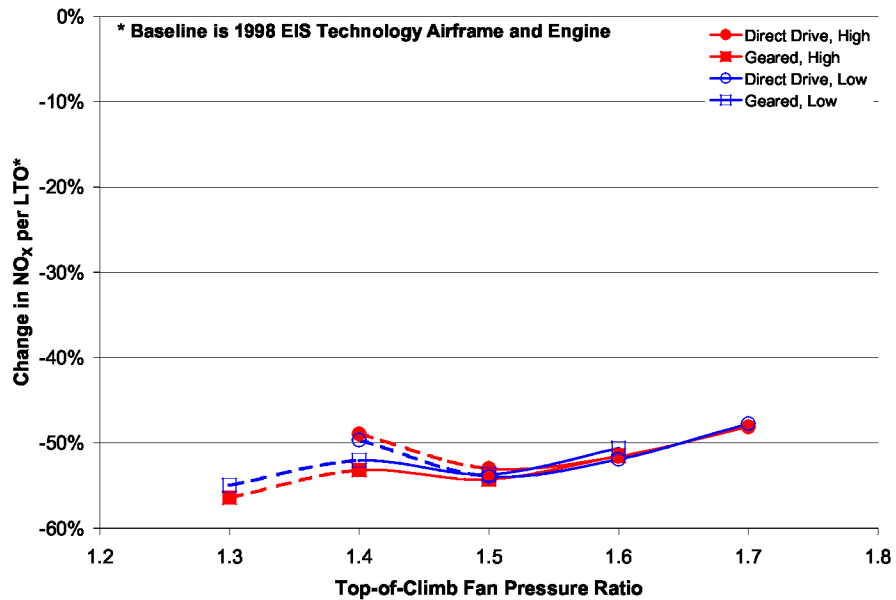


Figure 45. Potential LTO NO<sub>x</sub> reduction from application of ASAT, Spiral 2 technologies.

### 5.3 Spiral 2 Certification Noise Analysis

Certification noise results for the Spiral 2 configurations are presented in Figures 46 to 48, relative to the levels predicted for a 737-800 using similar noise analysis methodologies. These results are overlaid on the Spiral 1 results; however, the Spiral 1 and Spiral 2 noise results are nearly identical. The higher overall pressure ratio of Spiral 2 does not have an impact on the overall noise trends and the absolute values differ by less than 1 dB. Although the Spiral 2 configurations are generally lighter and have lower thrust engines, these differences are small and have negligible impacts on the noise. A limitation in the noise analysis methodology must be noted here. One of the shortcomings of the engine core noise module in the ANOPP noise prediction tool (ref. 32) is that the maximum overall pressure ratio considered is 30. The variation in overall pressure ratio between Spiral 1 and 2 is, therefore, not reflected in the core noise estimates. Core noise is a relatively small contributor to the overall noise level, however. The cumulative noise reductions predicted for the Spiral 2 configurations relative to a 737-800 are presented in Figure 49 and margins relative to Stage 4 regulations in Figure 50, again overlaid on Spiral 1 results. The maximum reduction relative to the 737-800 baseline realized for a practical design is ~25 EPNdB cumulative (high work, geared, FPR=1.4 case). For both FPR=1.4, geared engine cases, the predicted cumulative margin relative to Stage 4 regulations is ~24 EPNdB. If fan pressure ratio could be decreased to 1.3 (1.2 at sea level static conditions) in a practical aircraft design, the potential Stage 4 margin approaches 32 EPNdB.

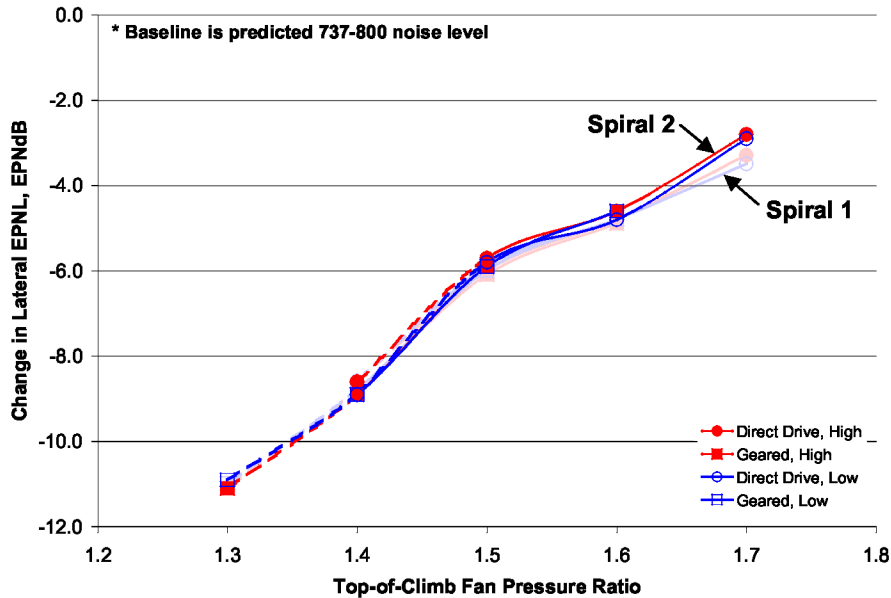


Figure 46. Variation in lateral (sideline) noise with fan pressure ratio and engine type, Spiral 2.

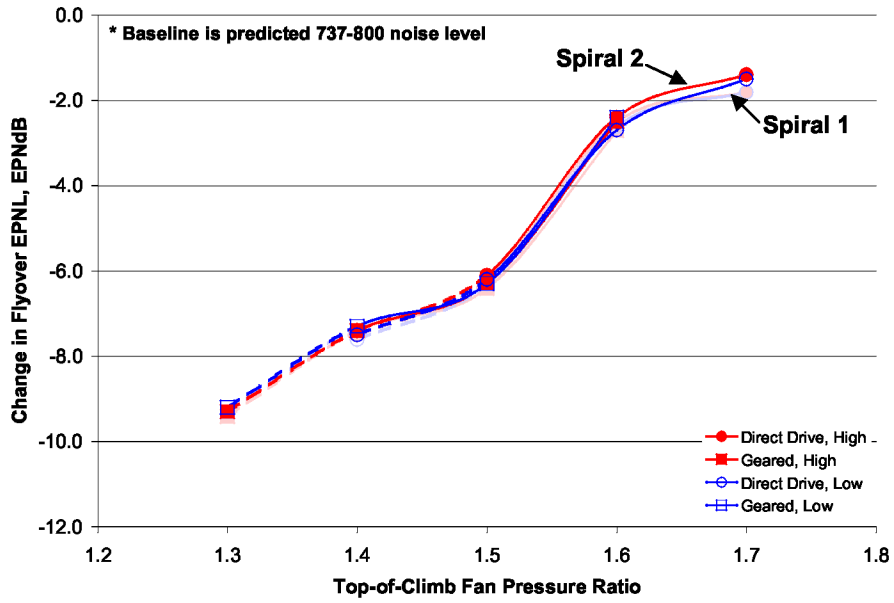


Figure 47. Variation in flyover noise with fan pressure ratio and engine type, Spiral 2.

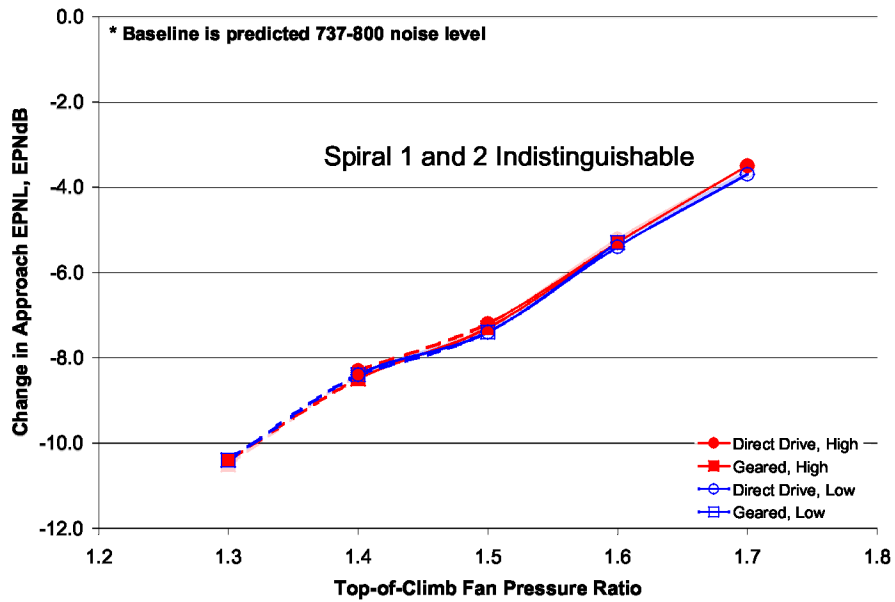


Figure 48. Variation in approach noise with fan pressure ratio and engine type, Spiral 2.

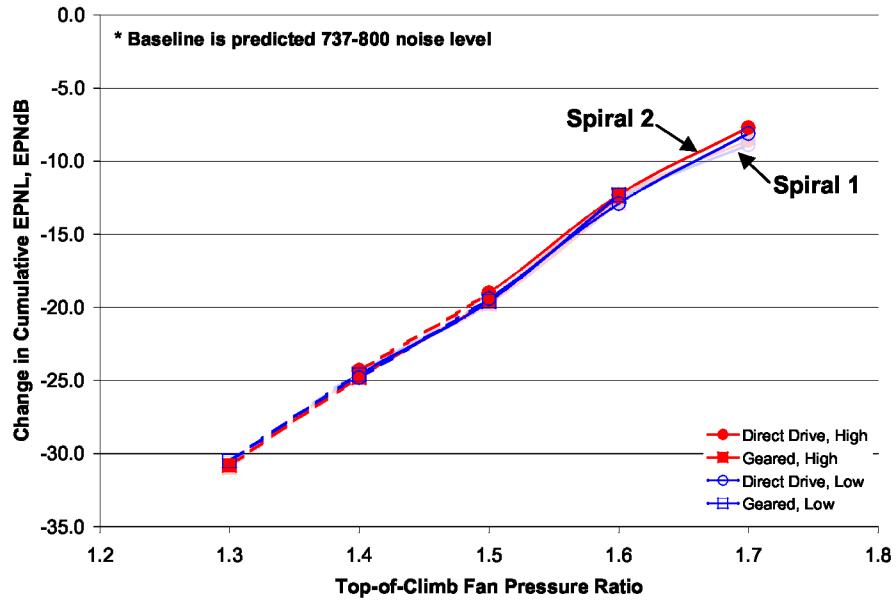


Figure 49. Variation in cumulative noise reduction with fan pressure ratio and engine type, Spiral 2.

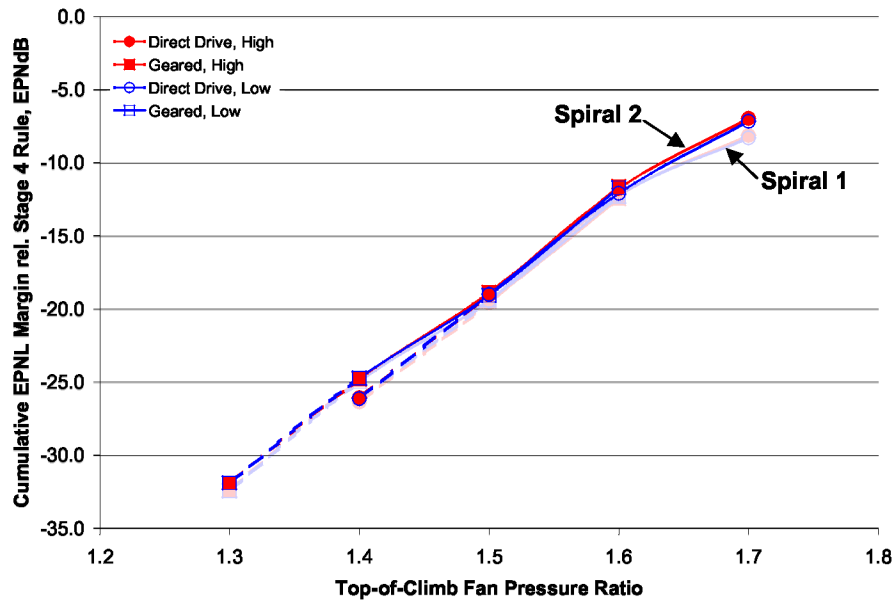


Figure 50. Stage 4 cumulative margin, Spiral 2.

## 6.0 Spiral 3

The design cruise Mach number selected for the Spiral 1 and Spiral 2 advanced vehicle designs was 0.80, compared to a long range cruise Mach number of 0.785 for the 737-800. The decision to increase cruise Mach for the advanced configurations assumed a continuation of the historical trend toward increasing speed for passenger transport aircraft. Some have suggested that to increase fuel efficiency the replacement aircraft for the Boeing 737 and Airbus A320 families will actually be designed to fly significantly slower. Because of environmental and economic pressures, some airlines may be willing to give up something in productivity (speed) for reduced fuel consumption. Cruise Mach numbers as low as 0.70 have been postulated. Despite this speculation, neither the actual Mach number(s) being considered by the manufacturers nor the speeds being suggested to the manufacturers by the airlines are known outside of company proprietary discussions. The conclusions drawn from the results in Spiral 1 and 2 are not necessarily applicable to designs with lower Mach numbers. It is possible that with a lower cruise Mach number, the optimum fan pressure ratio will shift. Given the uncertainty in what the cruise Mach number of the next generation single-aisle transport will be, it is prudent to investigate the sensitivity of the results to this parameter. For Spiral 3, the sensitivity of the results to cruise Mach number was assessed by repeating the Spiral 2 analysis with a cruise Mach number of 0.72.

### 6.1 Spiral 3 Engine Design

General characteristics of the Spiral 3 engines are shown in Table 10 and Table 11 for the low work and high work design approaches, respectively. The design approach for these engines is essentially the same as for the Spiral 2 engines, except for a change in the ADP conditions. The fan, LPC and HPC pressure ratio combinations for the Spiral 3 low work and high work engines are the same as for the corresponding Spiral 2 engines. ADP for the Spiral 3 engines is at an altitude of 35,000 ft and a Mach number 0.72. Target maximum thrust at that condition was set slightly lower at 4600 lb (compared to 5000 lb for Spirals 1 and 2) based on an initial assessment of the thrust required for the slower,  $M=0.72$  flight condition. The fan pressure ratios considered for Spiral 3 are the same as in Spiral 1 and 2; 1.3 to 1.6 for geared fan designs and 1.4 to 1.7 for direct drive designs. The  $FPR=1.3$  geared engine and  $FPR=1.4$  direct drive engine continue to be impractical designs for the reasons noted in Section 4.1. The Spiral 3 engines tend to be slightly smaller and lighter than their Spiral 2 counterparts. Weight estimates for the Spiral 3 engines are compared to Spiral 2 engines in Figure 51. Although the weight values are slightly less, the trends in weight with respect to fan pressure ratio, compressor work split, and fan drive approach are the same for Spiral 3 as for Spiral 2. The change in TSFC is more significant as shown in Figure 52. TSFC is ~5-7% lower for the lower design Mach number used in Spiral 3. This lower fuel consumption offers the potential for equally significant savings in block fuel, reducing fuel cost to the airlines. In addition to fuel savings, the lower design Mach number results in lower  $NO_x$  emissions.  $NO_x$  EIs at the TOC condition are presented in Figure 53 with Spiral 2 values plotted in the background. The ~25% decrease in  $NO_x$  EI can be attributed primarily to the reduced cruise Mach number, which reduces the total pressure and temperature of the air entering the engine. Although the Spiral 2 and 3 engines have the same overall pressure ratio of 42, combustor entrance pressure and temperature, which are key factors in  $NO_x$  formation, are lower for a Spiral 3 engine than for its Spiral 2 equivalent.

Table 10. General Characteristics of Spiral 3, Low Work Engine Models

	S3-Lo-g-1.3*		S3-Lo-g-1.4		S3-Lo-dd-1.4*		S3-Lo-g-1.5		S3-Lo-dd-1.5		S3-Lo-g-1.6		S3-Lo-dd-1.6		S3-Lo-dd-1.7	
Fan Drive/Gear Ratio	Geared/3.0		Geared/2.0		Direct Drive		Geared/1.5		Direct Drive		Geared/1.2		Direct Drive		Direct Drive	
Fan Diameter, in	89		79		79		72		72		66		66		63	
Fan Nozzle Geometry	Variable		Variable		Variable		Fixed		Fixed		Fixed		Fixed		Fixed	
Engine+Nacelle Weight, lb	9261		7701		9918		6794		7309		6599		6096		5622	
Nacelle Max Diameter, ft	9.1		8.1		8.1		7.3		7.3		6.8		6.8		6.4	
Operating Conditions	SLS	TOC	SLS	TOC	SLS	TOC	SLS	TOC	SLS	TOC	SLS	TOC	SLS	TOC	SLS	TOC
Fan Pressure Ratio	1.2	1.3	1.3	1.4	1.3	1.4	1.4	1.5	1.4	1.5	1.5	1.6	1.5	1.6	1.6	1.7
Bypass Ratio	25	25.6	17.7	18.0	17.9	18.2	14.0	13.8	14.1	14.0	11.3	11.0	11.4	11.2	9.5	9.3
Overall Pressure Ratio	31.2	42	33.3	42	33.3	42	34.8	42	34.8	42	36.2	42	36.2	42	37.4	42
Net Thrust, lb	23001	4600	22986	4600	23004	4600	22986	4600	23001	4600	22986	4600	23002	4600	23000	4600
TSFC, lb/(lb-h)	0.205	0.438	0.235	0.457	0.233	0.452	0.257	0.471	0.255	0.466	0.280	0.487	0.277	0.482	0.299	0.498
NO <sub>x</sub> Emission Index (g/kg)	23.5	7.6	25.6	6.6	25.6	6.6	26.8	6.1	26.9	6.1	28.1	5.8	28.1	5.8	29.4	5.5

\*Design ground rules lead to impractical design for these cases.

Table 11. General Characteristics of Spiral 3, High Work Engine Models

	S3-Hi-g-1.3*		S3-Hi-g-1.4		S3-Hi-dd-1.4*		S3-Hi-g-1.5		S3-Hi-dd-1.5		S3-Hi-g-1.6		S3-Hi-dd-1.6		S3-Hi-dd-1.7	
Fan Drive/Gear Ratio	Geared/3.5		Geared/2.5		Direct Drive		Geared/1.9		Direct Drive		Geared/1.6		Direct Drive		Direct Drive	
Fan Diameter, in	89		79		79		72		72		66		66		63	
Fan Nozzle Geometry	Variable		Variable		Variable		Fixed		Fixed		Fixed		Fixed		Fixed	
Engine+Nacelle Weight, lb	8464		7154		10610		6325		7970		5907		6654		6040	
Nacelle Max Diameter, ft	9.2		8.1		8.1		7.3		7.3		6.8		6.8		6.4	
Operating Conditions	SLS	TOC	SLS	TOC	SLS	TOC	SLS	TOC	SLS	TOC	SLS	TOC	SLS	TOC	SLS	TOC
Fan Pressure Ratio	1.2	1.3	1.3	1.4	1.3	1.4	1.4	1.5	1.4	1.5	1.5	1.6	1.5	1.6	1.6	1.7
Bypass Ratio	23.5	23.7	16.5	16.6	16.7	16.8	12.9	12.6	13.1	12.8	10.4	10.1	10.6	10.2	8.7	8.4
Overall Pressure Ratio	31.0	42	33.1	42	33.1	42	34.6	42	34.5	42	36.0	42	36.0	42	37.3	42
Net Thrust, lb	23001	4600	23001	4600	23002	4600	22999	4600	22995	4600	22993	4600	22999	4600	23000	4600
TSFC, lb/(lb-h)	0.209	0.443	0.240	0.463	0.237	0.458	0.264	0.478	0.261	0.473	0.287	0.494	0.284	0.489	0.307	0.505
NO <sub>x</sub> Emission Index (g/kg)	22.4	7.0	24.4	6.0	24.4	6.0	25.7	5.5	25.7	5.5	27	5.2	27.0	5.2	28.2	4.9

\*Design ground rules lead to impractical design for this case

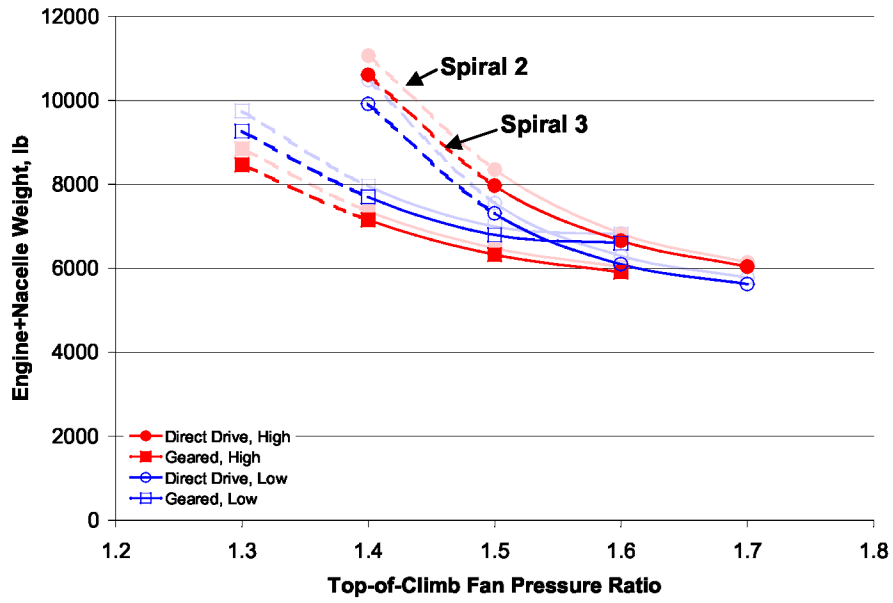


Figure 51. Variation of engine+nacelle weight with fan pressure ratio, Spiral 3.

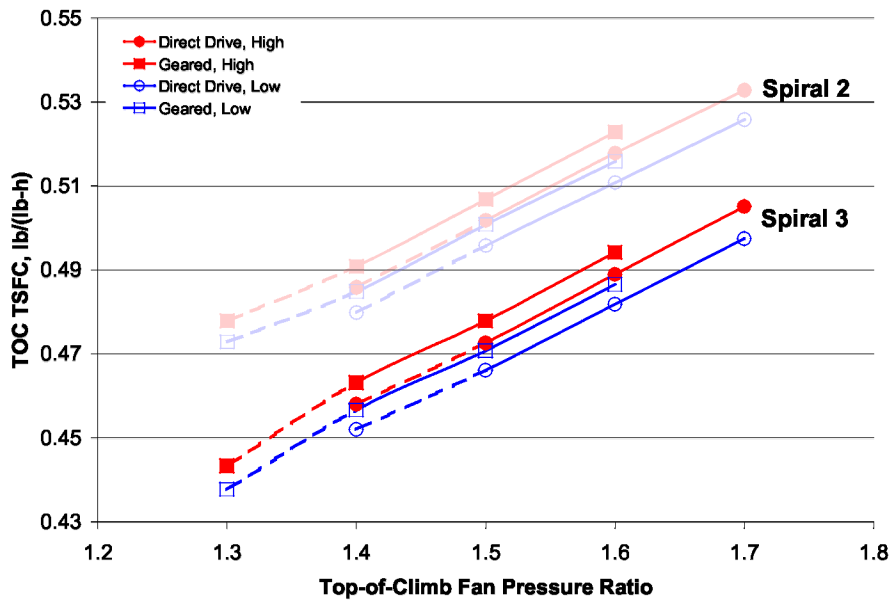


Figure 52. Relationship between fan pressure ratio and TSFC, top-of-climb conditions, Spiral 3.

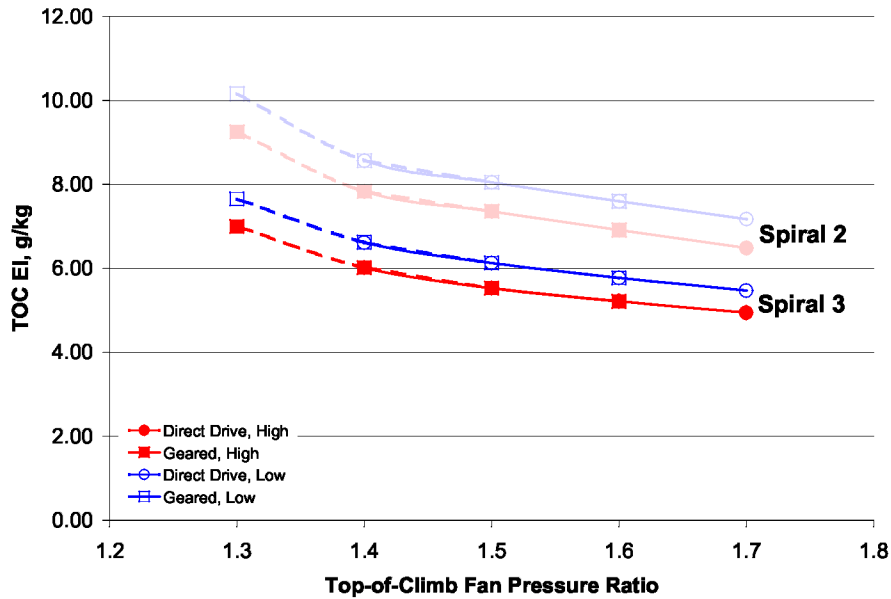


Figure 53. Variation in NO<sub>x</sub> Emission Index with fan pressure ratio and engine type, Spiral 3.

## 6.2 Spiral 3 Aircraft Sizing

### 6.2.1 Airframe Modifications

The wing sweep of the ASAT airframe used in Spirals 1 and 2 is much higher than needed for the M=0.72 cruise speed of the Spiral 3 configurations. As described in Section 3.2.2, the ASAT wing sweep was slightly increased relative to the baseline 737-800 geometry to account for the increased cruise Mach assumed (M=0.8 vs. M=0.785). For a cruise Mach of 0.72, wing sweep can be reduced even below that of the 737-800 wing, which has a 25° quarter-chord sweep. Although the Spiral 1/2 wing geometry could have been retained for the Spiral 3 analysis, the high drag-rise Mach number of this airframe would not have been representative of a future M=0.72 vehicle. Therefore, the quarter-chord wing sweep was reduced to 15° for the Spiral 3 configurations. This results in a leading-edge sweep of ~18°, and a normal Mach number at cruise of 0.685. The sweep of the horizontal tail was reduced as well. A comparison of the Spiral 1/2 and Spiral 3 basic airframe geometries is shown in Figure 54. Note that cruise Mach number is not the only factor that determines sweep angles. Other design considerations such as stability and control can dictate a required amount of sweep. Stability and control analysis was not performed for the new airframe geometry. It was assumed that adequate stability and control could be achieved with the selected wing and tail sweeps through proper positioning.

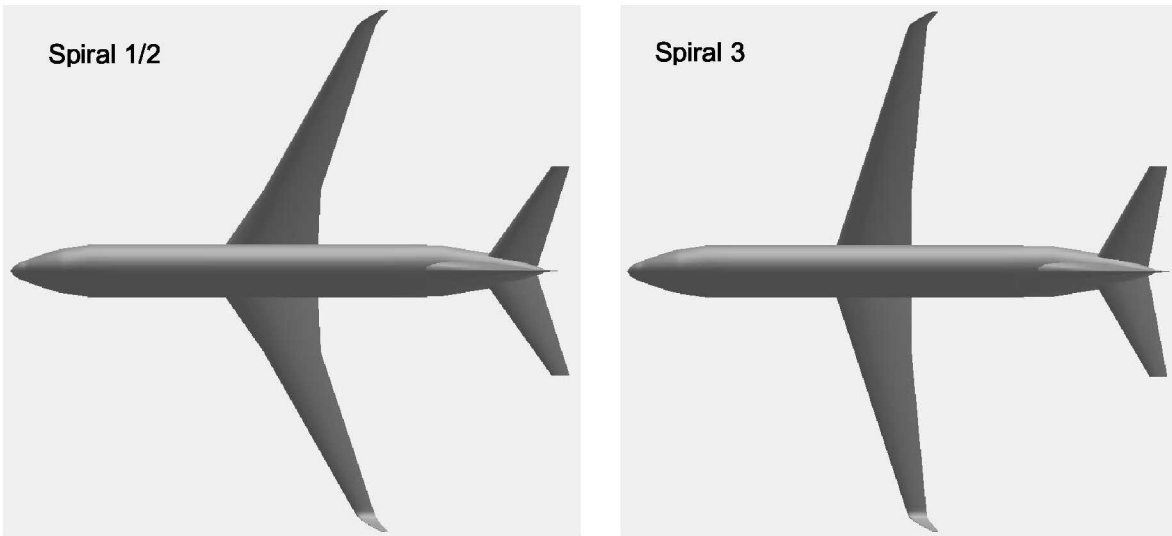


Figure 54. Comparison of Spiral 1/2 and Spiral 3 airframe geometry.

The close similarity between the 737-800 airframe geometry and the Spiral 1/2 airframe geometry provided confidence in the Spiral 1/2 aerodynamic model, which was based on calibration to 737-800 aerodynamic data. However, the Spiral 3 geometry is substantially different and the usefulness of the 737-800 data is limited in this case. The aerodynamic approximation approach used for the Spiral 3 model was to retain the calibration factors derived from the 737-800 calibration case even though the cruise Mach number and wing and tail geometries had changed. Comparisons were then made to the 737-800 data to check the reasonableness of the resulting aerodynamic predictions. In Figure 55, the predicted variation of drag with Mach number for the Spiral 3 airframe (with CFM56-7B engines installed) is compared to the 737-800 data. The reduction in wing sweep results in an expected shift in drag-rise Mach number to a lower value as evident from the figure.

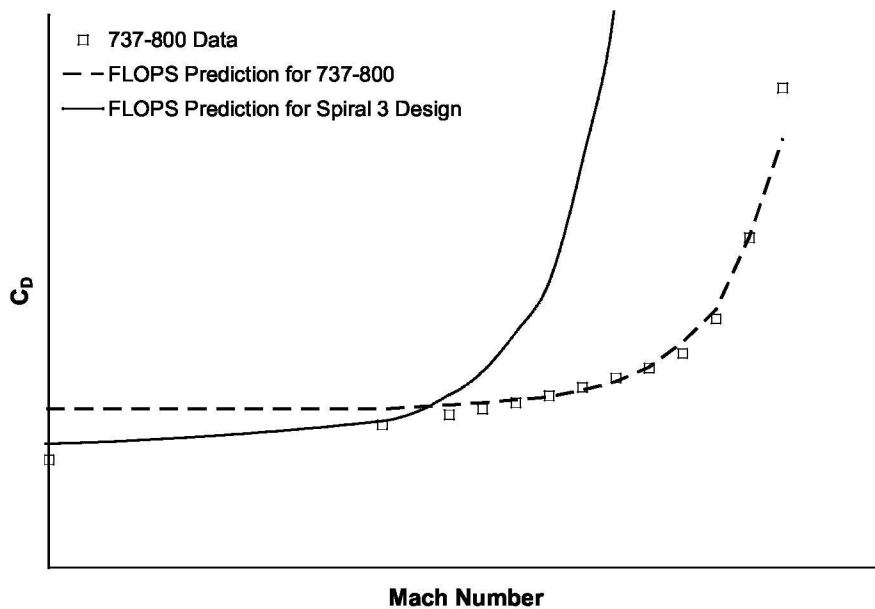


Figure 55. Comparison of 737-800 and Spiral 3 design drag rise.

Another way to visualize the change in aerodynamic performance for the Spiral 3 airframe is a plot of  $M(L/D)$  as a function of Mach number.  $M(L/D)$  is a basic metric for cruise aerodynamic efficiency found in the Breguet Range Equation, which can approximate cruise range capability for a jet aircraft under simplifying assumptions:

$$R = \frac{aM(L/D)}{TSFC} \ln \left( \frac{W_i}{W_f} \right); \text{ where}$$

- $R$  = range
- $a$  = speed of sound
- $M$  = Mach number
- $L/D$  = lift-to-drag ratio
- $TSFC$  = thrust specific fuel consumption
- $W_i$  = initial weight
- $W_f$  = ending weight ( $W_i$  minus amount of fuel consumed)

A comparison of  $M(L/D)$  for the Spiral 1/2 and Spiral 3 configurations is shown in Figure 56. The data in Figure 56 was generated at a lift coefficient typical of cruise conditions. There is little difference in  $M(L/D)$  for the two designs at low Mach numbers. As drag rise for the lower sweep, Spiral 3 configuration is reached the  $M(L/D)$  drops quickly, whereas  $M(L/D)$  continues to increase for the higher sweep, Spiral 1/2 configuration. Note that the higher drag rise Mach number for the Spiral 1/2 geometry enables a higher maximum  $M(L/D)$ . Although cruise  $L/D$  is higher for the Spiral 3 configuration (at  $M=0.72$ ) than for the Spiral 1/2 configuration (at  $M=0.8$ ), cruise  $M(L/D)$  is actually lower for the Spiral 3 design.

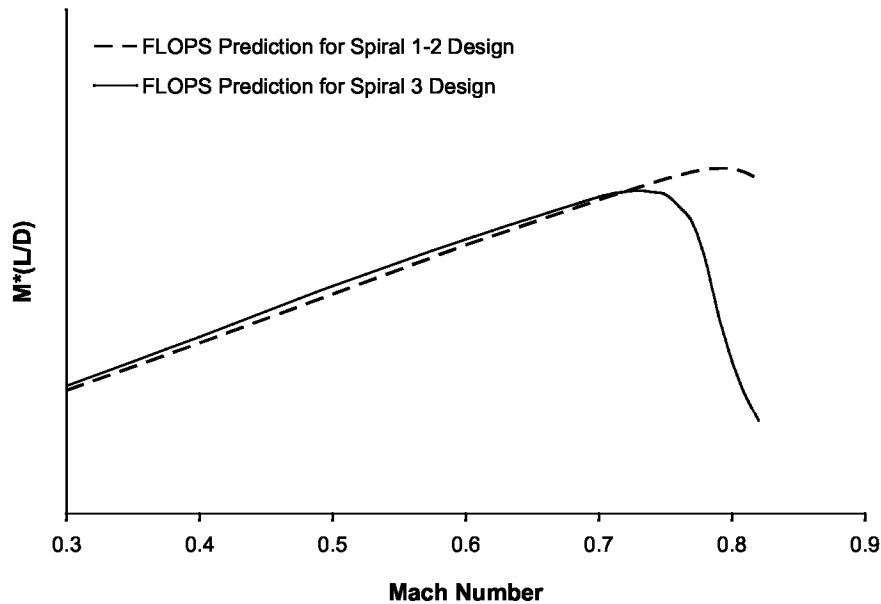


Figure 56. Comparison of aerodynamic efficiency for Spiral 1/2 and Spiral 3.

The change in wing sweep not only impacts the high speed aerodynamic characteristics, but the low speed characteristics as well. Reducing the wing sweep tends to increase the wing's maximum lift coefficient ( $C_{Lmax}$ ) and lift curve slope ( $C_{L\alpha}$ ). The low speed aerodynamic characteristics used for the Spiral 1/2 airframe model were derived from 737-800 data and input directly to the FLOPS analysis.

Unlike in the case of the high speed aerodynamics, there was no calibration of FLOPS internal estimates. Therefore, adjusting the low speed model for lower wing sweep would require direct modification to the aerodynamic data input ( $C_L$  and  $C_D$  versus angle of attack) based on estimated increments. Such modifications were not attempted for the Spiral 3 analysis; rather, the low speed aerodynamic data input used was the same as used in Spirals 1/2. Actual low speed performance would likely be better than that calculated with this unmodified aerodynamic model.

The lower wing sweep for Spiral 3 should lead to a decrease in wing structural weight (for a given size wing) compared to the Spiral 1/2 wing geometry. The affect of wing sweep on structural weight was captured with PDCYL.

### ***6.2.2 Comparison of Results***

Results of the Spiral 3 aircraft sizing and analysis are summarized in Table 12 for the low work engines and Table 13 for the high work engines. The numbers in bold indicate the “best” value for that particular parameter. Also shown for reference are results for a 1998 EIS technology level vehicle (equivalent technology to 737-800/CFM56-7B), designed to match the study design mission of 3250 nm with a cruise speed of  $M=0.72$ . As shown in Figures 51 and 52, the decrease in Mach number for Spiral 3 did not have a significant impact on the engine weight and TSFC trends versus fan pressure ratio and engine architecture. It is perhaps not surprising, therefore, that the “best” engine in each category is the same fan pressure ratio and drive approach as in Spiral 2. The primary motivation for Spiral 3 was the expectation that the trends with fan pressure ratio would be different for a lower cruise Mach number. Although the lower Mach number did not change which engines performed the best, it did alter the relative performance as can be seen in Figures 57 through 61. With the lower cruise Mach number in Spiral 3, the fan pressure ratio trend curves are flatter; that is, the penalties associated with low fan pressure ratio are less. This is especially true for fuel consumption. In Spiral 2, the  $FPR=1.3$  cases have a block fuel consumption which is 12-13% greater than the minimum block fuel case (low work,  $FPR=1.6$ , direct drive). In Spiral 3, the fuel consumption penalty associated with  $FPR=1.3$  is only 7%. Lowering the Mach number did improve the performance of the low fan pressure ratio engines more than that of the high fan pressure ratio engines, but this difference was not enough to change the optimum fan pressure ratios.

Table 12. Aircraft Sizing Results for Spiral 3, Low Work Engines (162 Passenger, 3250nm Design Mission)

	<i>1998 Tech. Baseline</i>	<b>S3-Lo-g-1.3*</b> (BPR ~ 26)	<b>S3-Lo-g-1.4</b> (BPR ~ 18)	<b>S3-Lo-dd-1.4*</b> (BPR ~ 18)	<b>S3-Lo-g-1.5</b> (BPR ~ 14)	<b>S3-Lo-dd-1.5</b> (BPR ~ 14)	<b>S3-Lo-g-1.6</b> (BPR ~ 11.0)	<b>S3-Lo-dd-1.6</b> (BPR ~ 11)	<b>S3-Lo-dd-1.7</b> (BPR ~ 9)
OEW, lb	92250	98900	87600	97750	82000	83600	80800	79150	<b>77400</b>
Mission Fuel, lb	48300	36600	35800	37150	34300	34450	35050	<b>34200</b>	34800
Payload Weight, lb	32400	32400	32400	32400	32400	32400	32400	32400	32400
Ramp Weight, lb	172950	167900	155800	167300	148700	150450	148250	145750	<b>144650</b>
Wing Area, ft <sup>2</sup>	1430	1740	1375	1670	1300	1310	1270	1250	1210
W/S, lb/ft <sup>2</sup>	121	97	113	100	114	115	117	116	120
Thrust(SLS), lb	25600	26450	25050	25350	22900	23300	22900	22550	22500
T/W (takeoff)	0.296	0.315	0.322	0.303	0.308	0.310	0.309	0.310	0.311
Takeoff field length, ft	7000	7000	7000	7000	7000	7000	6990	6990	7000
Landing field length, ft	6030	5190	5740	5320	5750	5790	5850	5830	5930
~Cruise Range Factor V*(L/D)/TSFC, nm	12700	<b>16600</b>	15700	16300	15600	15700	15200	15350	14950
Block Fuel, lb	40900	30900	30200	31400	29100	29200	29700	<b>29000</b>	29500
Block NO <sub>x</sub> , lb	461	213	180	199	158	158	152	149	<b>144</b>
LTO NO <sub>x</sub> , lb per cycle	21.8	<b>9.3</b>	10.4	10.4	10.9	10.9	11.4	11.1	12.0

\*Design ground rules lead to impractical design for these cases.

Table 13. Aircraft Sizing Results for Spiral 3, High Work Engines (162 Passenger, 3250nm Design Mission)

	<i>1998 Tech. Baseline</i>	<b>S3-Hi-g-1.3*</b> (BPR ~ 24)	<b>S3-Hi-g-1.4</b> (BPR ~ 17)	<b>S3-Hi-dd-1.4*</b> (BPR ~ 17)	<b>S3-Hi-g-1.5</b> (BPR ~ 13)	<b>S3-Hi-dd-1.5</b> (BPR ~ 13)	<b>S3-Hi-g-1.6</b> (BPR ~ 10)	<b>S3-Hi-dd-1.6</b> (BPR ~ 10)	<b>S3-Hi-dd-1.7</b> (BPR ~ 8)
OEW, lb	92250	95900	85950	101800	80750	86400	78900	81100	<b>78900</b>
Mission Fuel, lb	48300	36550	35800	39200	<b>34800</b>	36400	35500	35900	36450
Payload Weight, lb	32400	32400	32400	32400	32400	32400	32400	32400	32400
Ramp Weight, lb	172950	164850	154150	173400	147950	155200	<b>146800</b>	149400	147750
Wing Area, ft <sup>2</sup>	1430	1690	1380	1700	1290	1310	1240	1250	1210
W/S, lb/ft <sup>2</sup>	121	98	111	102	115	119	118	120	122
Thrust(SLS), lb	25600	26300	24550	26300	22890	24350	22800	23350	23200
T/W (takeoff)	0.296	0.319	0.319	0.304	0.309	0.314	0.311	0.313	0.314
Takeoff field length, ft	7000	7000	7000	6990	6980	6990	7000	6980	6980
Landing field length, ft	6030	5230	5680	5380	5780	5920	5896	5940	6020
~Cruise Range Factor V*(L/D)/TSFC, nm	12700	<b>16300</b>	15450	15950	15250	15300	14850	14950	14550
Block Fuel, lb	40900	30900	30300	33200	<b>29550</b>	30900	30100	30400	30850
Block NO <sub>x</sub> , lb	461	201	178	201	153	156	147	148	<b>144</b>
LTO NO <sub>x</sub> , lb per cycle	21.8	<b>9.2</b>	10.1	10.7	10.2	10.8	11.2	11.3	12.2

\*Design ground rules lead to impractical design for these cases.

The Spiral 3 fuel consumption results are presented graphically in Figure 57, overlaid on the Spiral 2 results. The lower cruise Mach number results in 2.5-9.6% lower block fuel consumption depending on the particular case. The minimum fuel consumption is ~4% less for Spiral 3 than for Spiral 2. This lower fuel consumption is primarily the result of lower engine TSFC and lower engine and structural weight. As noted above, the Spiral 3 configurations are less aerodynamically efficient (as measured by cruise  $M(L/D)$ ). Lower fuel consumption and lower empty weight leads to lower ramp weight as well, as shown in Figure 58. The reduction in ramp weight is on the order of 2.5% for the optimum ramp weight cases, more for the higher weight cases. A comparison of Spiral 2 and Spiral 3 total  $NO_x$  emissions is presented in Figure 59. The lower fuel consumption and lower  $NO_x$  EIs of the Spiral 3 engines results in a 22-30% reduction in total  $NO_x$  emissions for the design mission. The trends in  $NO_x$  emissions with fan pressure ratio and engine architecture are similar to Spiral 2. LTO  $NO_x$  emissions are presented in Figures 60 and 61.  $D_p/F_{\infty}$  for the Spiral 3 engines is actually slightly higher than for Spiral 2. Even though overall pressure ratio at ADP is 42 for both Spiral 2 and 3, overall pressure ratio at SLS conditions is slightly higher for the Spiral 3 engines.  $NO_x$  per LTO cycle values are similar to Spiral 2, with some cases higher and other cases lower, reflecting variations in engine thrust sizing between Spiral 2 and 3.

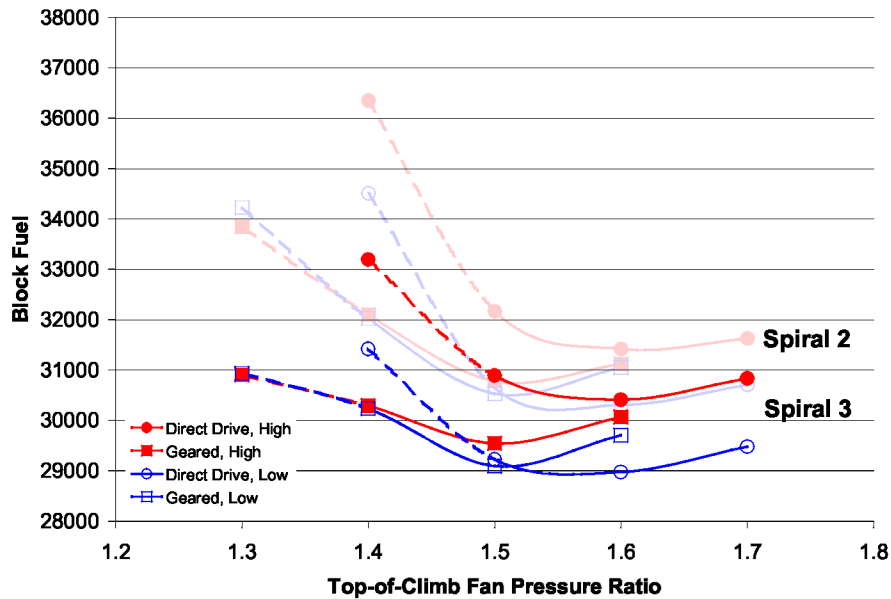


Figure 57. Variation of block fuel with fan pressure ratio and engine type, Spiral 3.

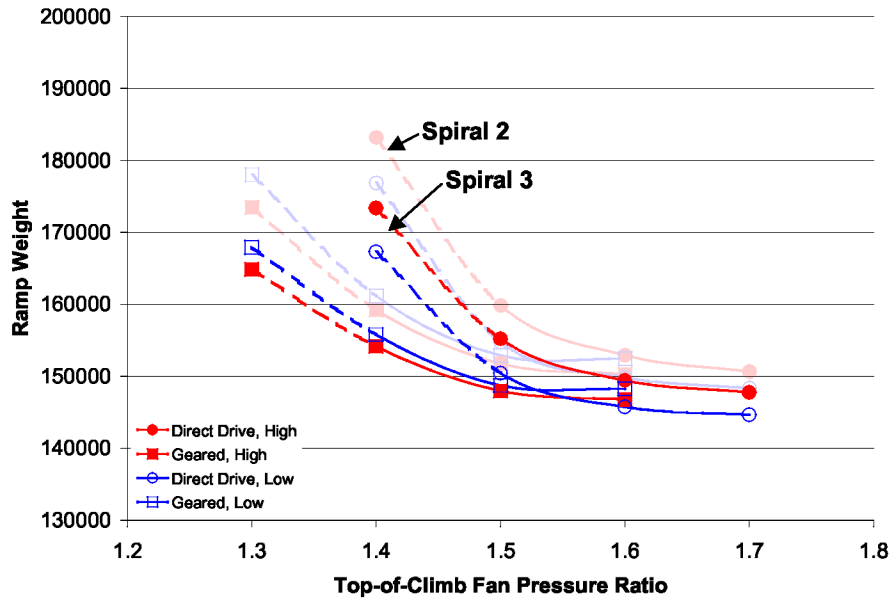


Figure 58. Variation of ramp weight with fan pressure ratio and engine type, Spiral 3.

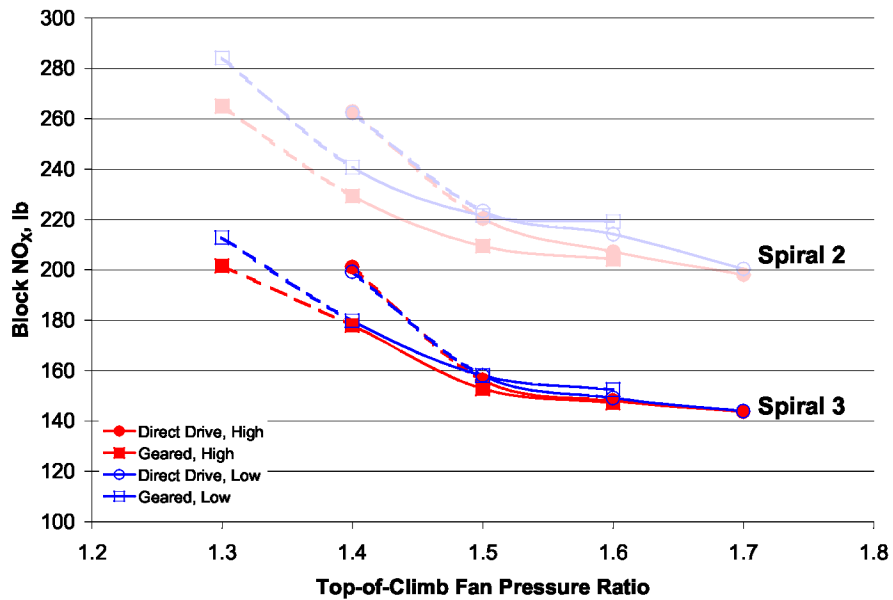


Figure 59. Variation in total mission NO<sub>x</sub> emissions with fan pressure ratio and engine type, Spiral 3.

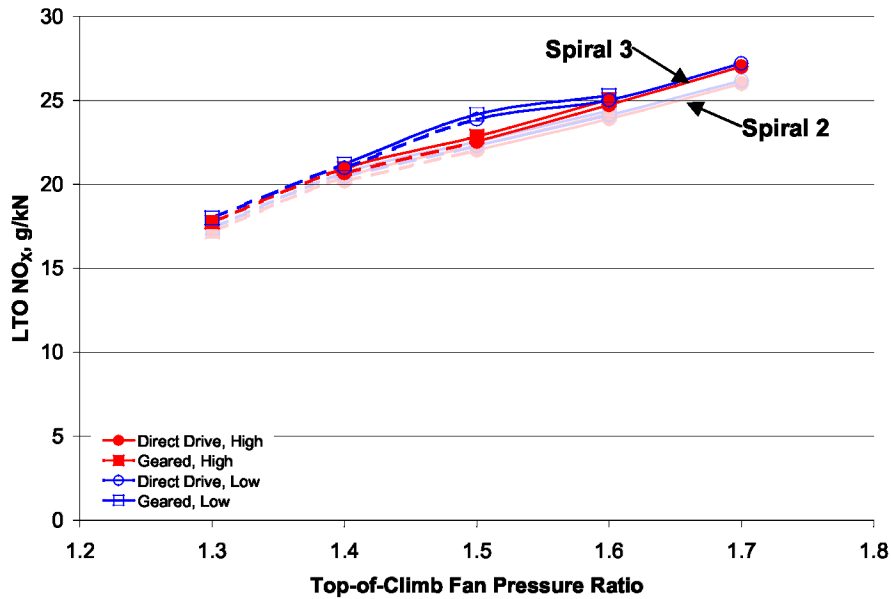


Figure 60. Variation in LTO NO<sub>x</sub> emissions with fan pressure ratio and engine type ( $D_p/F_{oo}$ ), Spiral 3.

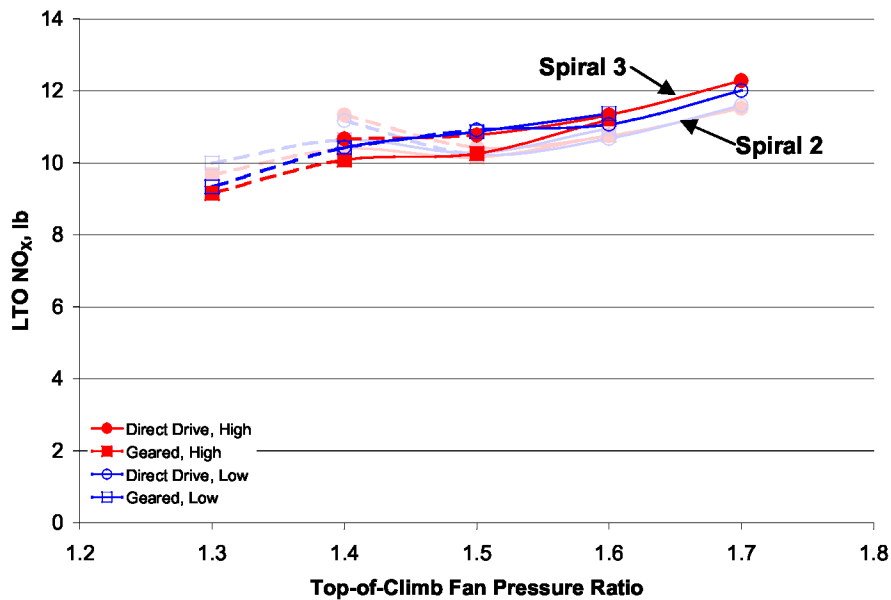


Figure 61. Variation in NO<sub>x</sub> emissions per LTO cycle with fan pressure ratio and engine type, Spiral 3.

### 6.2.3 Potential ASAT, Spiral 3 Technology Benefits

Since the technology assumptions for Spiral 3 are the same as for Spiral 2 (only the design Mach number is different), the benefits relative to a 1998 EIS technology airplane are approximately the same as well. In other words, the ASAT technology benefits have not been affected by the change in Mach number. The technology benefit of the ASAT, Spiral 3 configurations is up to a 29% reduction in fuel consumption compared to a 737-800 equivalent technology airplane *designed for the same mission* (M=0.72 cruise with modified wing sweep, etc.), the same benefit as found in Spiral 2. Note however, that reduction in fuel consumption of the Spiral 3 vehicles compared to a 737-800 type airplane

( $M=0.785$ ) is slightly greater because of the additional benefit of lower cruise Mach. One area where the Spiral 3 technology benefits do differ from Spiral 2 is block  $NO_x$ . The lower EIs associated with the lower cruise Mach lead to a larger reduction in block  $NO_x$  than in Spiral 2 (up to 69% compared to the 1998 EIS technology baseline airplane).

### 6.3 Spiral 3 Certification Noise Analysis

Certification noise results for the Spiral 3 configurations are presented in Figures 62 to 64, relative to the levels predicted for a 737-800 using similar noise analysis methodologies. These results are overlaid on the Spiral 2 results to facilitate easier comparison. The Spiral 2 and Spiral 3 noise results are similar. Overall the differences are relatively small, less than 1 EPNdB. The cumulative noise reductions predicted for the Spiral 3 configurations relative to a 737-800 are presented in Figure 65 and margins relative to Stage 4 regulations in Figure 66, again overlaid on Spiral 2 results. Differences in cumulative noise between Spiral 2 and Spiral 3 are less than 1.5 EPNdB. The Spiral 3 practical designs have up to a 25 EPNdB cumulative reduction relative to the 737-800 baseline. The margin relative to Stage 4 regulations is up to 25 EPNdB based on the ANOPP analysis model.

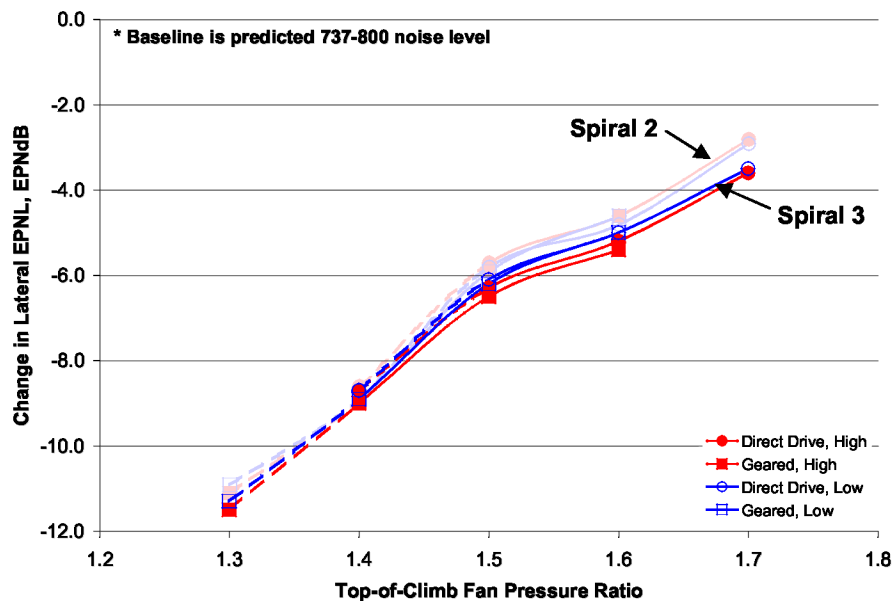


Figure 62. Variation in lateral (sideline) noise with fan pressure ratio and engine type, Spiral 3.

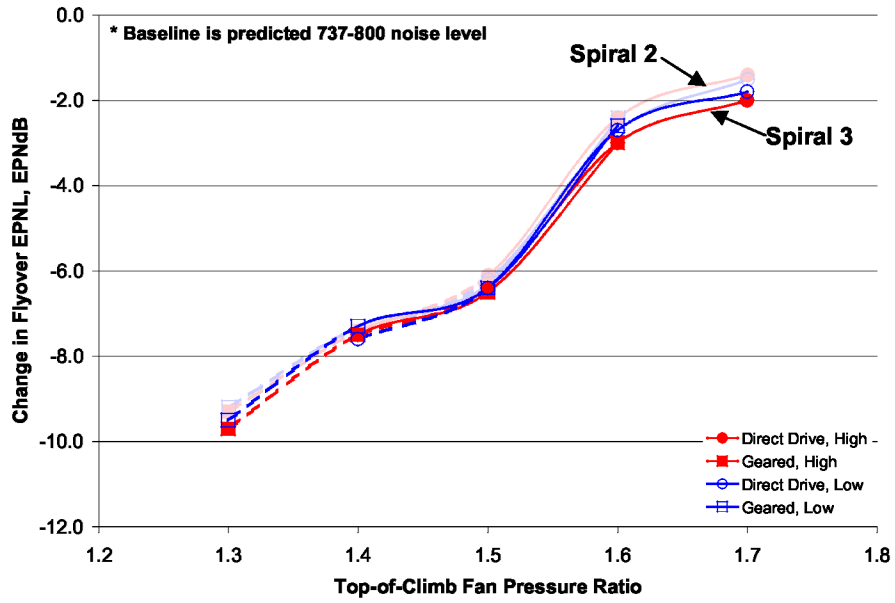


Figure 63. Variation in flyover noise with fan pressure ratio and engine type, Spiral 3.

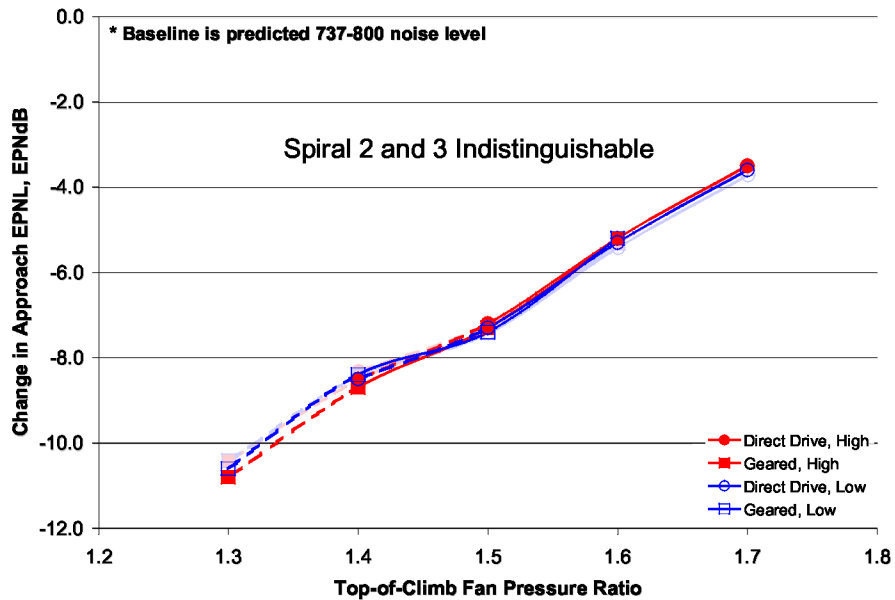


Figure 64. Variation in approach noise with fan pressure ratio and engine type, Spiral 3.

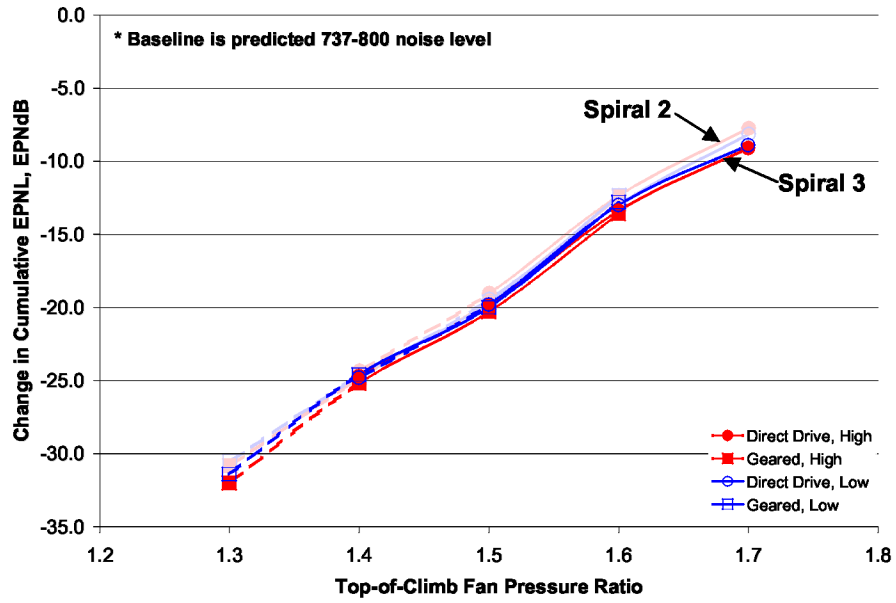


Figure 65. Variation in cumulative noise reduction with fan pressure ratio and engine type, Spiral 3.

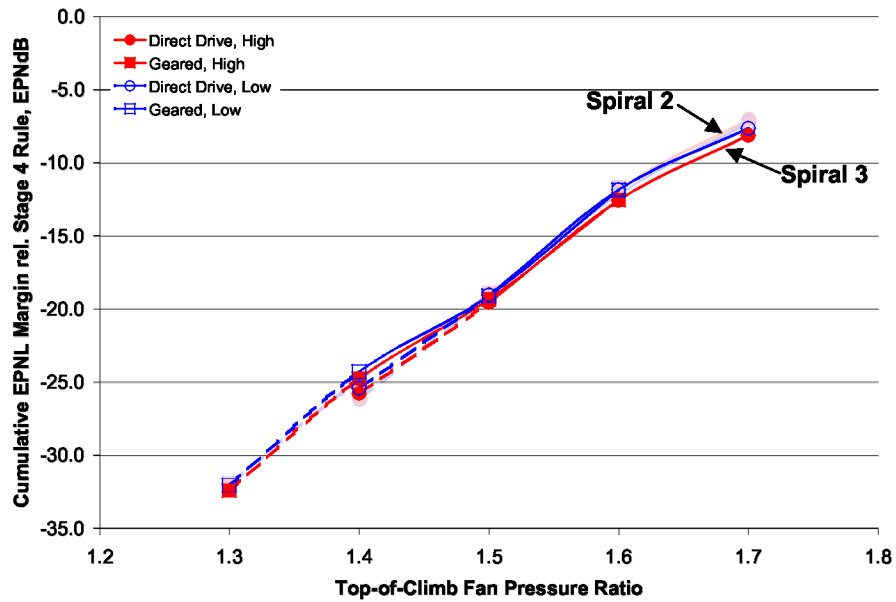


Figure 66. Stage 4 cumulative margin, Spiral 3.

## 7.0 Summary

When Boeing and Airbus launch replacement products for the 737 and A320 families respectively, they will likely tout significant gains in fuel efficiency, emissions, and noise over the current offerings in this vehicle class. One of the primary keys to obtaining those gains will be an advanced technology engine. The characteristics of that future engine are not yet known, although there is plenty of speculation surrounding the type of engine which will power the 737 and A320 replacements. In the past, the promise of higher fuel efficiency and lower noise has led technology developers and engine designers to push toward higher bypass ratio engines. The next step in this evolution is so-called “Ultra-High Bypass” or UHB engines. It is possible that the 737/A320 replacement aircraft will incorporate UHB engine technology. However, there are drawbacks to large diameter, UHB engines which can erode their fundamental efficiency and noise benefits. The advantages and disadvantages of very-high or ultra-high bypass ratio engines have been studied numerous times over the course of several decades with varying conclusions depending on the application and metrics of interest. The primary objective of the current study was to determine whether or not the TSFC and noise benefits of advanced, low fan pressure ratio (high bypass ratio) engines translate into overall aircraft system level benefits for a 737 class vehicle with a conventional airframe-engine layout. Fan pressure ratio or bypass ratio alone does not fully describe the trades available for an advanced engine, however. To more fully investigate the engine design space, an engine design trade study was conducted which considered not only the fan pressure ratio, but also the fan drive approach (geared vs. direct drive), the compression work split between the low pressure and high pressure compressors, the overall pressure ratio, and the bypass nozzle type (variable or fixed geometry). The relative merits of the different engine designs was determined by integrating the engines with a common airframe, sizing the airplane to a fixed mission, and comparing aircraft system level metrics such as block fuel consumption.

Figures 67 to 71 attempt to consolidate and summarize the large amount of data generated during this study. In these figures, the four different engine architectures (low work-geared, low work-direct drive, high work-geared, and high work-direct drive) have been collapsed into a single curve with the minimum value for a given fan pressure ratio plotted for each Spiral and the engine configuration to which this value corresponds indicated. (Note that in many cases the minimum value at a given fan pressure ratio is not significantly less than that obtained from other engine architectures.) Figure 67, ramp weight, indicates the weight penalty associated with low fan pressure ratio which was consistently found across the analysis Spirals. Also, there is a clear preference for high work, geared designs at fan pressure ratios up to 1.5 and low work, direct drive engines at higher fan pressure ratios. Higher overall pressure ratio (Spirals 2 & 3) and lower Mach (Spiral 3) both reduce ramp weight. For block fuel, shown in Figure 68, there is again consistently a penalty for low fan pressure ratio engines. The minimum block fuel consumption consistently occurs in the 1.55 to 1.6 fan pressure ratio range (analysis was only conducted at 1.5 and 1.6; the minimum shown between those two points is the result of curve fitting the data and may not be the true minimum). As with ramp weight, geared engines are preferred below FPR=1.5 and direct drive engines above. Comparing the Spirals it is evident that both higher overall pressure ratio and lower cruise Mach reduce fuel consumption. In the block  $\text{NO}_x$  chart, Figure 69, all the minimum points are high work engines since as noted previously the low work engines have slightly higher  $\text{NO}_x$  emissions. Similar to ramp weight, the trend is for block  $\text{NO}_x$  to decrease with increasing fan pressure ratio, at least up to the highest fan pressure ratio analyzed. In the case of block  $\text{NO}_x$ , gearing is beneficial up to a fan pressure ratio of 1.6. The increase in overall pressure ratio for Spiral 2 significantly increases the block  $\text{NO}_x$ , while the lower cruise Mach in Spiral 3 results in a reduction in block  $\text{NO}_x$ . The trends for LTO  $\text{NO}_x$ , shown in Figure 70, are not as consistent as the other metrics. High fan pressure ratio certainly leads to higher LTO  $\text{NO}_x$ , but between FPR=1.3 and 1.5 the variation with fan pressure ratio is not monotonic. LTO  $\text{NO}_x$  results depend on a combination of the engine characteristics and the aircraft

sizing results (e.g., trade between engine thrust and wing area necessary to meet takeoff performance), and therefore they exhibit more variability. For certification noise the dominant factor is clearly fan pressure ratio as evident in Figure 71. Although the minimum noise cases were mostly with high work, geared engines, there was in fact little variability in noise results among the different engine architectures. Regardless of the type of engine, the overall pressure ratio, or the airplane/engine design Mach number, noise for a given fan pressure ratio was approximately the same.

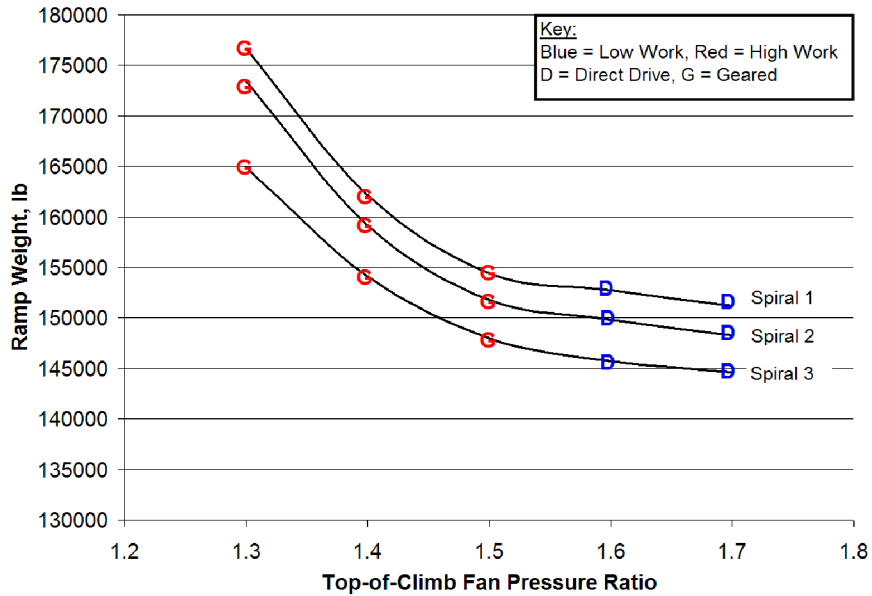


Figure 67. Minimum ramp weight.

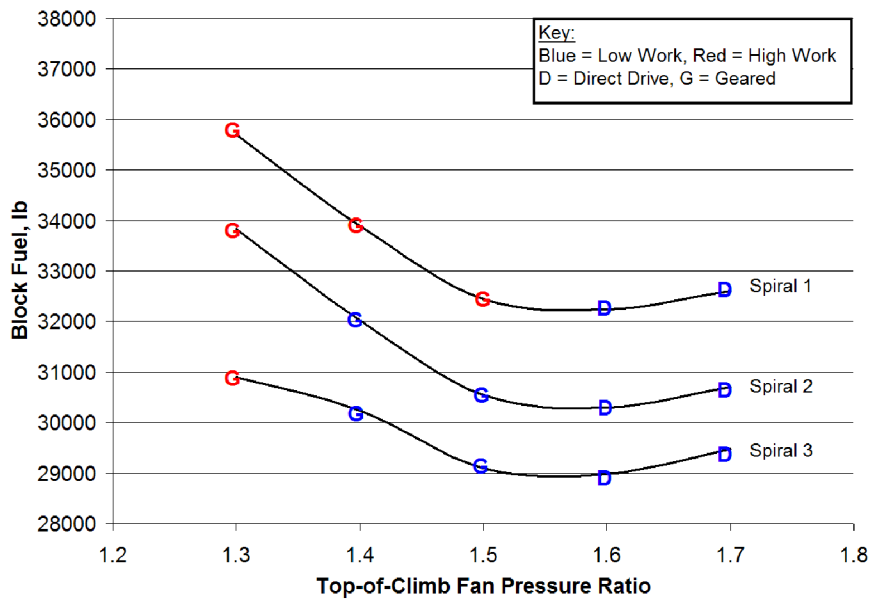


Figure 68. Minimum block fuel.

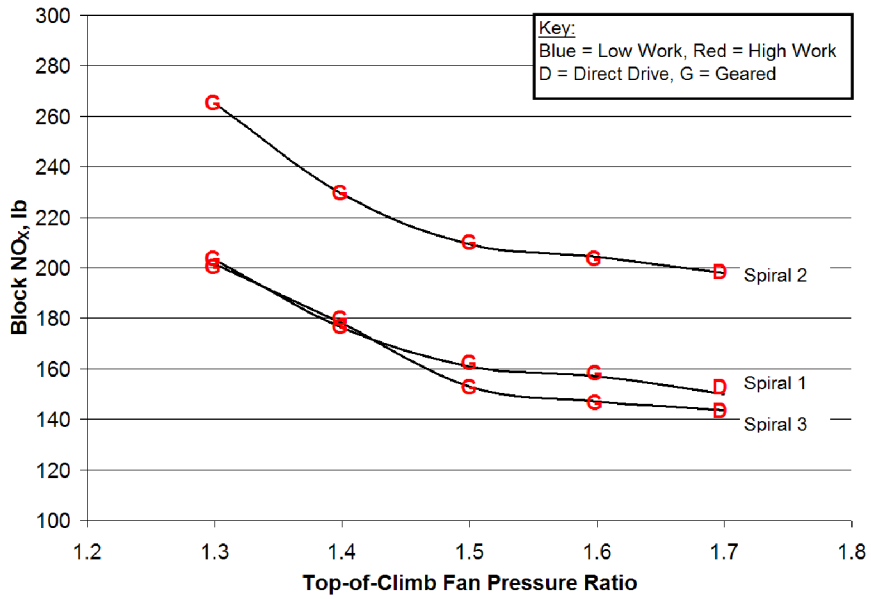


Figure 69. Minimum block NO<sub>x</sub>.

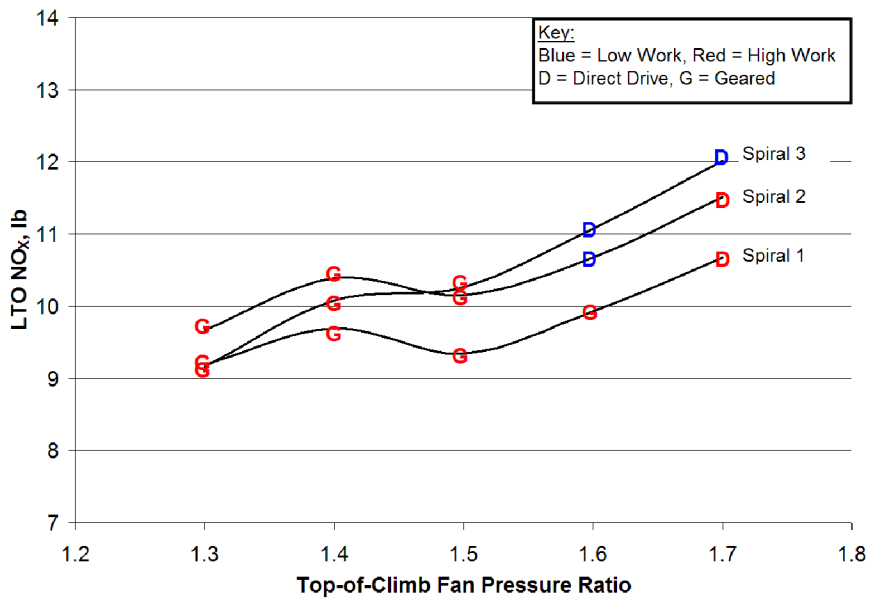


Figure 70. Minimum LTO NO<sub>x</sub>.

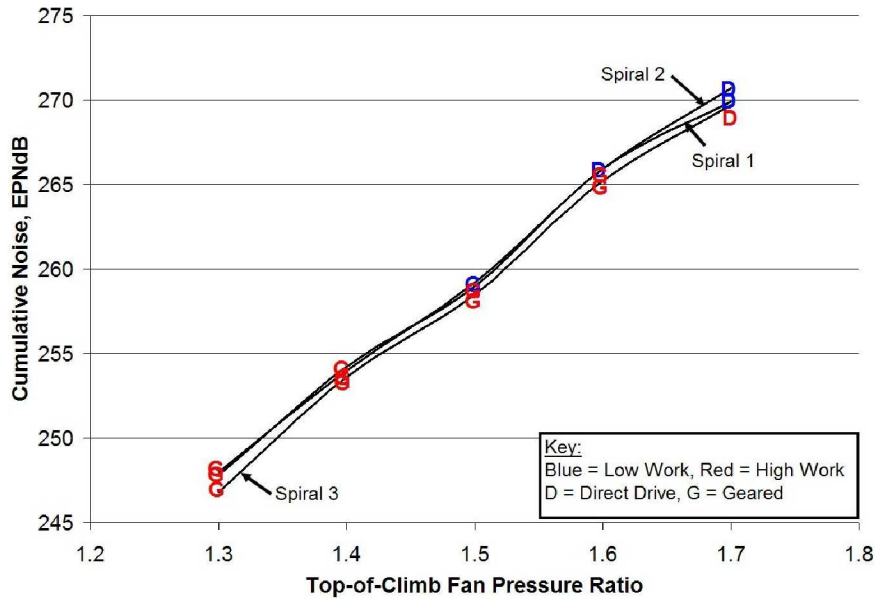


Figure 71. Minimum noise.

As evidenced by the varying colors, letters, and trend lines in Figures 67-71, the study results did not lead to a clear “winner” in terms of the best engine design for this application. The low fan pressure ratio, UHB engines studied do lead to lower aircraft noise, but at the expense of fuel consumption and total NO<sub>x</sub> emissions. For an isolated engine, lower fan pressure ratio (higher bypass ratio) is beneficial for both reducing fuel consumption and reducing noise. However, once incorporated into an aircraft system, a desire for low noise and a desire for low fuel consumption may not lead to the same optimum fan pressure ratio. Aircraft noise and LTO NO<sub>x</sub> are reduced by driving fan pressure ratio as low as practically possible, whereas optimum vehicle weight, block fuel, and block NO<sub>x</sub> occur towards the other end of the fan pressure ratio range analyzed. The relative importance of efficiency, noise, and emissions will dictate the overall best engine design.

Since no single engine provides the best performance across all of the metrics, there are a series of design trade-offs that must be accepted. For example, choosing a low fan pressure ratio because of the noise benefits incurs an increase in fuel consumption compared to what could be achieved with a higher fan pressure ratio design. The magnitudes of these various trade-offs are presented in Tables 14-16 for Spirals 1 through 3. For each metric column, the minimum value is used as the baseline for the remaining cases. The values in the remaining rows indicate the magnitude of the penalty incurred from selecting that particular engine, relative to the best possible result. For example, in Table 14 the direct drive, low work, FPR=1.5 case has 4.3% higher ramp weight than the minimum (direct drive, low work LPC, FPR=1.7); 1.1% greater block fuel consumption than the minimum (direct drive, low work LPC, FPR=1.6); 17.3% greater block NO<sub>x</sub> than the minimum (direct drive, high work LPC, FPR=1.7); 4.1% greater LTO NO<sub>x</sub> than the minimum (geared, high work LPC, FPR=1.5); and 5.1 EPNdB higher cumulative noise than the minimum (geared, high work LPC, FPR=1.4). (The geared, FPR=1.3 and direct drive, FPR=1.4 cases are not included in these tables because of the practicality issues with these designs that have been previously discussed.)

Table 14. Spiral 1 Trade-Off Analysis

	<b>Ramp Weight</b>	<b>Block Fuel</b>	<b>Block NO<sub>x</sub></b>	<b>LTO NO<sub>x</sub></b>	<b>Cum. EPNdB</b>
Low, Geared, FPR=1.4	+8.9%	+5.8%	+24.1%	+10.9%	+0.1
<b>High, Geared, FPR=1.4</b>	<b>+7.2%</b>	<b>+5.1%</b>	<b>+17.6%</b>	<b>+3.8%</b>	<b>Minimum</b>
Low, Geared, FPR=1.5	+3.2%	+0.8%	+16.9%	+4.5%	+5.0
<b>High, Geared, FPR=1.5</b>	<b>+2.1%</b>	<b>+0.6%</b>	<b>+7.2%</b>	<b>Minimum</b>	<b>+4.8</b>
Low, Direct, FPR=1.5	+4.3%	+1.1%	+17.3%	+4.1%	+5.1
High, Direct, FPR=1.5	+6.5%	+4.2%	+11.5%	+2.4%	+5.2
Low, Geared, FPR=1.6	+2.5%	+2.1%	+15.0%	+10.8%	+12.0
High, Geared, FPR=1.6	+1.2%	+2.0%	+4.6%	+6.3%	+11.7
<b>Low, Direct, FPR=1.6</b>	<b>+1.0%</b>	<b>Minimum</b>	<b>+12.5%</b>	<b>+8.5%</b>	<b>+11.9</b>
High, Direct, FPR=1.6	+2.9%	+2.8%	+5.5%	+6.9%	+12.1
<b>Low, Direct, FPR=1.7</b>	<b>Minimum</b>	<b>+1.1%</b>	<b>+9.1%</b>	<b>+15.4%</b>	<b>+15.7</b>
<b>High, Direct, FPR=1.7</b>	<b>+1.1%</b>	<b>+3.4%</b>	<b>Minimum</b>	<b>+14.2%</b>	<b>+16.0</b>

Table 15. Spiral 2 Trade-Off Analysis

	<b>Ramp Weight</b>	<b>Block Fuel</b>	<b>Block NO<sub>x</sub></b>	<b>LTO NO<sub>x</sub></b>	<b>Cum. EPNdB</b>
Low, Geared, FPR=1.4	+8.6%	+5.7%	+21.6%	+4.8%	+0.2
<b>High, Geared, FPR=1.4</b>	<b>+7.3%</b>	<b>+5.9%</b>	<b>+15.8%</b>	<b>+2.3%</b>	<b>Minimum</b>
Low, Geared, FPR=1.5	+3.1%	+0.8%	+11.9%	+1.3%	+5.2
<b>High, Geared, FPR=1.5</b>	<b>+2.3%</b>	<b>+1.6%</b>	<b>+5.8%</b>	<b>Minimum</b>	<b>+5.3</b>
Low, Direct, FPR=1.5	+4.3%	+1.1%	+12.8%	+0.8%	+5.4
High, Direct, FPR=1.5	+7.8%	+6.2%	+11.2%	+2.8%	+5.8
Low, Geared, FPR=1.6	+2.8%	+2.5%	+10.7%	+7.9%	+12.5
High, Geared, FPR=1.6	+1.3%	+2.7%	+3.1%	+6.1%	+12.4
<b>Low, Direct, FPR=1.6</b>	<b>+1.0%</b>	<b>Minimum</b>	<b>+8.1%</b>	<b>+5.1%</b>	<b>+11.9</b>
High, Direct, FPR=1.6	+3.1%	+3.7%	+4.7%	+5.9%	+12.5
<b>Low, Direct, FPR=1.7</b>	<b>Minimum</b>	<b>+1.3%</b>	<b>+1.2%</b>	<b>+14.3%</b>	<b>+16.7</b>
<b>High, Direct, FPR=1.7</b>	<b>+1.6%</b>	<b>+4.4%</b>	<b>Minimum</b>	<b>+13.4%</b>	<b>+17.1</b>

Table 16. Spiral 3 Trade-Off Analysis

	<b>Ramp Weight</b>	<b>Block Fuel</b>	<b>Block NO<sub>x</sub></b>	<b>LTO NO<sub>x</sub></b>	<b>Cum. EPNdB</b>
Low, Geared, FPR=1.4	+7.7%	+4.4%	+25.1%	+3.4%	+0.6
<b>High, Geared, FPR=1.4</b>	<b>+6.6%</b>	<b>+4.5%</b>	<b>+23.8%</b>	<b>Minimum</b>	<b>Minimum</b>
Low, Geared, FPR=1.5	+2.8%	+0.4%	+9.9%	+7.8%	+5.2
High, Geared, FPR=1.5	+2.3%	+2.0%	+6.3%	+1.8%	+4.9
Low, Direct, FPR=1.5	+4.0%	+0.9%	+10.0%	+8.3%	+5.4
High, Direct, FPR=1.5	+7.3%	+6.6%	+8.8%	+6.9%	+5.3
Low, Geared, FPR=1.6	+2.5%	+2.5%	+6.0%	+12.8%	+12.4
High, Geared, FPR=1.6	+1.5%	+3.8%	+2.4%	+11.1%	+11.6
<b>Low, Direct, FPR=1.6</b>	<b>+0.8%</b>	<b>Minimum</b>	<b>+3.8%</b>	<b>+9.8%</b>	<b>+12.2</b>
High, Direct, FPR=1.6	+3.3%	+5.0%	+3.0%	+12.4%	+11.8
<b>Low, Direct, FPR=1.7</b>	<b>Minimum</b>	<b>+1.7%</b>	<b>+0.2%</b>	<b>+19.2%</b>	<b>+16.3</b>
<b>High, Direct, FPR=1.7</b>	<b>+2.2%</b>	<b>+6.4%</b>	<b>Minimum</b>	<b>+21.8%</b>	<b>+16.1</b>

For Spiral 1 (Table 14), pursuing minimum noise (geared, high work LPC, FPR=1.4), leads to a penalty in fuel consumption of greater than 5%. Note that, as discussed previously, the performance of the low fan pressure ratio cases could potentially be improved through better matching of engine design thrust to the aircraft thrust requirements. Conversely, pursuing minimum fuel consumption (direct drive, low work LPC, FPR=1.6) leads to ~12 EPNdB higher cumulative noise. The trade-off is similar for Spiral 2. As previously discussed in Section 6.2.2, the lower Mach number of Spiral 3 reduces the fuel consumption penalty associated with low fan pressure ratio. The fuel consumption penalty of pursuing minimum noise in a Spiral 3 design is only 4.5%, while the noise penalty of pursuing minimum fuel consumption remains ~12 EPNdB cumulative. Which design is better overall depends, in part, on the relative value of low noise and low fuel consumption to the airlines, which in turn depends on external factors such as fuel cost and airport noise restrictions.

In the absence of an overall “goodness” metric, the results in Tables 14-16 can indicate some potential balanced designs which perform fairly well across all the metrics of interest without giving up too much in any one area. Selecting a balanced design is somewhat subjective; however, for all three Spirals the FPR=1.5 cases seem to offer the best overall performance. In particular, the low work, geared and direct drive cases and the high work, geared case have relatively good weight, fuel efficiency, noise, and emissions results. (The high work, direct drive, FPR=1.5 case has inferior performance to the other FPR=1.5 cases.) Bypass ratios for these engines are in the ~12.5-14.5 range, at the lower end of what is usually considered ultra-high bypass ratio. The emergence of FPR=1.5 as the best balanced design is a function of the approach and assumptions in this study. Changes in engine or airframe design rules and technology assumptions could lead to a different result. It is interesting to compare the general characteristics of the FPR=1.5 engines to those of the geared engine being offered by Pratt and Whitney for the Bombardier C Series aircraft. Although the details of the Pratt and Whitney engine are not known publically (including the fan pressure ratio), there are some similarities in the general parameters. The target thrust level for the C Series engine is 23,000 lb (ref. 48), the same SLS target thrust used in this

study. The fan diameter for the CSeries engine is 73 inches (ref. 48), the same as the Spiral 1 and 2 FPR=1.5 engines. Bypass ratio is expected to be 12 (ref. 49), again similar to the FPR=1.5 engines in the study. Cumulative noise margin for the P&W engine is projected to be Stage 4 minus 20 EPNdB (ref. 49). The FPR=1.5 configurations in this study result in a Stage 4 margin of ~19 EPNdB.

## 8.0 Conclusions

- UHB engines are feasible for a 737/A320-class vehicle. In general, the larger diameter associated with UHB engines can be accommodated on this class of vehicle with relatively simple measures such as increased landing gear length or changes to wing dihedral (changes to wing dihedral were not explored in this study).
- Optimum engine fan pressure ratio depends on the metric of interest, as well as the ground rules, basic engine architectures, and assumptions used in the analysis. With the ground rules, architectures, and assumptions used in this study: empty and ramp weight (often surrogate indicators of cost) are minimized with high fan pressure ratio; block fuel consumption is minimized with a fan pressure ratio of ~1.6; block NO<sub>x</sub> emissions are minimized with high fan pressure ratio; and LTO NO<sub>x</sub> and certification noise are minimized with fan pressure ratio as low as possible. These fan pressure ratio trends do not change with variation in engine overall pressure ratio or design Mach number.
- The primary benefit of the geared fan approach is to enable viable propulsion systems at lower fan pressure ratios than possible with a direct drive fan. The geared fan approach is preferred for fan pressure ratios (top-of-climb) below 1.5 (roughly BPR >13). At a fan pressure ratio of 1.5, a low work LPC, direct drive engine can provide outcomes similar to a geared engine. Above a fan pressure ratio of 1.5, a low work, direct drive engine provides a better overall aircraft system (for the metrics tracked in this study) than the geared engines do.
- If the design goal is to minimize ramp weight, block fuel, or block NO<sub>x</sub>, with the design ground rules and technology assumptions of this study geared fan engine technology is not necessary (since the minimums for these metrics occur at fan pressure ratios greater than 1.5.).
- If the design goal is to minimize airport area environmental impacts (i.e., aircraft noise and LTO NO<sub>x</sub>), a geared system would be the preferred approach because it enables a practical low fan pressure ratio engine design.
- Among the cases analyzed, the best balanced designs, performing well across all the metrics of interest (ramp weight, fuel consumption, emissions, and noise), are fan pressure ratio 1.5 designs; either the high work LPC with a geared fan, or the low work LPC with either a geared or direct drive fan.
- Relative to 1998 EIS technology, the advanced 2015 EIS configurations have the potential for significant benefits: up to 29% reduction in fuel consumption and 25 EPNdB cumulative noise reduction. These benefits do not occur with the same engine design, however. The minimum fuel consumption designs have ~12 EPNdB (cumulative) higher noise than the minimum noise designs and the minimum noise designs have up to 6% higher fuel consumption than the minimum fuel consumption designs.

## 9.0 References

1. Norris, G.: *THE 737 STORY: Smoke and mirrors obscure 737 and Airbus A320 replacement studies*. Flight International, February 7, 2006. <http://www.flightglobal.com/articles/2006/02/07/204506/the-737-story-smoke-and-mirrors-obscure-737-and-airbus-a320-replacement.html>. Accessed 4/9/2007.
2. Lyon, T. A. and Hillery, R. D.: *Geared Fan Engine Systems – Their Advantages and Potential Reliability*. AIAA 72-1173, November 1972.
3. Dunican, M. G.: *Installation of Innovative Turbofan Engines on Current Transport Airplanes*. AIAA 87-2921, September 1987.
4. Daggett, D. L.; Brown, S. T.; and Kawai, R. T.: *Ultra-Efficient Engine Diameter Study*. NASA CR-2003-212309, May 2003.
5. *Current Market Outlook 2008*. Boeing Commercial Airplanes, 2008.
6. Norris, G.: *P&W researches next generation airliner geared turbofan engines*. Flight International, February 7, 2006. <http://www.flightglobal.com/articles/2006/02/07/204523/pw-researches-next-generation-airliner-geared-turbofan.html>. Accessed 4/9/2007.
7. Lytle, J.K.: *The Numerical Propulsion System Simulation: An Overview*. NASA TM-2000-209915.
8. NPSS User Guide Software Release: NPSS\_1.6.3 AL.
9. NPSS Reference Sheets Software Release: NPSS\_1.6.3 AL.
10. Onat, E.; and Klees, G.: *A Method to Estimate Weight and Dimensions of Large and Small Gas Turbine Engines*. NASA CR 159481, 1979.
11. Tong, M.T.; Halliwell, I.; Ghosn, L.J.: *A Computer Code for Gas Turbine Engine Weight and Life Estimation*, ASME Journal of Engineering for Gas Turbine and Power, volume 126, no. 2, April 2004
12. Tong, M.T.; Naylor, B.A.: *An Object-Oriented Computer Code for Aircraft Engine Weight Estimation*, GT2008-50062, ASME Turbo-Expo 2008, June 9-13, 2008.
13. ICAO Committee on Aviation Environmental Protection: *Environmental Design Space (EDS) Prototype*. CAEP/7 WG2 – Aircraft Operations and Modeling, TG2 Meeting –Sixth Meeting, Tucson, AZ, 7-8 February 2006.
14. McCullers, L.: *Aircraft Configuration Optimization Including Optimized Flight Profiles*. Proceedings of the Symposium on Recent Experiences in Multidisciplinary Analysis and Optimization, NASA CP 2327, April 1984.
15. Ardema, M. D.; Chambers, M. C.; Patron, A. P; Hahn, A. S.; Miura, H.; and Moore, M. D.: *Analytical Fuselage and Wing Weight Estimation of Transport Aircraft*. NASA TM 110392, May 1996.
16. *737 Airplane Characteristics for Airport Planning*. D6-58325-6, Boeing Commercial Airplanes, October 2005. <http://www.boeing.com/commercial/airports/737.htm>. Accessed 4/9/2007.
17. Advanced Blended Winglets. <http://www.b737.org.uk/winglets.htm>. Accessed 4/12/2007.

18. Faye, R.; Laprete, R.; and Winter, M.: *Blended Winglets for Improved Airplane Performance*. Aero, January 2002. [http://www.boeing.com/commercial/aeromagazine/aero\\_17](http://www.boeing.com/commercial/aeromagazine/aero_17). Accessed 9/25/2007.
19. Baughcum, S. L.; Tritz, T. D.; Henderson, S. C.; and Pickett, D. C.: *Scheduled Civil Aircraft Emission Inventories for 1992: Database Development and Analysis*. NASA CR-4700, April 1996.
20. 787 Dreamliner Program Fact Sheet. <http://www.boeing.com/commercial/787family/programfacts.html>. Accessed 4/9/2007.
21. 737-800 Technical Characteristics. [http://www.boeing.com/commercial/737family/pf/pf\\_800tech.html](http://www.boeing.com/commercial/737family/pf/pf_800tech.html). Accessed 4/9/2007.
22. Torenbeek, E.: *Synthesis of Subsonic Airplane Design*. Kluwer Academic Publishers, 1982.
23. Gunston, B., ed.: *Jane's Aero-Engines*. Jane's Information Group, 2006.
24. CFM56-3 Technology. <http://www.cfm56.com/index.php?level2=engines&level3=cfm56-3&level4=1043>. Accessed 4/9/2007.
25. Code of Federal Regulations, Title 14, Chapter I, Part 25. *Airworthiness Standards: Transport Category Airplanes*.
26. Pendergraft, O. C., Jr.; Ingraldi, A. M.; Re, R. J.; Kariya, T. T.: *Installation Effects of Wing-Mounted Turbofan Nacelle-Pylons on a 1/17-Scale, Twin-Engine, Low-Wing Transport Model*. NASA TP 3168, March 1992.
27. Gillian, Ronnie E.: *Aircraft Noise Prediction Program User's Manual*. NASA TM-84486, 1983.
28. Zorumski, William E.: *Aircraft Noise Prediction Program Theoretical Manual*. NASA TM-83199, 1981, Parts 1 and 2 (Currently maintained at NASA LaRC by the ANOPP team in electronic format and provided upon request; Latest revision: December 2005).
29. Code of Federal Regulations, Title 14, Chapter I, Part 36. *Noise standards: Aircraft type and airworthiness certification*.
30. Kontos, K.; Janardan, B.; and Gliebe, P.: *Improved NASA-ANOPP Noise Prediction Computer Code for Advanced Subsonic Propulsion Systems Volume 1: ANOPP Evaluation and Fan Noise Model Improvement*. NASA CR-195480, 1996.
31. Stone, J.R.; Krejsa, E.A.; Clark, B.J.; and Berton, J.J.: *Jet Noise Modeling for Suppressed and Unsuppressed Aircraft in Simulated Flight*. NASA TM-2009-215524, 2009.
32. Emmerling, J.J.; Kazin, S.B.; and Matta, R.K.: *Core Engine Noise Control Program. Volume III, Supplement 1 - Prediction Methods*. FAA-RD-74-125, III-I, Mar. 1976 (Available from DTIC as AD A030 376.)
33. Kontos, K.B.; Kraft, R.E.; and Gliebe, P.R.: *Improved NASA-ANOPP Noise Prediction Computer Code for Advanced Subsonic Propulsion Systems. Volume 2: Fan Suppression Model Development*. NASA CR-202309, 1996.
34. Fink, M.: *Airframe Noise Prediction Method*. FAA-RD-77-29, March, 1977.

35. Dahl, Milo D.: *A Process for Assessing NASA's Capability in Aircraft Noise Prediction Technology*. AIAA Paper 2008-2813, NASA TM-2008-215268, 2008.
36. Burley, Casey L.; Rawls, John W., Jr.; Berton, Jeffrey J.; and Marcolini, Michael A.: *Aircraft System Noise Prediction*. NASA report to be published, 2009.
37. Envia, Edmane; Woodward, Richard P.; Elliott, David M.; Fite, E. Brian; Hughes, Christopher E.; Podboy, Gary G.; Sutliff, Daniel L.: *An Assessment of Current Fan Noise Prediction Capability*. NASA TM-2008-215415, 2008.
38. Hunter, Craig A.; Bridges, James E.; Khavaran, Abbas: *Assessment of Current Jet Noise Prediction Capabilities*. AIAA Paper 2008-2933; NASA TM-2008-215275, 2008.
39. Humphries, W.M.; Burley, C.L.; and Brooks, T.F.: *Scale-Model Landing Gear Noise Spectra and Directivity*. Acoustics Technical Working Group Meeting, 23-24 Sep. 2008, Williamsburg, VA, United States.
40. Society of Automotive Engineers, Committee A-21, *Aircraft Noise: Procedure for the Computation of Airplane Noise in the Vicinity of Airports*. Aerospace Information Report No. 1845, Warrendale, PA: Society of Automotive Engineers, Inc., March 1986.
41. Janardan, B.A.; Hoff, G.E.; Barter, J.W.; Martens, S.; Gliebe, P.R.; Mengle, V.; and Dalton, W.N.: *AST Critical Propulsion and Noise Reduction Technologies for Future Commercial Subsonic Engines – Separate-Flow Exhaust System Noise Reduction Evaluation*. Final Report: NAS3-27720, Area of Interest 14.3, General Electric Report R98AEB152, May 1998.
42. Neubert, R.; Bock, L.; Malmberg, E.; and Owen-Peer, W.: *Advanced Low Noise Research Fan Stage Design*. NASA CR 97-206308, 1997.
43. Sutliff, Daniel; Jones, Mike; Hartley, Tom: *Collaboration with Williams International to Demonstrate the Characteristics of a Foam-Metal-Liner Installed Over-the-Rotor of a Turbofan Engine*. Acoustics Technical Working Group Meeting, 23-24 Sep. 2008, Williamsburg, VA, United States.
44. Jones, M.; Parrott, T.; Sutliff, D.; Hughes, C.: *Assessment of Soft Vane and Metal Foam Engine Noise Reduction Concepts*. 15th AIAA/CEAS Aeroacoustics Conference, AIAA-2009-3142, 2009.
45. Envia, Edmane: *Progress Toward N+1 Noise Goal*. Fundamental Aeronautics Program, Subsonic Fixed Wing Project, 12-Month Program Review, Washington, DC, November 5-6, 2008.
46. Norris, G. and Wall, R.: *Boeing Goes Back to Drawing Board for 737 Follow-on*. Aviation Week and Space Technology, May 18, 2008. [http://www.aviationweek.com/aw/generic/story\\_generic.jsp?channel=awst&id=news/aw051908p2.xml](http://www.aviationweek.com/aw/generic/story_generic.jsp?channel=awst&id=news/aw051908p2.xml). Accessed 5/28/2008.
47. Mintz, J.: *Boeing delays plan for replacing popular 737*. USA Today.com. [http://www.usatoday.com/travel/flights/2008-05-23-737-replacement\\_N.htm](http://www.usatoday.com/travel/flights/2008-05-23-737-replacement_N.htm). Accessed 5/29/2008.
48. Norris, G.: *Simplified GTF*. Aviation Week and Space Technology, March 3, 2008. pp 26-27.
49. Flint, P.: *Gearing Up for the Future*. Air Transport World, February 2008. <http://www.atwonline.com/magazine/article.html?articleID=2220>. Accessed 5/28/2008.

REPORT DOCUMENTATION PAGE				Form Approved OMB No. 0704-0188	
<p>The public reporting burden for this collection of information is estimated to average 1 hour per response, including the time for reviewing instructions, searching existing data sources, gathering and maintaining the data needed, and completing and reviewing the collection of information. Send comments regarding this burden estimate or any other aspect of this collection of information, including suggestions for reducing this burden, to Department of Defense, Washington Headquarters Services, Directorate for Information Operations and Reports (0704-0188), 1215 Jefferson Davis Highway, Suite 1204, Arlington, VA 22202-4302. Respondents should be aware that notwithstanding any other provision of law, no person shall be subject to any penalty for failing to comply with a collection of information if it does not display a currently valid OMB control number.</p> <p><b>PLEASE DO NOT RETURN YOUR FORM TO THE ABOVE ADDRESS.</b></p>					
1. REPORT DATE (DD-MM-YYYY) 01-08 - 2009		2. REPORT TYPE Technical Memorandum		3. DATES COVERED (From - To)	
4. TITLE AND SUBTITLE Engine Concept Study for an Advanced Single-Aisle Transport			5a. CONTRACT NUMBER		
			5b. GRANT NUMBER		
			5c. PROGRAM ELEMENT NUMBER		
6. AUTHOR(S) Guynn, Mark D.; Berton, Jeffery J.; Fisher, Kenneth L.; Haller, William J.; Tong, Michael T.; and Thurman, Douglas R.			5d. PROJECT NUMBER		
			5e. TASK NUMBER		
			5f. WORK UNIT NUMBER 561581.02.08.07.13.04		
7. PERFORMING ORGANIZATION NAME(S) AND ADDRESS(ES) NASA Langley Research Center Hampton, VA 23681-2199			8. PERFORMING ORGANIZATION REPORT NUMBER  L-19712		
9. SPONSORING/MONITORING AGENCY NAME(S) AND ADDRESS(ES) National Aeronautics and Space Administration Washington, DC 20546-0001			10. SPONSOR/MONITOR'S ACRONYM(S)  NASA		
			11. SPONSOR/MONITOR'S REPORT NUMBER(S) NASA/TM-2009-215784		
12. DISTRIBUTION/AVAILABILITY STATEMENT Unclassified - Unlimited Subject Category 01 Availability: NASA CASI (443) 757-5802					
13. SUPPLEMENTARY NOTES An electronic version can be found at <a href="http://ntrs.nasa.gov">http://ntrs.nasa.gov</a>					
14. ABSTRACT The desire for higher engine efficiency has resulted in the evolution of aircraft gas turbine engines from turbojets, to low bypass ratio, first generation turbofans, to today's high bypass ratio turbofans. Although increased bypass ratio has clear benefits in terms of propulsion system metrics such as specific fuel consumption, these benefits may not translate into aircraft system level benefits due to integration penalties. In this study, the design trade space for advanced turbofan engines applied to a single aisle transport (737/A320 class aircraft) is explored. The benefits of increased bypass ratio and associated enabling technologies such as geared fan drive are found to depend on the primary metrics of interest. For example, bypass ratios at which mission fuel consumption is minimized may not require geared fan technology. However, geared fan drive does enable higher bypass ratio designs which result in lower noise. The results of this study indicate the potential for the advanced aircraft to realize substantial improvements in fuel efficiency, emissions, and noise compared to the current vehicles in this size class.					
15. SUBJECT TERMS Aircraft Design, Engine Design, Engine Airframe Integration, Aircraft Noise, Turbofan Engines, Propulsion System Performance					
16. SECURITY CLASSIFICATION OF:			17. LIMITATION OF ABSTRACT	18. NUMBER OF PAGES	19a. NAME OF RESPONSIBLE PERSON
a. REPORT	b. ABSTRACT	c. THIS PAGE			STI Help Desk (email: <a href="mailto:help@sti.nasa.gov">help@sti.nasa.gov</a> )
U	U	U	UU	97	19b. TELEPHONE NUMBER (Include area code) (443) 757-5802